STATUS REPORTS

to the

PAPERMAKING

PROJECT ADVISORY COMMITTEE

VOLUME II

March 18 - 19, 1996

INSTITUTE OF PAPER SCIENCE AND TECHNOLOGY

Atlanta, Georgia

ANNUAL RESEARCH REVIEW

PAPERMAKING

VOLUME II

March 18 - 19, 1996

TABLE OF CONTENTS

FUNDAMENTALS OF COATING SYSTEMS

STATUS REPORT

FOR

PROJECT F003 (3674)

Cyrus K. Aidun

March 18 - 19, 1996

Institute of Paper Science and Technology
500 10th Street, N.W.
Atlanta, Georgia 30318

TECHNICAL PROGRAM REVIEW

Project Title: FUNDAMENTALS OF COATING SYSTEMS
Project Code: COATS
Project Number: F003/3674
Division: Engineering and Paper Materials
Project Staff: Cyrus Aidun
Project Budget: $46,000

M.S. students: 2
Ph.D. students: 3

OBJECTIVES: (1) To investigate the cause and origin of coat weight nonuniformities reported in high-speed blade coating of paper and board, (2) to explore novel coating systems for application of a more uniform coat weight profile at higher machine speeds.

SUMMARY OF RESULTS:

The focus of the project is on examination of new concepts for coating application. The original vortex-free coater, exmained and explained in the previous progress reports (PAC report 1994-95), suffer from large flow rate requirement which has been a deterant in prgress to pilot scale experiments. This coater has been modified such that an air layer exists between the coating liquid and the lower solid boundary. The air layer serves as a carrier fluid. This arrangement will allow the pressure inside the channel to be increased above ambient pressure, if necessary, in order to prevent air entrainment. However, the system may also operate at ambient pressure if air entrainment is not an issue. The revised vortex-free coater and computational simulation of the flow in the system are presented below. The computational simulations assume ambient pressure in the air layer and, therefore, consider only the coating layer just upstream of the blade.

A REVISED VORTEX-FREE COATER

The coater consists of two inlet channels and an outlet channel, as shown in the schematic below. The first inlet channel carries the coating liquid. The second channel can be used to pump air into the coating head in order to pressurize the chamber and to keep the contact line at the upstream section attached to the substrate and therefore prevent any kind of air entrainment into the coating liquid. The air pressure can vary from zero to any level appropriate for the coating operation. If air entrainment is not a problem, there is no need to have forced air into the second channel. In this case, the air layer serves as a carrier fluid.

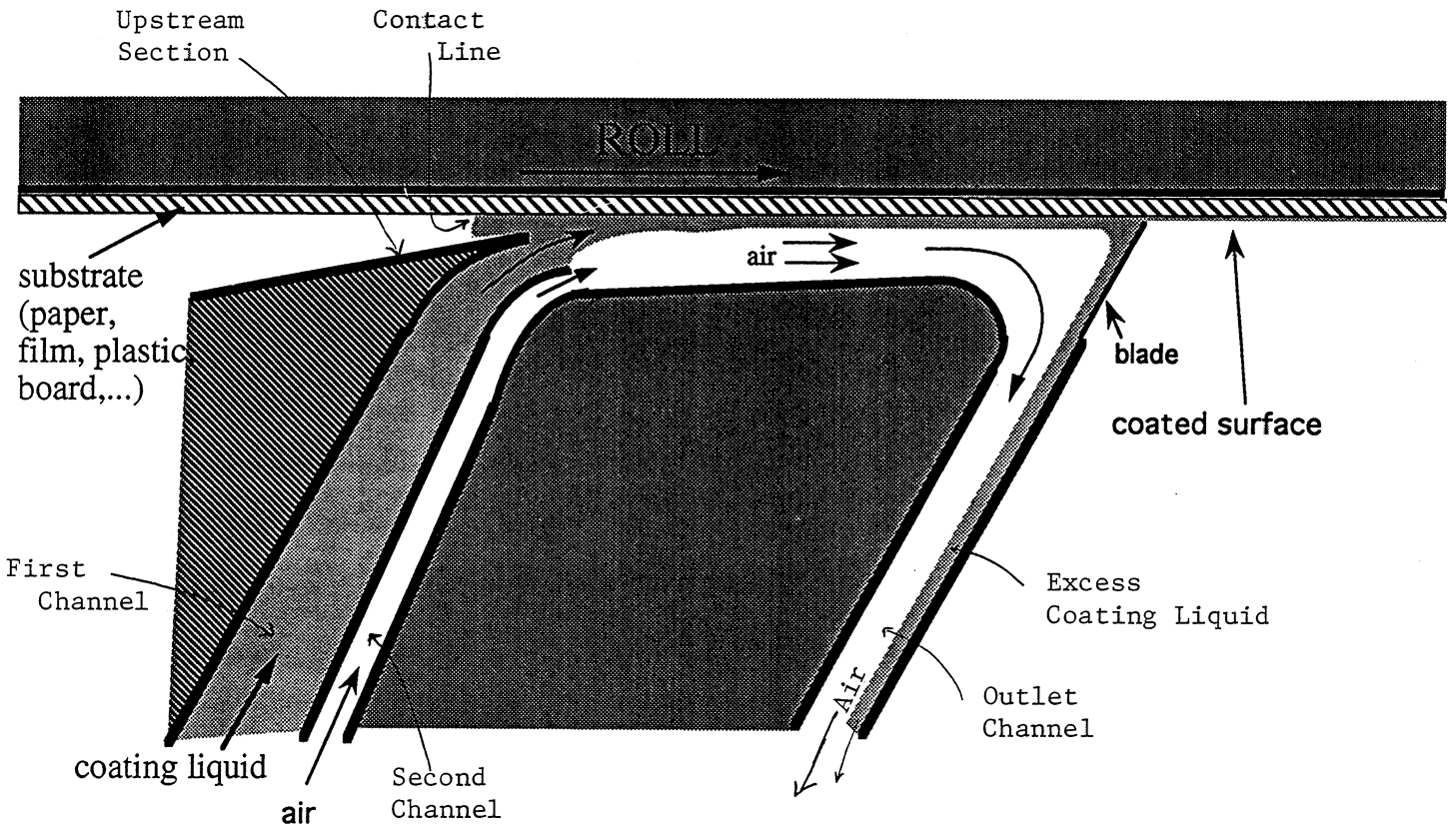

Schematic of the Modified Vortex Free Coater

By removing the wall shear stress on the coating liquid in the channel, the total coating flow rate for the operation of this device without flow separation from the wall (i.e., in a vortex-free mode) becomes very low and appropriate for today's commercial applications. The excess coating liquid and all of the air leave the coater head at the outlet channel. The blade is used to meter the excess coating from the substrate. Details of the computational analysis without including the air layer is presented in the next section.

ANALYSIS OF A MODIFIED VORTEX-FREE COATER

Charlotte Song (Cody) and Cyrus K. Aidun

The present study considers the modified vortex-free coater configurations in an effort to investigate the hydrodynamic behavior of the current system at very low flow rates. We show that in all cases, flow separation and recirculation are avoided. The flow field and the free surface boundary location are solved using a Galerkin finite element approach for web speeds ranging from 15m/s to 30m/s and flowrates from 4 to 7 liter/sec./mete (l/s/m).

Development of high speed blade coating is of particular interest in the industry to enhance production and reduce cost. The analysis of this process is very complex since the governing equations of fluid motion are nonlinear and the free-surface position is part of the unknown. The nonlinear constitutive behavior of typical coating fluids increases the complexity. Boundaries are also complicated; flexible, permeable, and unknown in different regions.

Several mechanisms of instability are present due to the complexity of the domain. The flow is nearly parallel throughout the majority of the domain, with the important exception of the region in which the web and the blade converge forcing some of the liquid under the blade tip and the rest to curve and flow down the blade. In the gap region, between the substrate and the blade tip, the flow is nearly parallel and experiences high shear rates. Squires theorem requires that the first instability in parallel shear flows occur due to a two-dimensional instability. In the turning flow, the possibility of centrifugal instabilities to three-dimensional disturbances exist. Aidun (1991) gives a detailed description of the mechanisms of instability in coating flows.

Pranckh & Scriven (1988) have provided a detailed analysis of blade coating using a finite element approximation method including the complex interactions of the boundary in addition to the solution of the flow field and free surface location. The blade was modeled as a thin, inextensible, elastic solid and the substrate deformed due to normal stresses.

Aidun & Kovacs (1995) have worked towards alleviating recirculations in a fixed domain pressurized pond coating system. The combination of a moving applicator wall and a sufficient flowrate have allowed the design of a vortex-free coater configuration.

The present study seeks to examine the flow field of a blade coater with a lower free surface. The flow is assumed to be incompressible, two-dimensional and steady. The effects of flowrate and web speed variation on the design will provide insight into the optimal operating conditions. A further analysis of the stability of the resulting solutions to 2-D and 3-D disturbances will provide additional information.

The present study seeks to determine the velocity field, pressure field, and location of the two free surfaces of the blade coater depicted in Figure 1 with parameters detailed in Tables

1 and 2. The region of particular interest is shown in Figure 2, here the blade (Γ_4) and the web (Γ_2), converge to form a gap with a vertical cross-section length (blade gap) of 50 microns. A portion of the fluid pumped in at the inlet (Γ_1) proceeds through the gap and coats the substrate, while the excess is scraped off and flows nearly parallel to the blade.

Table 1: Fluid Parameters

ρ	density	1200 kg/m^3
μ_o	zero shear rate viscosity	1.0 kg/(m-s)
μ_∞	infinite shear rate viscosity	0.05 kg/(m-s)
γ	surface tension	0.05 kg/s^2
c	Carreau exponent	0.65
K	time constant	0.01 s
U_{web}	web velocity	varies from 15-30 m/s
U_{inlet}	centerline velocity on inlet	varies from 2-5 m/s
q_{inlet}	inlet flowrate	varies from 4-7 l/s/m

Table 2: Geometry Parameters

L_{inlet}	inlet length	0.0025 m
L_{gap}	gap length	50 E-6 m
L_{ace}	applicator channel exit	0.5 mm
L_{thick}	blade thickness	1.25 mm
L_{blade}	blade length (modeled)	60.104 mm
L_{web}	web length (modeled)	59.551 mm
$<_{blade}$	angle of blade	45°
C_t	coating thickness	O(10 μm)
W_t	vertical distance from web to free surface at C-C	O(100 μm)

The problem can be defined in a dimensionless manner. The inlet cross-section length and web velocity are used as the length and velocity scales. Table 3 relates the dimensionless quantities to the parameters given in Tables 1 and 2.

Table 3: Dimensionless Quantities

Re	Reynolds Number	$Re = \frac{\rho U_{web} L_{in}}{\mu}$
Ca	Capillary Number	$Ca = \frac{\mu U_{web}}{\gamma}$
We	Weber Number	$We = \frac{1}{ReCa} = \frac{\gamma}{\rho U_{web}^2 L_{in}}$

The equations governing the flow in the coater are continuity and momentum

$$\nabla \bullet \vec{v} = u_{i,j} = 0 \qquad (1)$$

$$\rho\left[\frac{\partial u_i}{\partial t} + u_j u_{i,j}\right] = \sigma_{ij,j} + \rho f_i \qquad (2)$$

Here σ_{ij} denotes the stress tensor, is assumed to be of the form

$$\sigma_{ij} = -p\delta_{ij} + \tau_{ij}$$

Where τ_{ij} denotes the deviatoric stress tensor with the constitutive relation

$$\tau_{ij} = 2\mu\varepsilon_{ij}$$

Where ε_{ij} is the rate of strain tensor, given by

$$\varepsilon_{ij} = \frac{1}{2}\left(u_{i,j} + u_{j,i}\right)$$

The fluid for the current application is assumed to be shear thinning, the dynamic viscosity is approximated by the Carreau constitutive model

$$\mu = \mu_\infty + (\mu_o - \mu_\infty)\left[1 + K^2\varepsilon_{ij}\varepsilon_{ij}\right]^{(n-1)/2} \qquad (3)$$

where μ_o and μ_∞ denote the zero and infinite shear rate viscosities. The parameters in the Carreau model are determined based on the behavior of typical coating colors.

The above equations are non-dimensionalized using the velocity of the web and the width of the inlet channel as the velocity and length scales respectively

$$U_s = U_{web}, \quad L_s = L_{inlet}$$

The velocity and pressure are scaled using the velocity and dynamic pressure scales

$$u_i^* = \frac{u_i}{U_s}, \quad p^* = \frac{p}{\rho U_s^2}$$

The superscript * denotes dimensionless variable. The independent variables, position and time, are scaled using the velocity and length scales

$$x_i^* = \frac{x_i}{L_s}, \quad t^* = t\frac{U_s}{L_s}$$

The body force f_i is non-dimensionalized

$$f_i^* = f_i \frac{L_s}{U_s^2}$$

The continuity, momentum, and constitutive relations can respectively be expressed in dimensionless form as

$$u^*_{i,j^*} = 0, \tag{4}$$

$$\left[\frac{\partial u^*_i}{\partial t^*} + u^*_j u^*_{i,j^*}\right] = \sigma^*_{ij,j^*} + f^*_i, \tag{5}$$

and

$$\frac{1}{Re} = \frac{1}{Re_\infty} + \left(\frac{1}{Re_o} - \frac{1}{Re_\infty}\right)\left[1 + K^{*2}\varepsilon^*_{ij}\varepsilon^*_{ij}\right]^{(c-1)/2} \tag{6}$$

where

$$\sigma^*_{ij} = -p^*\delta_{ij} + \tau^*_{ij}$$

$$\tau^*_{ij} = 2\varepsilon^*_{ij}\frac{\mu}{\rho U_s L_s} = 2\varepsilon^*_{ij}\frac{1}{Re}$$

$$\varepsilon^*_{ij} = \frac{1}{2}\left(u^*_{i,j} + u^*_{j,i}\right)$$

$$K^* = K\frac{U_s}{L_s}$$

The Dirichlet boundary conditions for this coating system are specified as

$$u^*_i\big|_{\Gamma_1} = \frac{U_{inlet}}{U_s}, \qquad \Gamma_1 \Rightarrow \text{inlet}$$

$$u^*_i\big|_{\Gamma_2} = \frac{U_{web}}{U_s} = 1 \qquad \Gamma_2 \Rightarrow \text{web}$$

$$u^*_i\big|_{\Gamma_3} = u^*_i\big|_{\Gamma_3} = 0 \qquad \Gamma_3 \Rightarrow \text{applicator channel, } \Gamma_4 \Rightarrow \text{blade}$$

Neumann conditions are applied at the outflow boundaries

$$\sigma^*_n\big|_{\Gamma_5} = \sigma^*_n\big|_{\Gamma_6} = 0 \qquad \Gamma_5 \Rightarrow \text{exit, } \Gamma_6 \Rightarrow \text{gap exit}$$

On the free surfaces (Γ_7 and Γ_8) the kinematic condition is given by

$$\frac{d\eta^*}{dt^*} = \frac{\partial \eta^*}{\partial t^*} + \frac{\partial \eta^*}{\partial x^*_i}u^*_i$$

When the flow is independent of time this condition reduces to

$$u_i^* n_i = 0 \tag{7}$$

where n_i is the unit vector normal to the surface.

The dynamic boundary condition requires the stress to be continuous across the interface, therefore the normal and tangential stresses are respectively given by

$$\sigma_n = 2\gamma H - p_a$$

$$\sigma_t = \hat{t}_i \frac{\partial \gamma}{\partial x_i}$$

The fluid surface tension, γ, is constant, therefore the tangential component of the traction vector is zero. The above dynamic boundary condition is non-dimensionalized by

$$\sigma_n^* = \frac{2H^*}{ReCa} - p_a^* = \frac{2H^*}{We} - p_a^*$$

$$\sigma_t^* = 0$$

The above non-dimensional equations (4) and (5) with the constitutive relation (6) and appropriate boundary conditions completely describe the flow field. The finite element method is employed via FIDAP to solve for the velocity and pressure at discrete points within the domain. The unknown boundary location is determined in a fully coupled manner by simultaneously requiring the condition (7) be satisfied on the free surfaces.

The governing equations, constitutive relation, and boundary conditions completely define the given blade coating problem. The domain is discretized using 9-noded, isoparametric, quadrilateral elements. The velocity is approximated over the element using biquadtratic basis functions and the pressure with bilinear basis functions. The free surface boundary is determined by satisfying the steady state kinematic and dynamic conditions in a fully coupled manner.

The nonlinearity of the governing equations requires an iterative solution approach. The stokes flow in the fixed domain provides an initial guess for the Newton-Raphson iteration procedure. Parameter continuation methods are used to assist in the variation of the parameters to reach the desired solution for given boundary conditions. Convergence is achieved when the norm of the solution change in between iterations is less than 10^{-3}.

The resulting coater configurations and streamlines are shown in Figures 3 and 4 for the cases listed in Table 4. A noticeable change in the free surface location is apparent as the flowrate is varied. An increase in flowrate results in a larger vertical cross-section under the web, a decrease in exit cross-section width on Γ_5, and an increase in the exit velocity magnitude on the same boundary.

The desire to avoid recirculating flow and minimize surface defects leads us to examine closely three regions where flow separation and recirculation is possible; the meniscus just aft of the applicator channel, the corner where the blade and web converge to construct the gap, and the blade tip where a meniscus forms and the substrate is coated. The mesh,

streamlines, and pressure contours are plotted for these three regions in Figures 5-14. As demonstrated in these figures, the results show no flow separation or flow recirculation. A true vortex-free coating flow system exists at low flow rates (4 l/s/m) and high coating speeds (20 m/s).

The velocity profiles in the gap region provide insight into the coating quality. Figure 15 shows the horizontal, non-dimensional velocity profile at a location A-A on the blade tip while Figure 16 depicts the profile at location B-B, the endpoint of the blade tip. At the static contact line it is clear that the formation of the meniscus slightly affects the velocity profile. The apparently linear pressure distribution along the blade tip, Figure 20, indicates an almost constant pressure gradient in the gap that increases with the flowrate. These velocity profiles and pressure distribution demonstrate a nearly Poiseuille-Couette velocity distribution, the linear combination of flow between two walls at a relative velocity to one another and flow between stationary walls with a constant pressure gradient. Thus, the coating flowrate and thickness increase slightly with the increase in the inlet flowrate due to the larger pressure gradient, see Figures 21 and 22. The portion of the coater where the blade and web form a converging channel is much more affected by the flowrate variation.

Examination of the corner region formed by web and blade, presented in Figure 8, shows significant free surface shape variation with flowrate variation. As the flowrate is decreased the free surface migrates toward the gap threatening to entirely disappear into the gap with further reduction of the inlet flowrate. The corresponding streamlines are shown in Figure 9.

The pressure along the blade and substrate are shown in Figures 18 and 19, all graphed quantities are non-dimensionalized. Table 6 can be used to convert all variables to dimensional quantities. Away from the gap the pressure remains fairly constant. Within the gap region the pressure peaks at the leading edge of the blade, just upstream of the gap. The maximum pressure increases as flowrate increases. At higher flowrates, the pressure increases in a more gradual manner, exhibiting a more distinct plateau. Following the peak, the flow field experiences sub-ambient pressures and then adjusts to the ambient exit pressure. The pressure contours in the gap region, shown in Figure 11, indicate that a decrease in flowrate causes a larger pressure gradient but decreases the value of the maximum pressure.

Table 5 gives results for the variation of the web speed for two flowrates; 6 and 7 l/s/m. The resulting domain and streamlines are plotted in Figures 24, 25, 42, & 43. Again we look at the formation of the meniscus and the turning flow, Figures 26-35 and 44-53 show the mesh, streamlines, and pressure fields in these regions.

The increase in web speed is effectively an increase in the two non-dimensional parameters characterizing the flow, the Reynolds Number and the Capillary Number. Let us consider the pressure distribution along the blade and the web presented in Figures 39, 57, 40, and 58 respectively. Here we find that as the inertial effects are magnified, the pressure gradient increases while the maximum pressure decreases. Along the web, a gradual pressure adjustment followed by a sharp pressure peak is observed at lower Reynolds Numbers. The effects of increase in web speed appear to have a qualitative relation to the effects of decreasing the flowrate.

A nearly Poiseuille-Couette velocity profile is again present in the gap region. Increasing web speed forces a greater amount of fluid to exit the gap through viscous shear and the nearly constant pressure gradient. Coating thickness increase is observed with an increase of web speed, as shown in Figures 60-62.

The results of the present analysis exhibit qualitative agreement with those of Pranckh & Scriven (1988). The graphical flow solution in the present study, Figures 8-14, should be compared to those of Pranckh & Scriven (P&S) See Figure 3† for the velocity field, streamlines, and pressure contours of their base case, Table 1†.

P&S looked at the pressure distribution along the substrate for their base case and another case where both the Reynolds Number and flowrate were increased, see Figure 5† and Figure 8†. In their base case they found the pressure distribution had an inflection point, or plateau, followed by a peak just prior to the leading edge of the blade. They found increasing the Reynolds Number and flowrate decreased the maximum pressure and eliminated the pressure plateau. In the present study, we similarly find that the pressure profile along the substrate has a peak just prior to the gap. The slope of the pressure plateau and the dimensionless pressure peak were also found to decrease with increasing Reynolds Number.

The effects of changing the parameters in their base case, including the Reynolds Number, Capillary Number, and flowrate were computed by P&S, see Figure 6†. The present study also investigated the effects of the variation of the web speed (or $Re|_{q=const}$ and $Ca|_{q=const}$) and flowrate ($q|_{Uweb=const}$) on the coating thickness, see Figures 60-62. Similar to P&S, we find that the coating thickness varies nearly linearly with the increase in Reynolds Number, Capillary Number, and flowrate.

† Pranckh, F.R., and Scriven, L.E., "The Physics of Blade Coating of Deformable Substrate," 1988 Coating Conference Proc., TAPPI Press, Atlanta, GA, 1988.

Table 4: Case Study - Effect of Flowrate Variation

Case	U_{web}	U_{inlet}	q_{inlet}	q_{film}	q_{exit}	C_t	W_t	Re	Ca	We
	m/s	m/s	l/s/m	l/s/m	l/s/m	µm	µm			1/ReCa
C4V20	20	2.4	4	.5481175	3.61508	27.465	208.4447	60	400	1/24000
C5V20	20	3	5	.550354	4.611883	27.575	259.0522	60	400	1/24000
C6V20	20	3.6	6	.552128	5.60895	27.66575	309.472	60	400	1/24000
C7V20	20	4.2	7	.553462	6.52	27.7325	354.6727	60	400	1/24000

Table 5: Case Study - Effect of Web Speed Variation

Case	U_{web} m/s	U_p m/s	q_{inlet} l/s/m	q_{film} l/s/m	C_t µm	Re	Ca	We 1/ReCa
C6V15	15	3.6	6	0.409921	27.42438	45	300	1/13500
C6V20	20	3.6	6	0.552128	27.66575	60	400	1/24000
C6V25	25	3.6	6	0.695813	27.873	75	500	1/37500
C6V30	30	3.6	6	0.841083	28.0655	90	600	1/54000
C7V15	15	4.2	7	0.410793	27.48275	45	300	1/13500
C7V20	20	4.2	7	0.553462	27.7325	60	400	1/24000
C7V25	25	4.2	7	0.698024	27.9615	75	500	1/37500
C7V30	30	4.2	7	0.844202	28.1695	90	600	1/54000

Table 6: Conversion to Dimensional Units

dimensionless quantity	scale	web speed	multiply by	dimensional units
p^*	$\rho U_s^2 = \rho U^2_{web}$	15 m/s	0.270 E+6	Pa
p^*	$\rho U_s^2 = \rho U^2_{web}$	20 m/s	0.480 E+6	Pa
p^*	$\rho U_s^2 = \rho U^2_{web}$	25 m/s	0.750 E+6	Pa
p^*	$\rho U_s^2 = \rho U^2_{web}$	30 m/s	1.080 E+6	Pa
q^*	$U_s L_s = U_{web} L_{inlet}$	15 m/s	37.5	l/s/m
q^*	$U_s L_s = U_{web} L_{inlet}$	20 m/s	50.0	l/s/m
q^*	$U_s L_s = U_{web} L_{inlet}$	25 m/s	62.5	l/s/m
q^*	$U_s L_s = U_{web} L_{inlet}$	30 m/s	75.0	l/s/m
u_i^*	$U_s = U_{web}$	15 m/s	15	m/s
u_i^*	$U_s = U_{web}$	20 m/s	20	m/s
u_i^*	$U_s = U_{web}$	25 m/s	25	m/s
u_i^*	$U_s = U_{web}$	30 m/s	30	m/s
x_i^*	$L_s = L_{inlet}$	all	0.0025	m

References

Aidun, C.K., "Principles of Hydrodynamic Instability In Coating Systems," *Tappi J.*, Parts I, II, and III, TAPPI Press, Atlanta, GA, 1991.

Aidun, C.K., Progress report on Fundamentals of Coating to the Papermaking Project Advisory Committee, Institute of Paper Science and Technology, Spring 1994 and Spring 1995.

Aidun, C.K., and Kovacs, A., "A Vortex-Free Pressurized Pond Coating System", 1995 Coating Conference Proc., TAPPI Press, Atlanta, GA, 1995.

Eklund, D.E., "Review of Surface Application," Trans. of the Ninth Fund. Research Symp., ed. Baker and Punton, Mech. Eng. Pub., 1989.

Pranckh, F.R., and Scriven, L.E., "The Physics of Blade Coating of Deformable Substrate," 1988 Coating Conference Proc., TAPPI Press, Atlanta, GA, 1988.

Nomenclature

δ_{ij}	Kronecker delta
ε_{ij}	rate of strain tensor
γ	surface tension
Γ_i	boundary
η	height of free surface
μ	dynamic viscosity
μ_o	zero shear rate viscosity
μ_∞	infinite shear rate viscosity
ρ	density
σ_{ij}	stress tensor
σ_n	normal component of the traction vector
σ_t	tangential component of the traction vector
τ_{ij}	deviatoric stress tensor
Ca	Capillary Number
C_t	coating thickness
c	Carreau exponent
f_i	component of gravitational acceleration
H	Gaussian mean curvature of the free surface
K	time constant
L_{ace}	applicator channel exit
L_{blade}	blade length (modeled)
L_{gap}	gap length
L_{inlet}	inlet length
L_s	length scale

L_{thick}	blade thickness
L_{web}	web length (modeled)
l/s/m	(liter/sec)/meter
m/s	meter/sec
n_i	unit normal vector
p	pressure
p_a	ambient pressure
q_{exit}	flowrate exiting along blade
q_{film}	flowrate exiting gap
q_{inlet}	inlet flowrate
Re	Reynolds Number
S	singularity
t	time
$\hat{t}_i$	unit tangent vector
U_{inlet}	centerline velocity on inlet Poiseuille profile
U_s	length scale
U_{web}	web velocity
u_i	velocity
We	Weber Number
W_t	vertical distance from web to free surface at C-C
x_i	Cartesian coordinate
$<_{blade}$	angle of blade
*	superscript denotes dimensionless variable

List of Figures

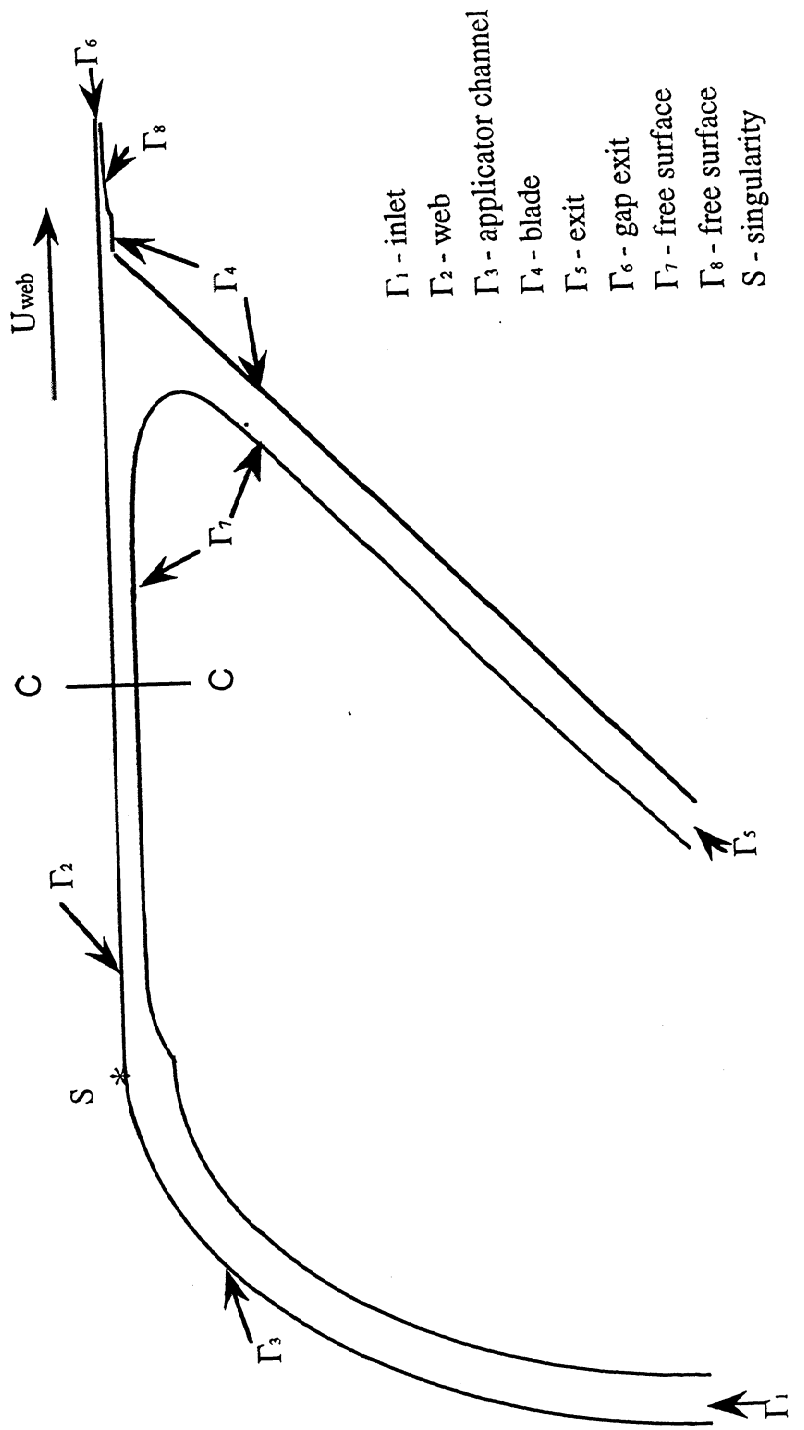
Γ1 - inlet
Γ2 - web
Γ3 - applicator channel
Γ4 - blade
Γ5 - exit
Γ6 - gap exit
Γ7 - free surface
Γ8 - free surface
S - singularity
Uweb
Γ1
Γ2
Γ3
Γ4
Γ5
Γ6
Γ7
Γ8
S
C
C

Figure 1

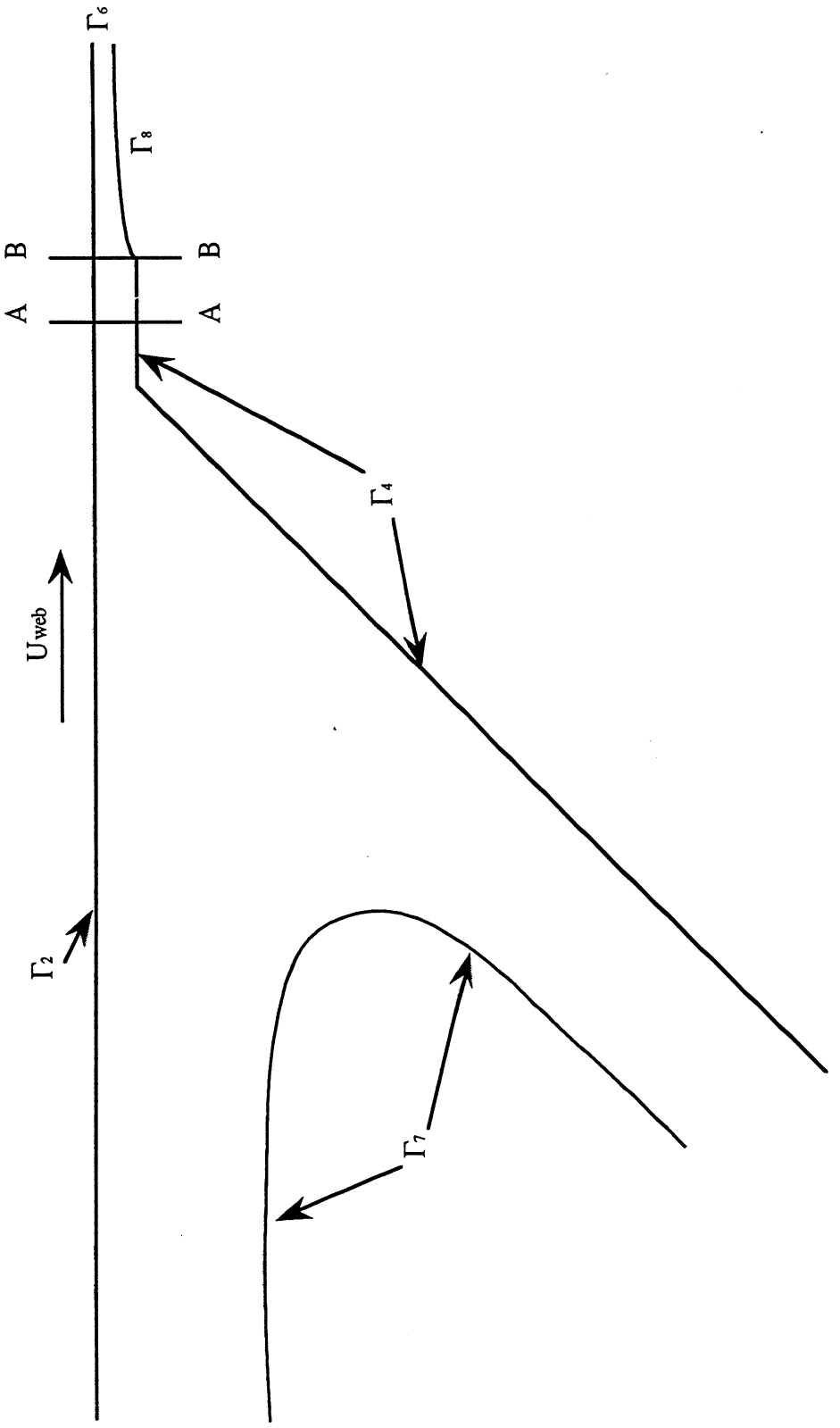

Figure 2

Figure 3

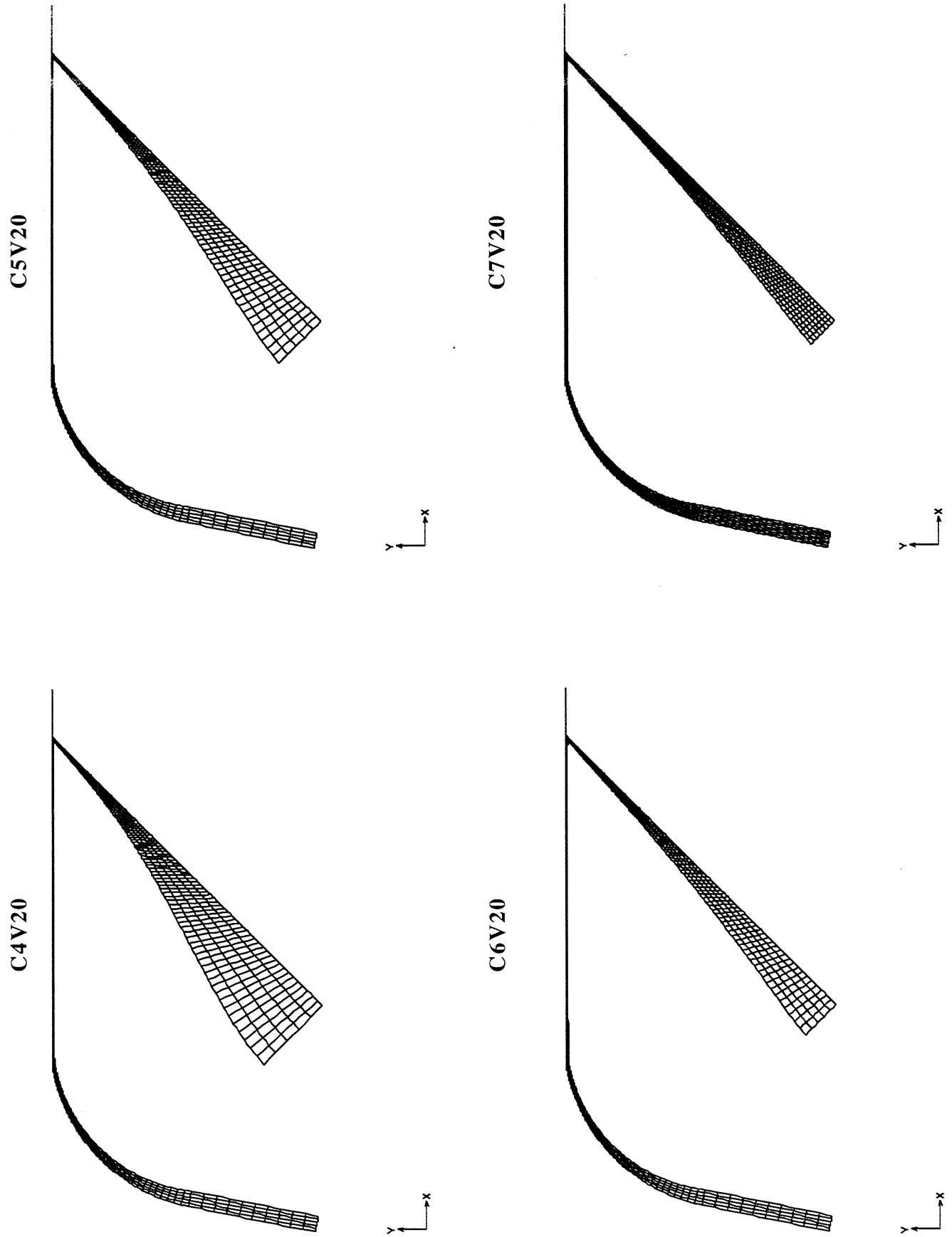

Figure 4

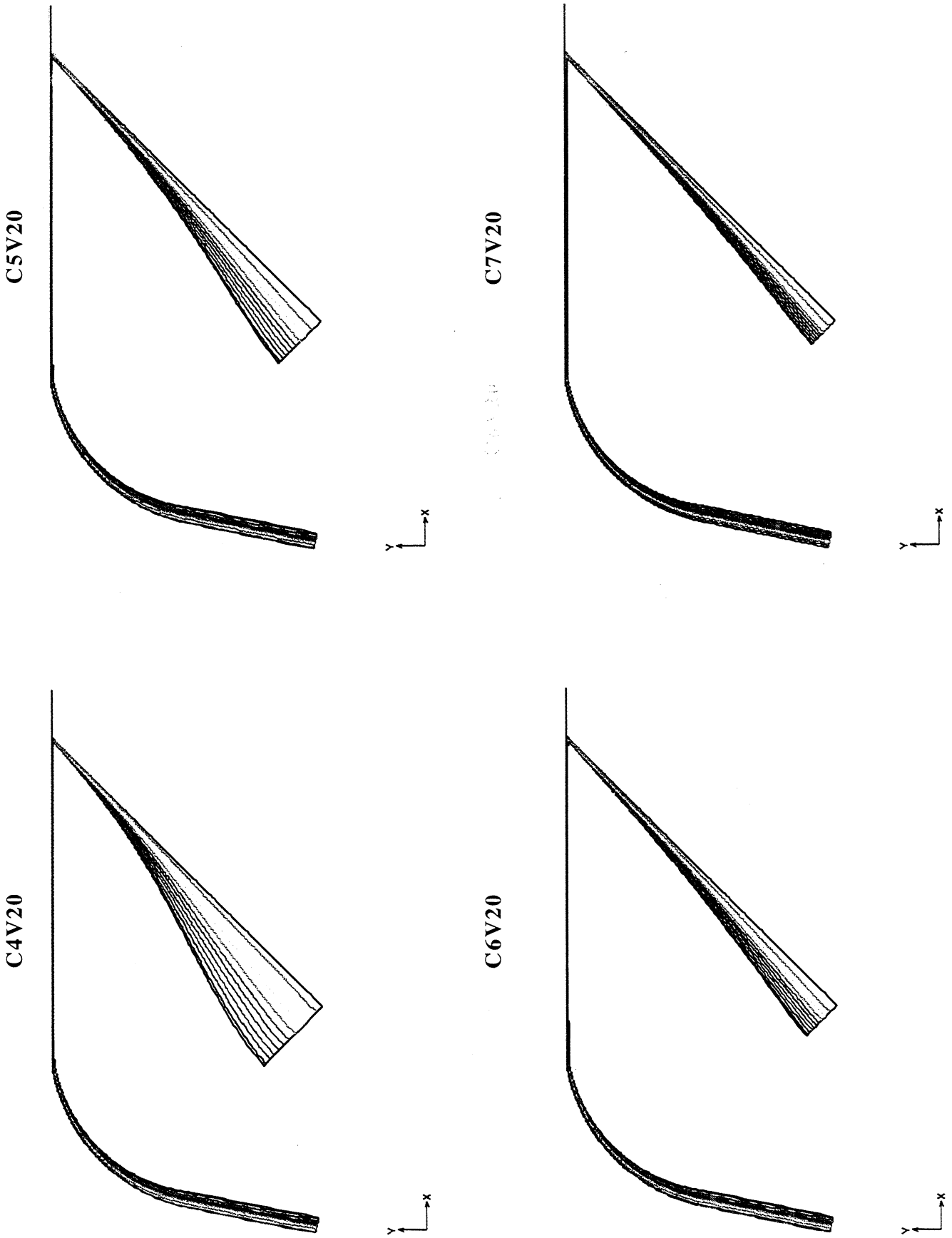

Figure 5

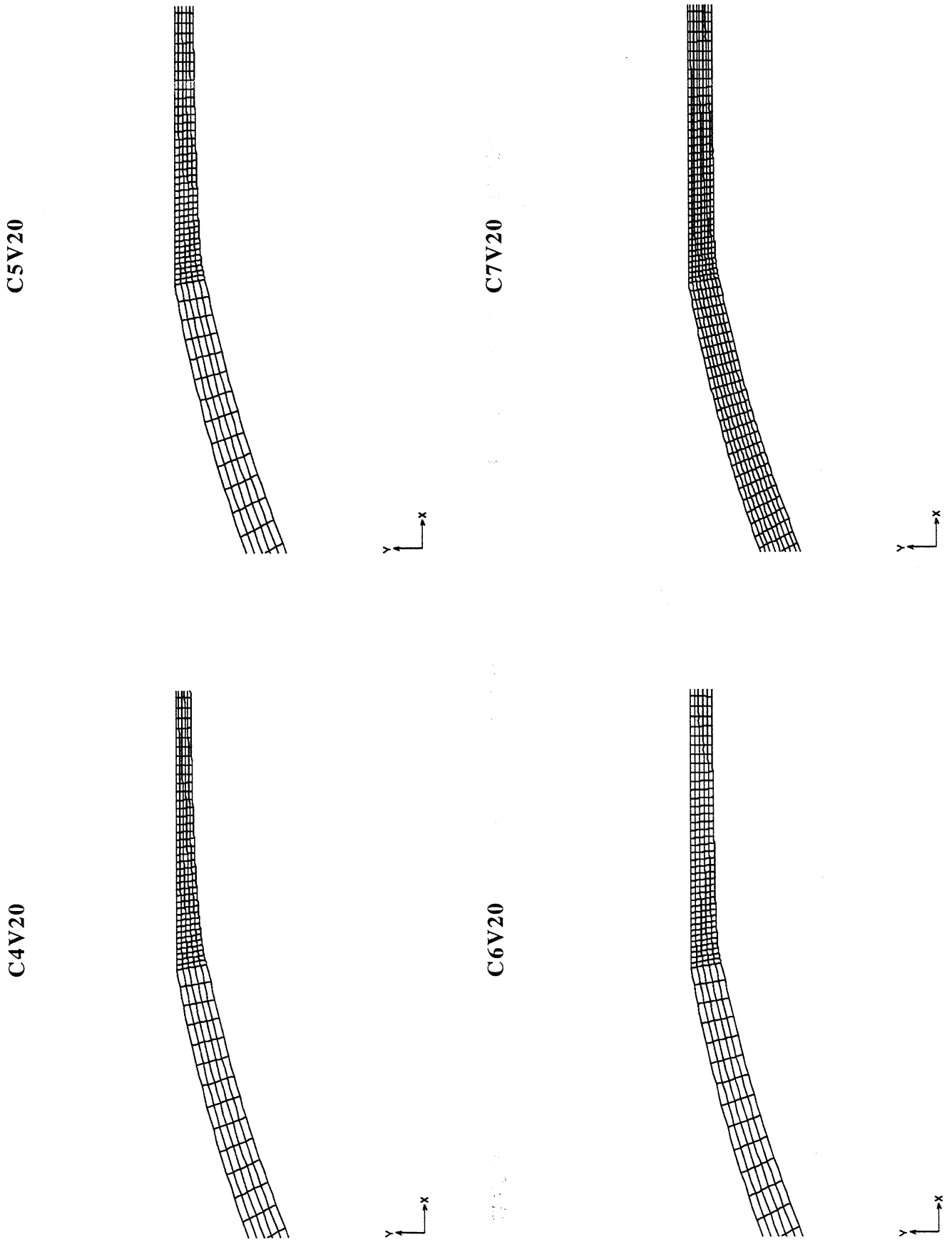

Figure 6

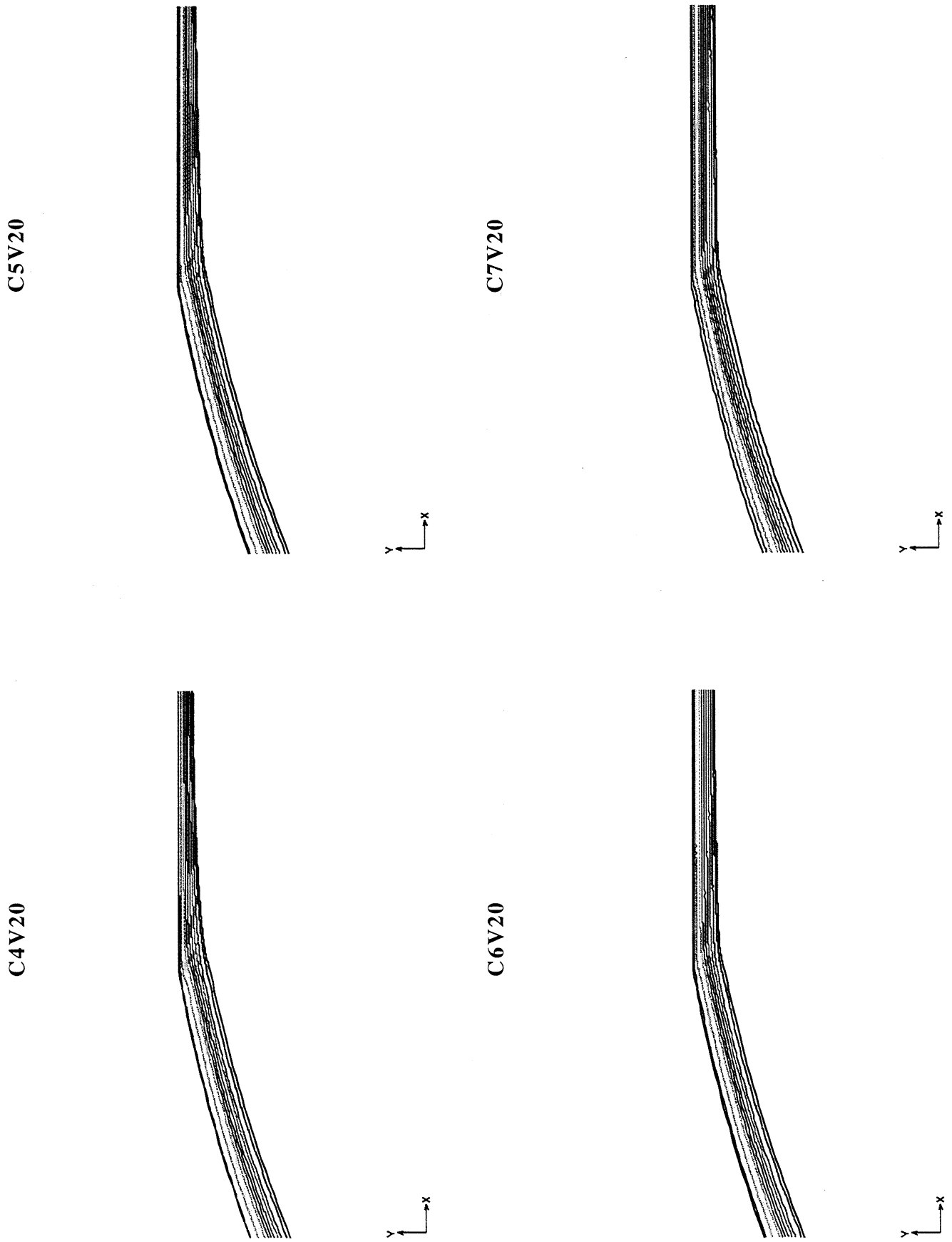

Figure 7

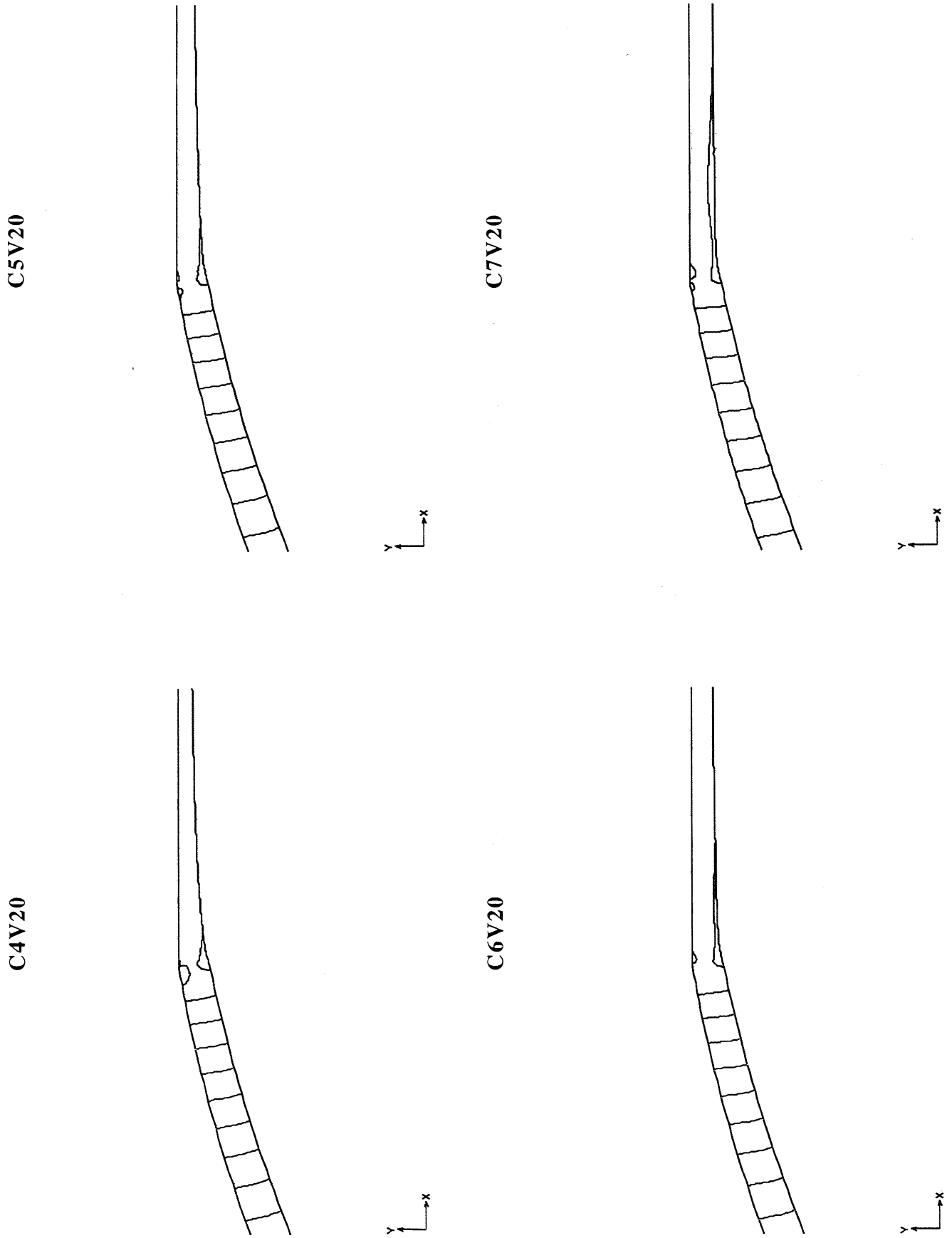

Figure 8

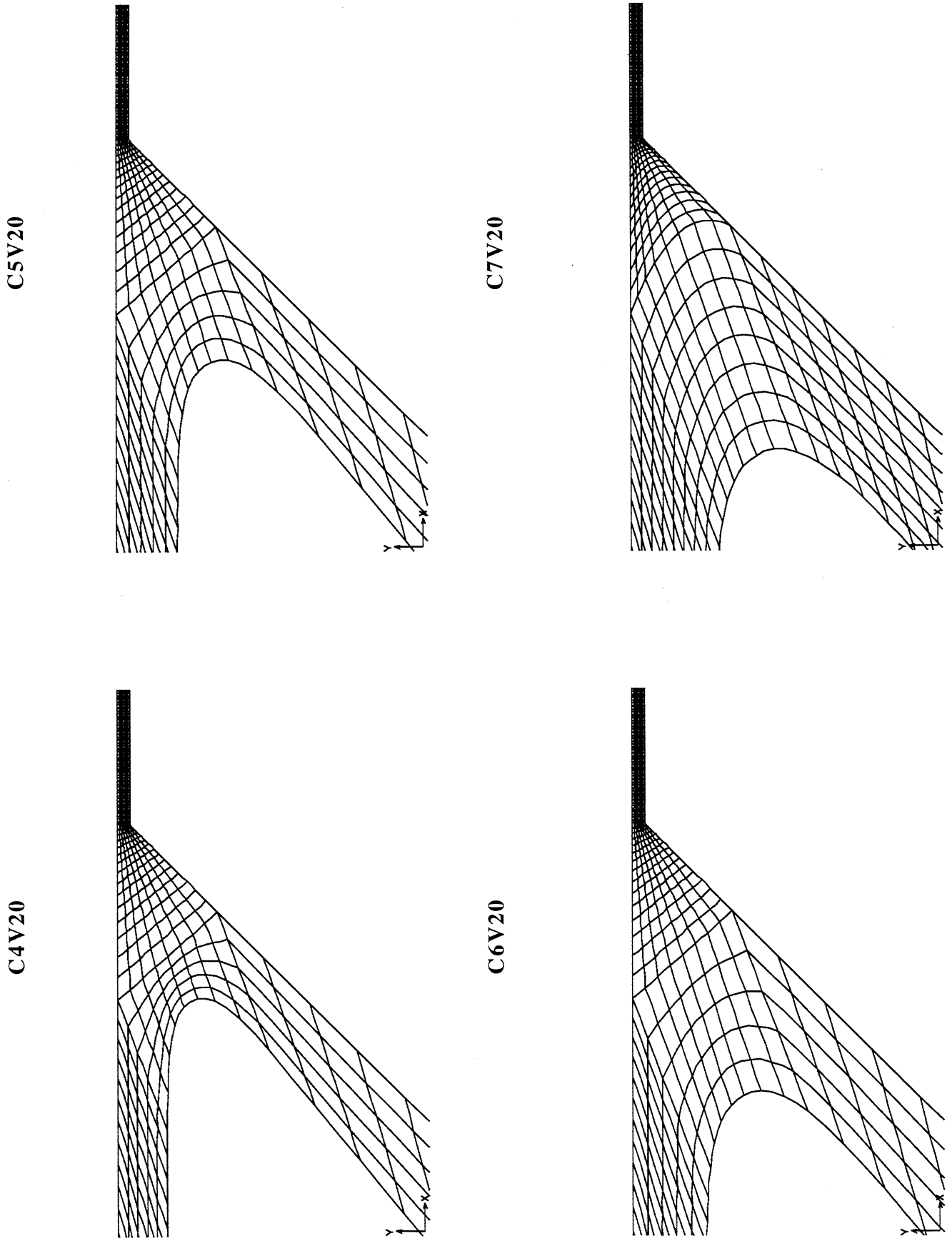

Figure 9

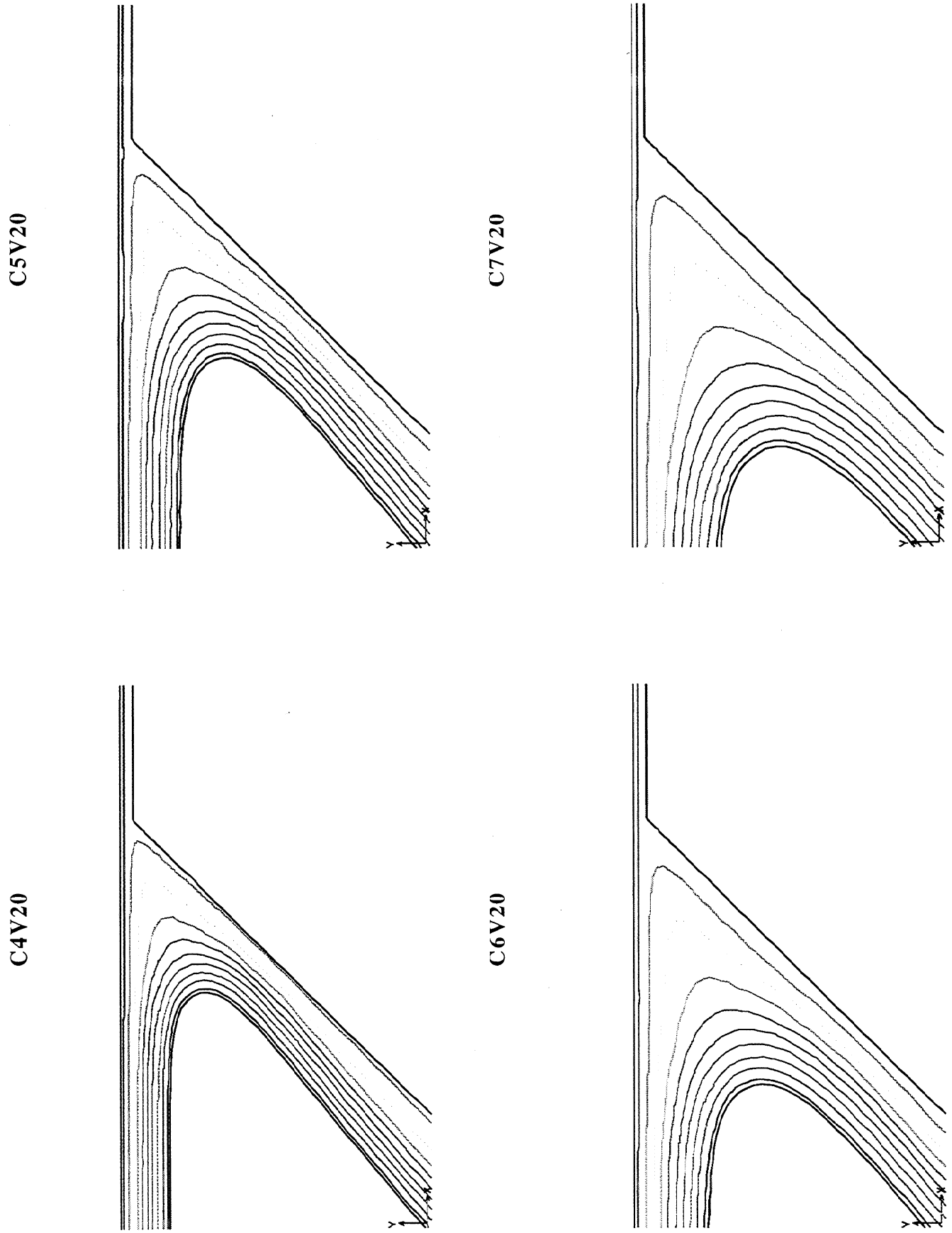

Figure 10

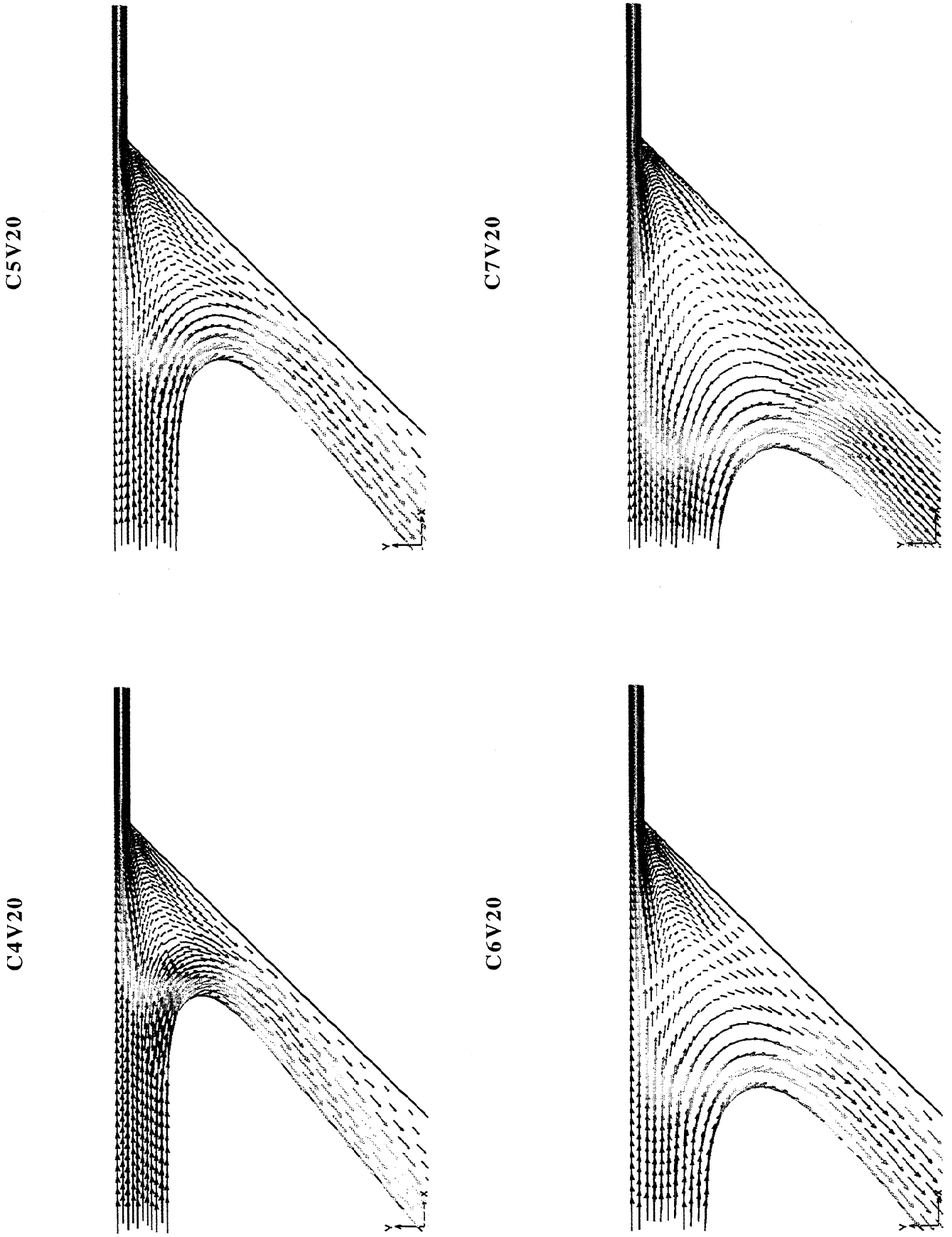

Figure 11

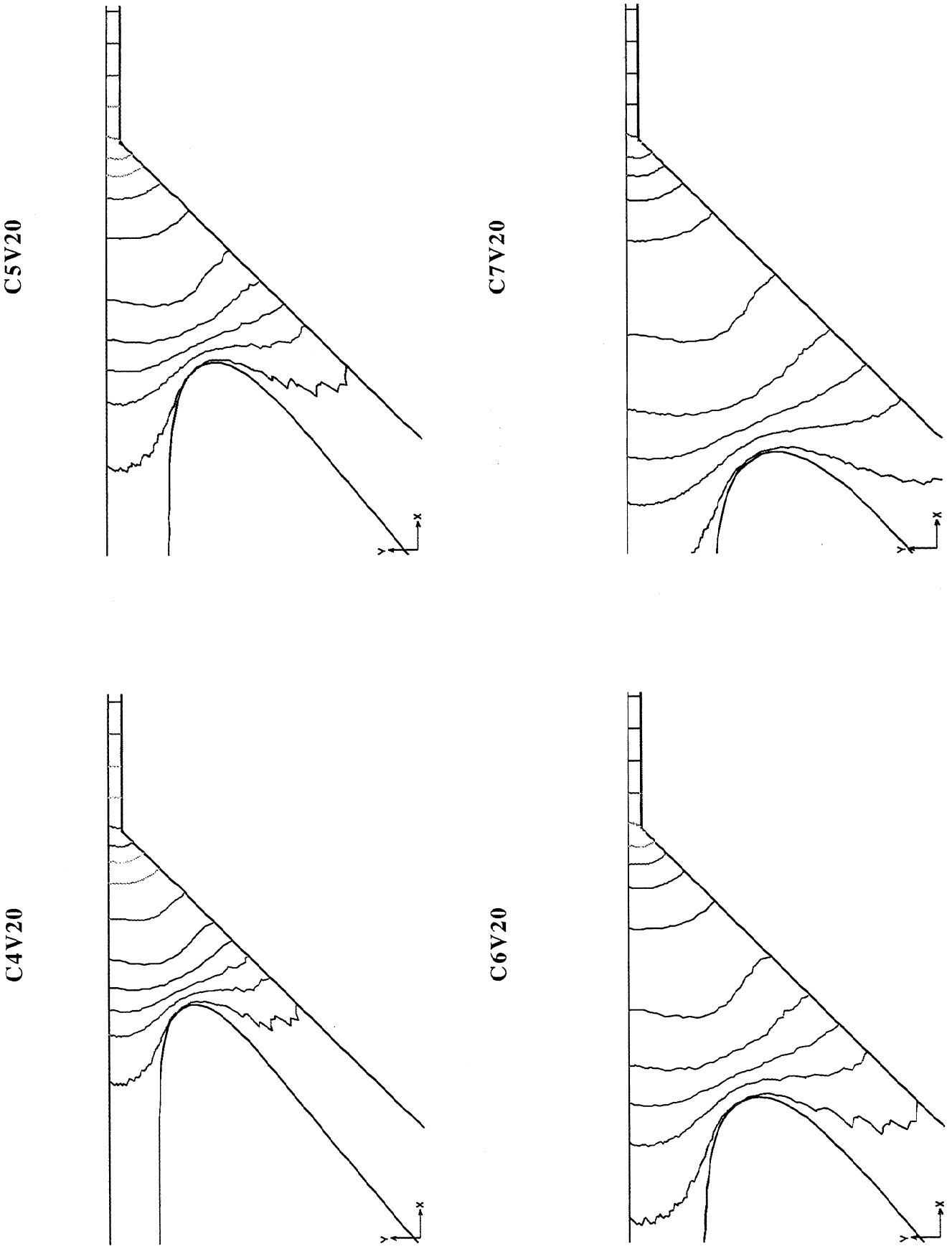

Figure 12

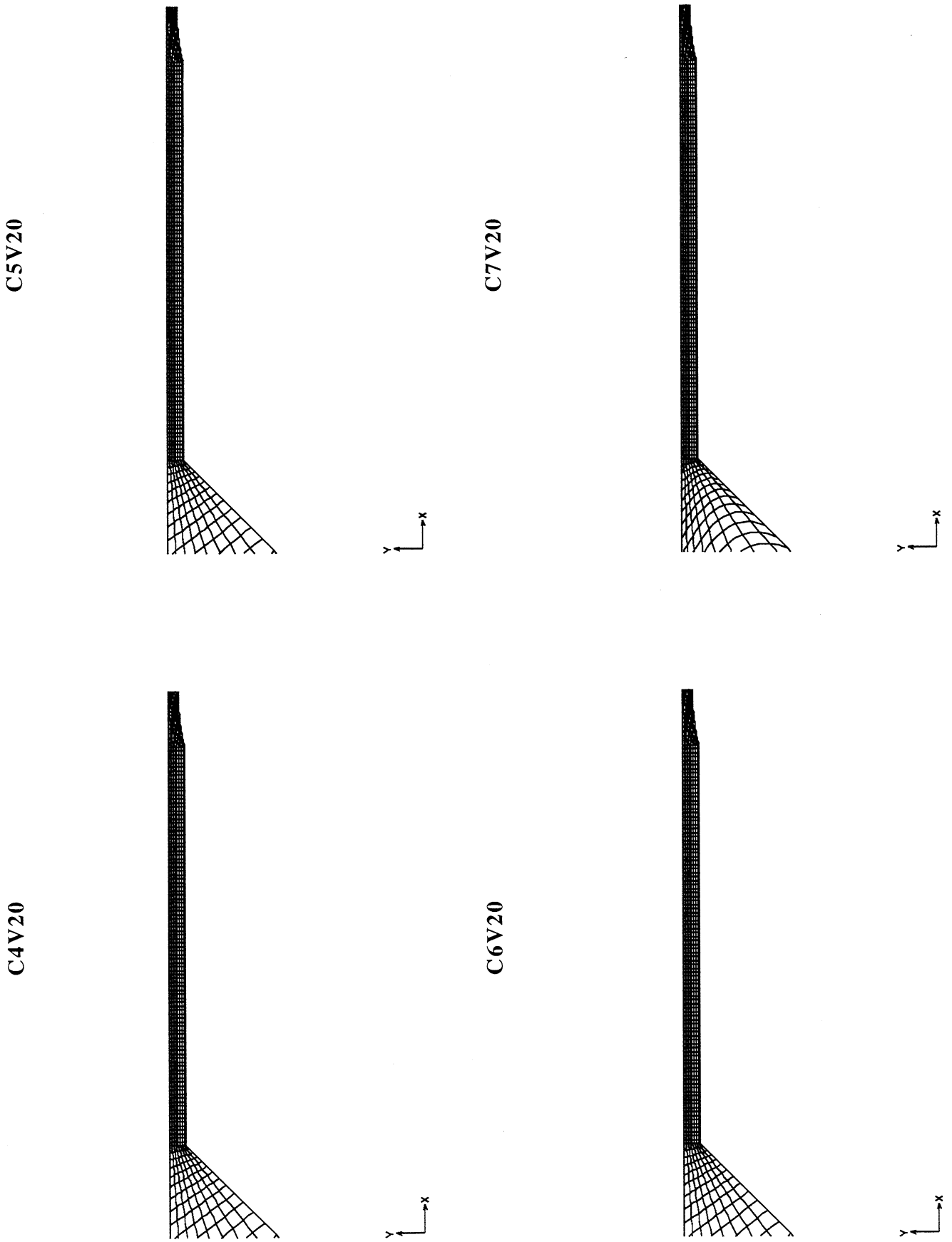

Figure 13

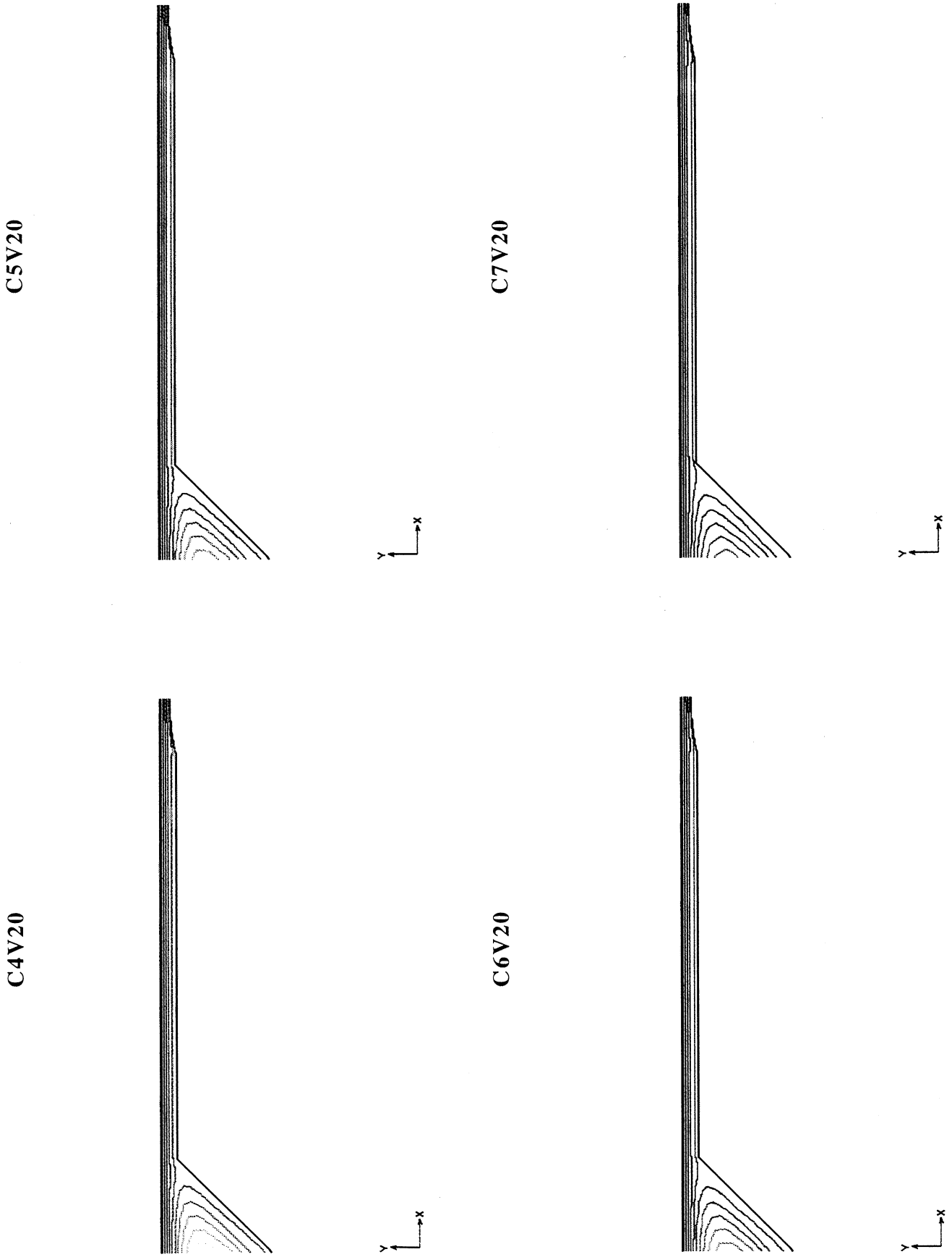

HAPID Sheet Strength

- STFI Compression strrength increased with platen temperature.
- Limit seems to have been reached.

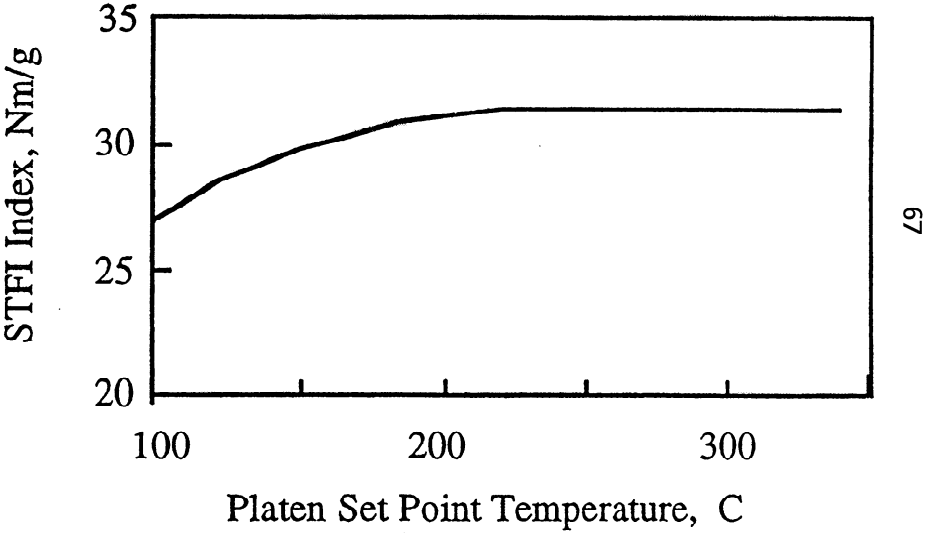

Figure 15

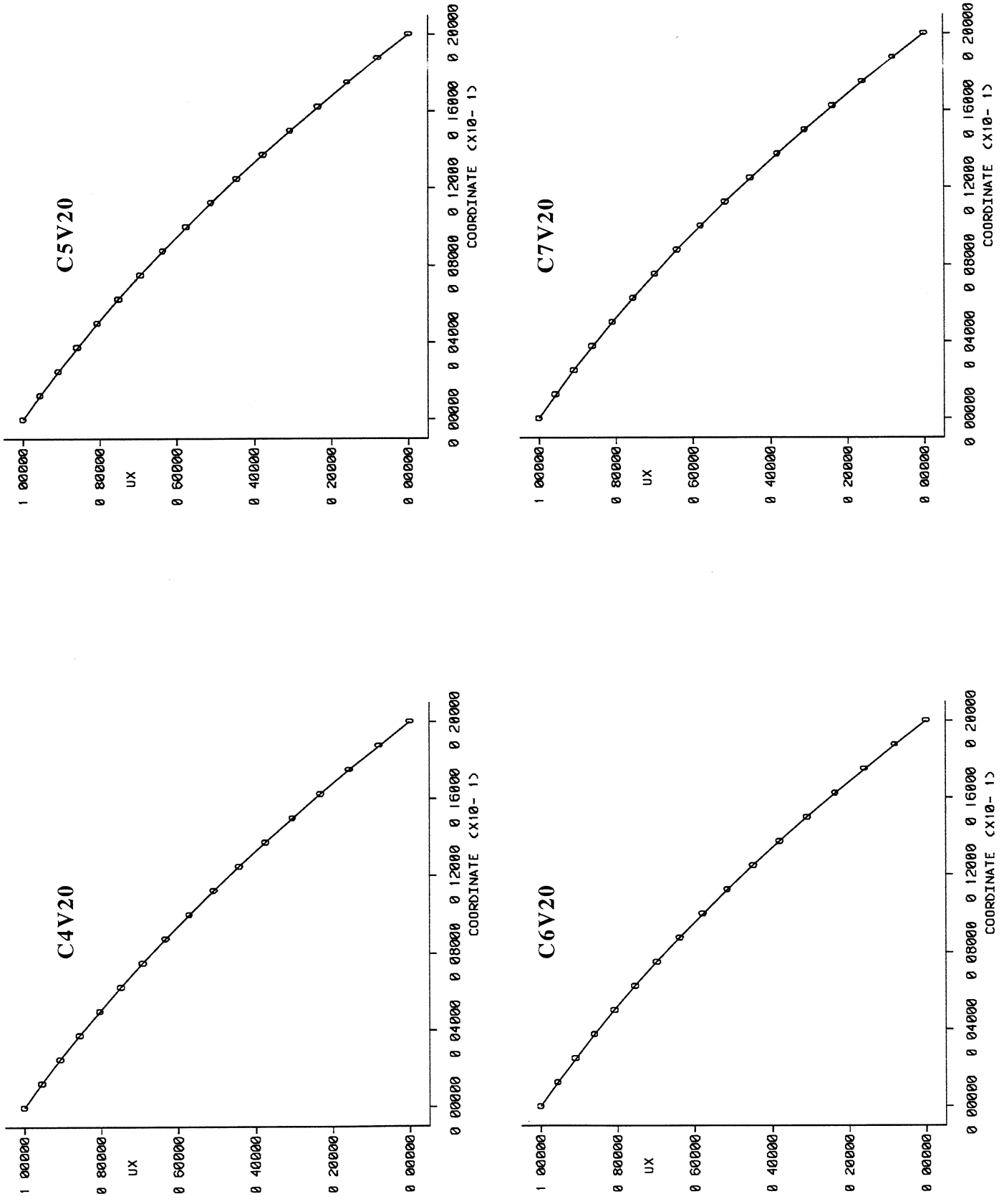
C4V20
C5V20
C6V20
C7V20
UX
COORDINATE (X10- 1)
1 00000
0 80000
0 60000
0 40000
0 20000
0 00000
0 00000
0 04000
0 08000
0 12000
0 16000
0 20000

Figure 16

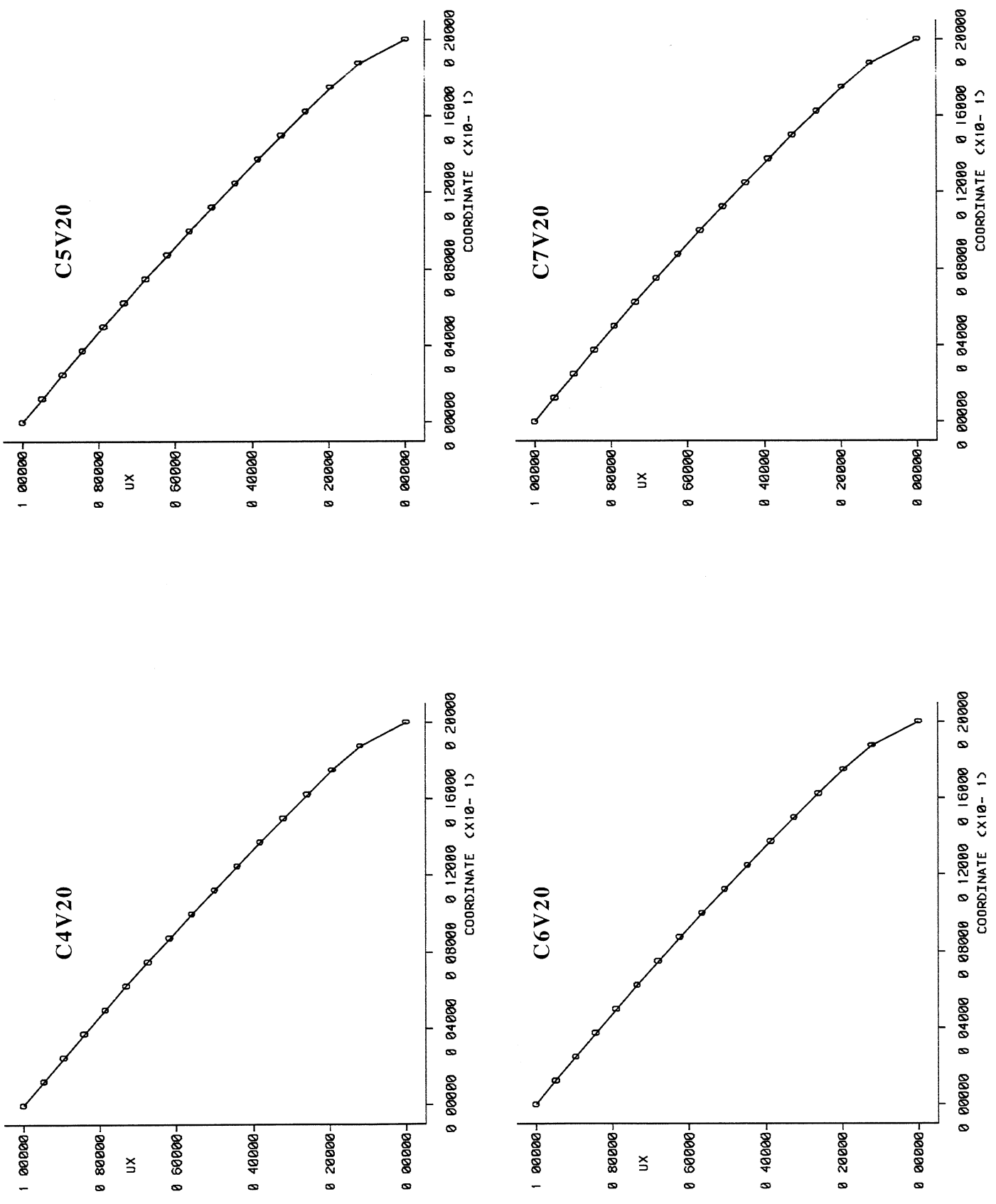
C5V20
C4V20
C7V20
C6V20
UX
COORDINATE (X10- 1)
1 00000
0 80000
0 60000
0 40000
0 20000
0 00000
0 00000
0 04000
0 08000
0 12000
0 16000
0 20000

Figure 17

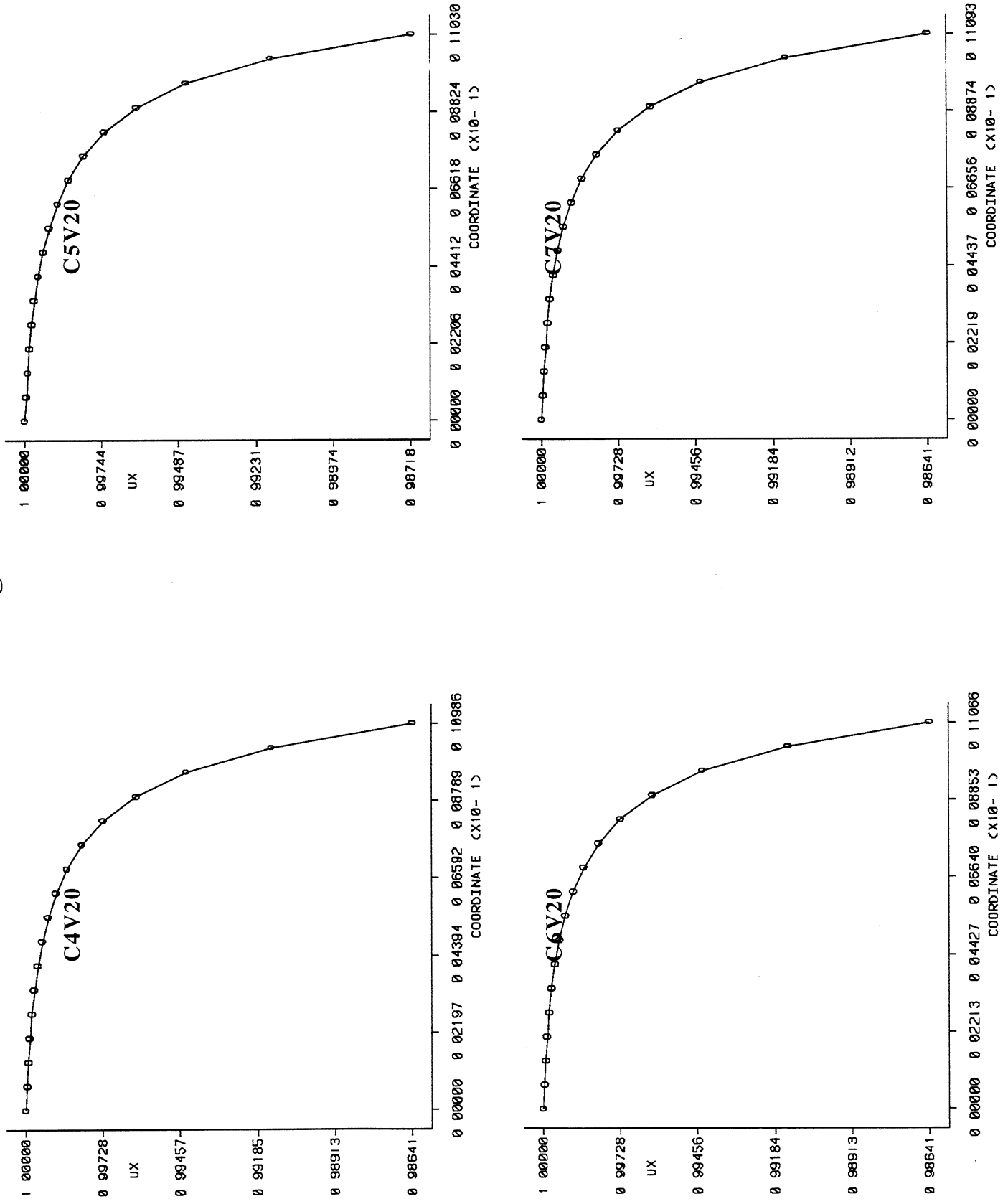
C5V20
C4V20
C7V20
C6V20
UX
COORDINATE (X10- 1)
1 00000
0 99744
0 99487
0 99231
0 98974
0 98718
0 99728
0 99457
0 99185
0 98913
0 98641
0 99456
0 99184
0 98912
0 00000
0 02206
0 04412
0 06618
0 08824
0 11030
0 02197
0 04394
0 06592
0 08789
0 10986
0 02219
0 04437
0 06656
0 08874
0 11093
0 02213
0 04427
0 06640
0 08853
0 11066

Figure 18

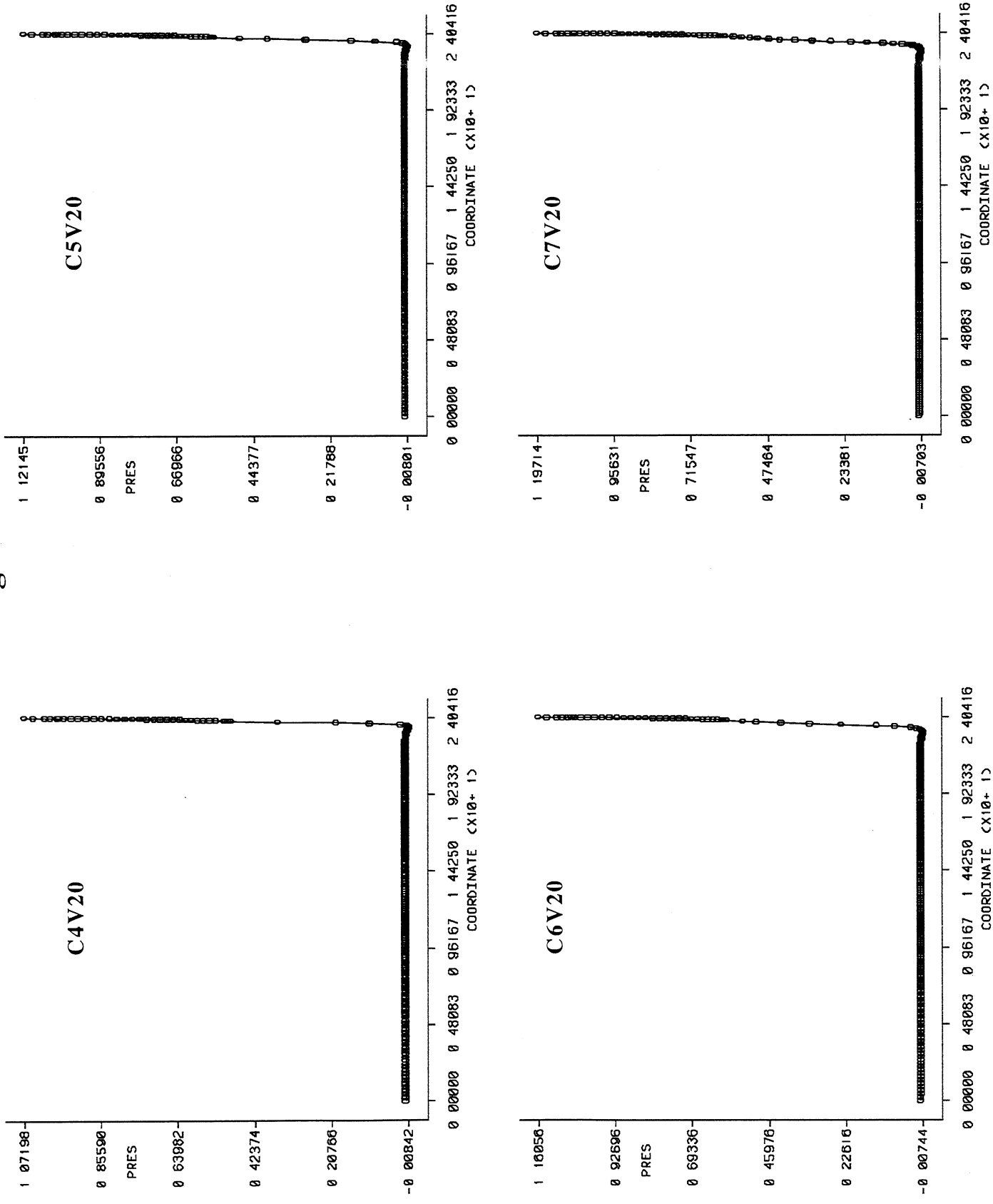

Figure 19

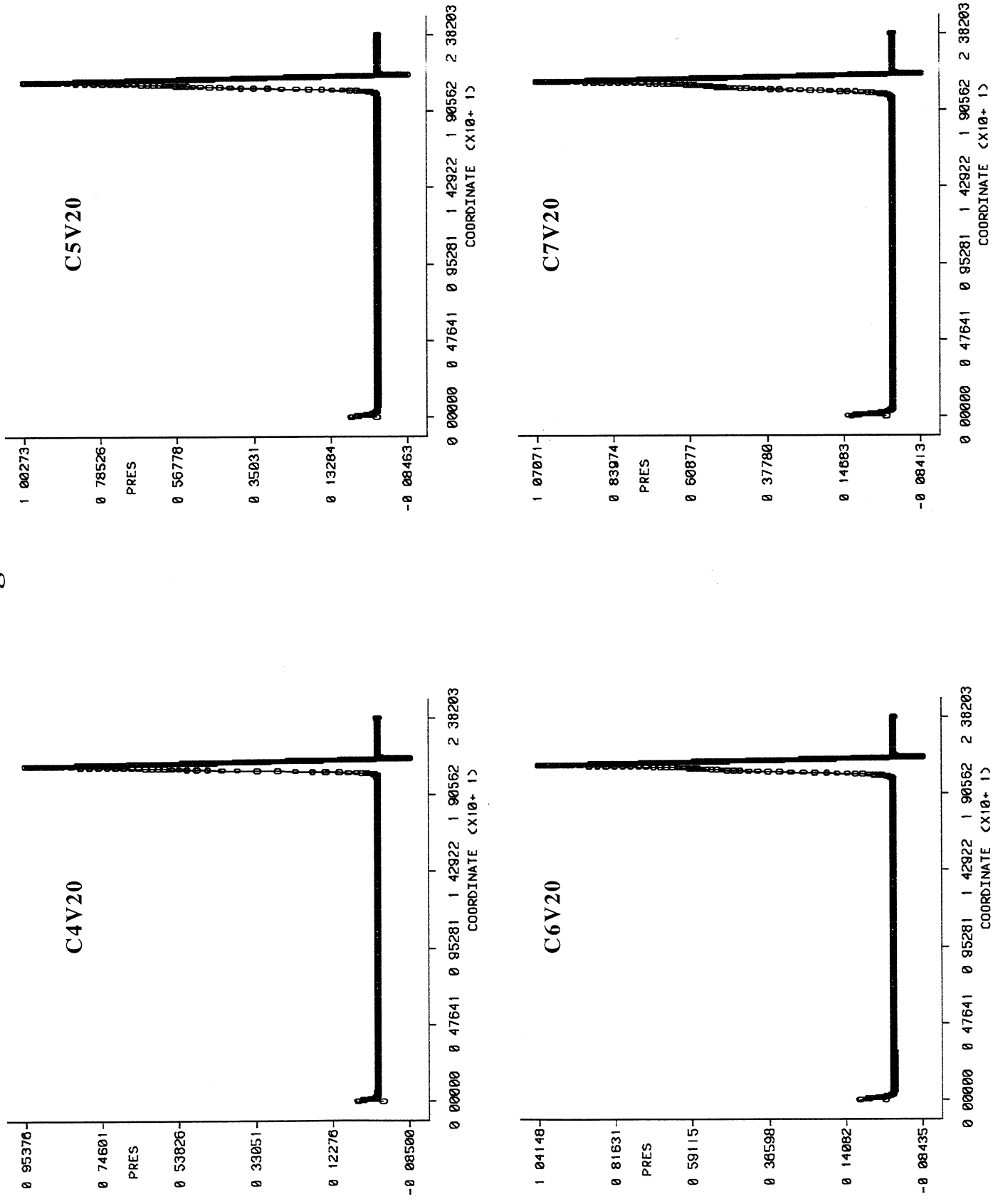
C5V20
C4V20
C7V20
C6V20
PRES
COORDINATE (X10+ 1)
1 00273
0 78526
0 56778
0 35031
0 13284
-0 08463
0 95376
0 74601
0 53826
0 33051
0 12276
-0 08500
1 07071
0 83974
0 60877
0 37780
0 14683
-0 08413
1 04148
0 81631
0 59115
0 36598
0 14082
-0 08435
0 00000
0 47641
0 95281
1 42922
1 90562
2 38203

Figure 20

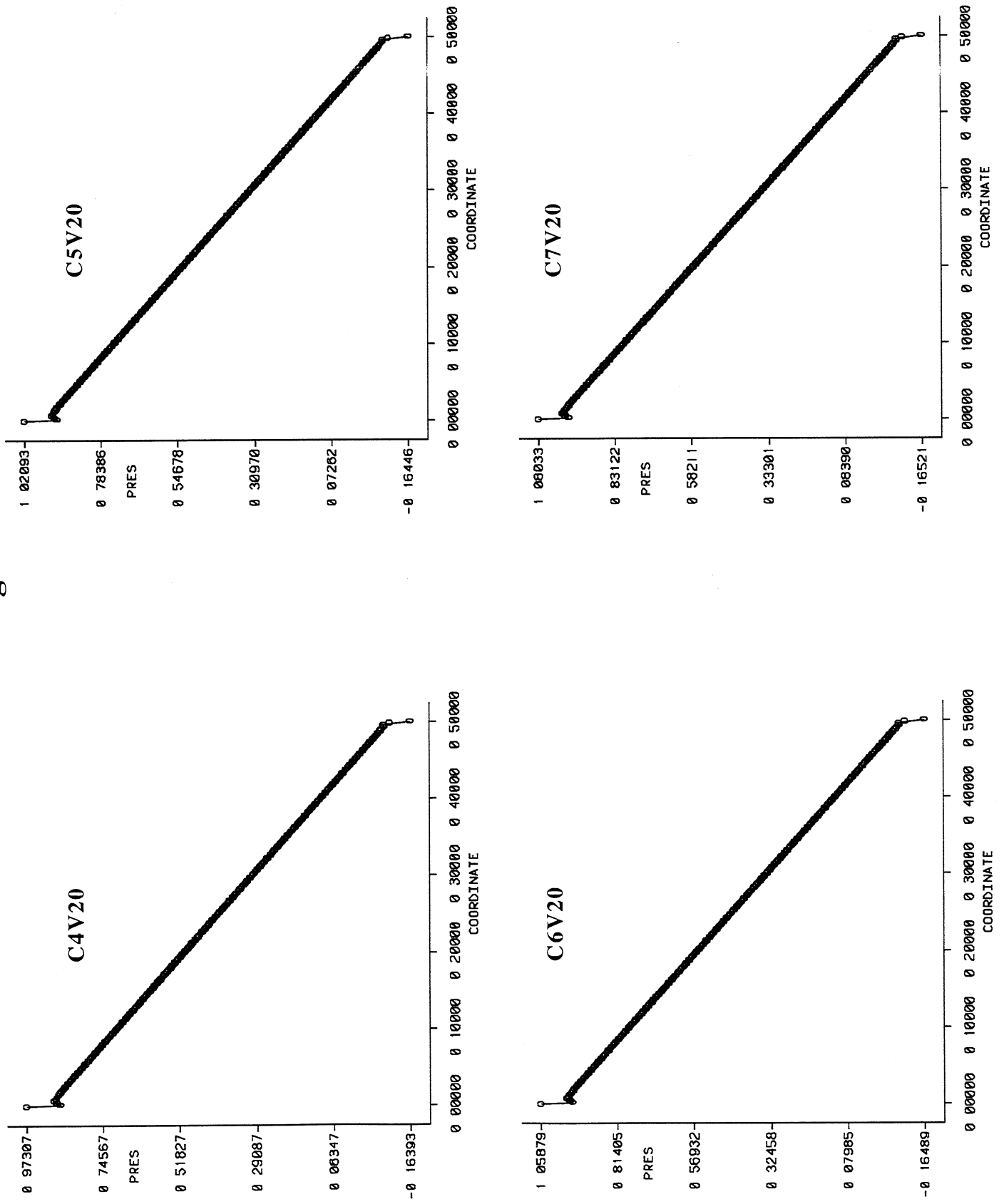
C4V20
C5V20
C6V20
C7V20
PRES
COORDINATE
0 97307
0 74567
0 51827
0 29087
0 06347
-0 16393
1 02093
0 78386
0 54678
0 30970
0 07262
-0 16446
1 05879
0 81405
0 56932
0 32458
0 07985
-0 16489
1 08033
0 83122
0 58211
0 33301
0 08390
-0 16521
0 00000
0 10000
0 20000
0 30000
0 40000
0 50000

Figure 21

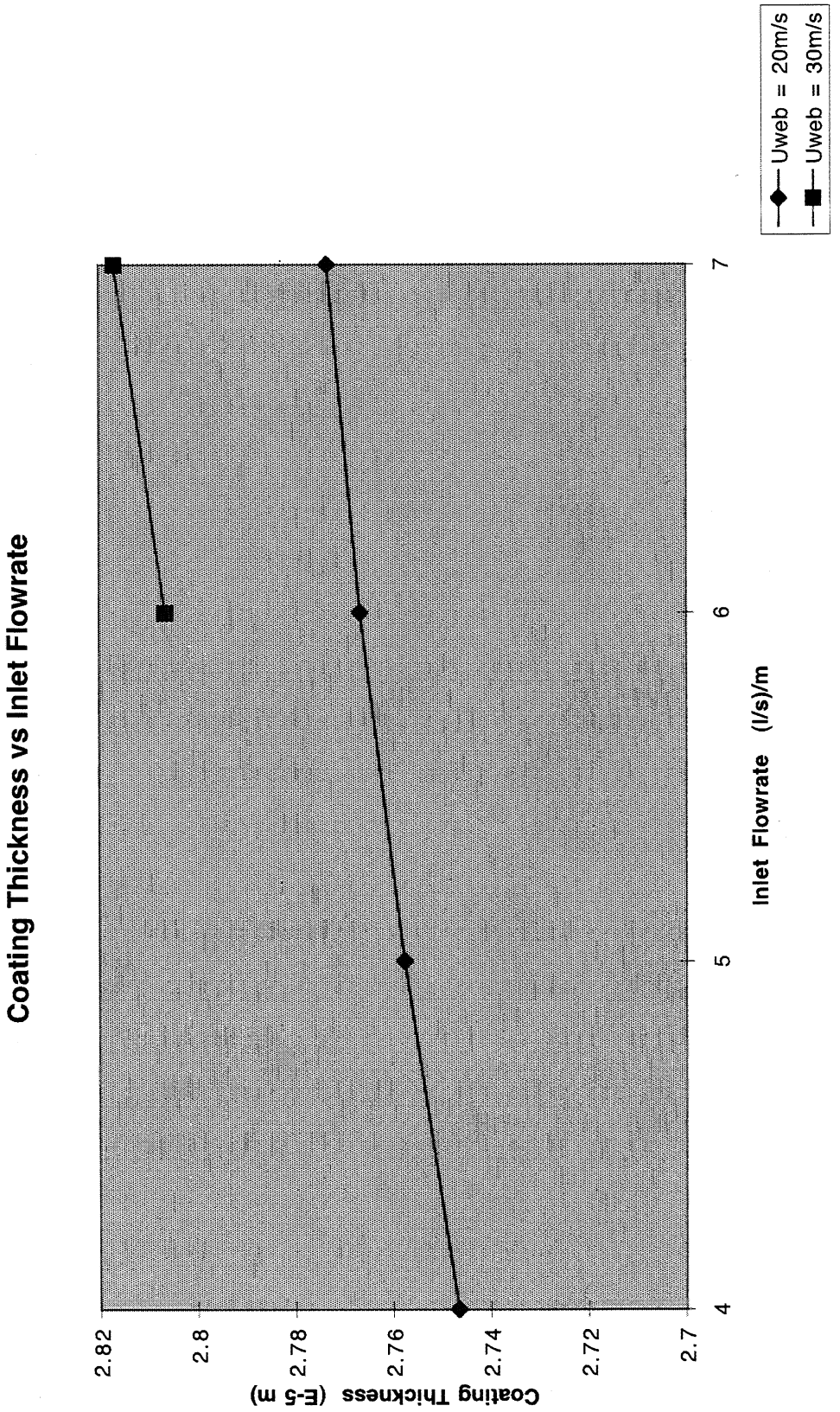
Coating Thickness vs Inlet Flowrate
Coating Thickness (E-5 m)
2.82
2.8
2.78
2.76
2.74
2.72
2.7
4
5
6
7
Inlet Flowrate (l/s)/m
Uweb = 20m/s
Uweb = 30m/s

Conservation of Momentum

Vapor

$$\frac{\partial}{\partial \tau}\left(\rho_v u_v\right)+\frac{\partial}{\partial z}\left(P_v\right)+\frac{\mu_v u_v}{K}=0 \qquad \textbf{(13)}$$

Liquid

$$\frac{\partial}{\partial \tau}\left(\rho_l u_l\right)+\frac{\partial}{\partial z}\left(P_l\right)+\frac{\mu_l u_l}{K}=0 \qquad \textbf{(14)}$$

Figure 23

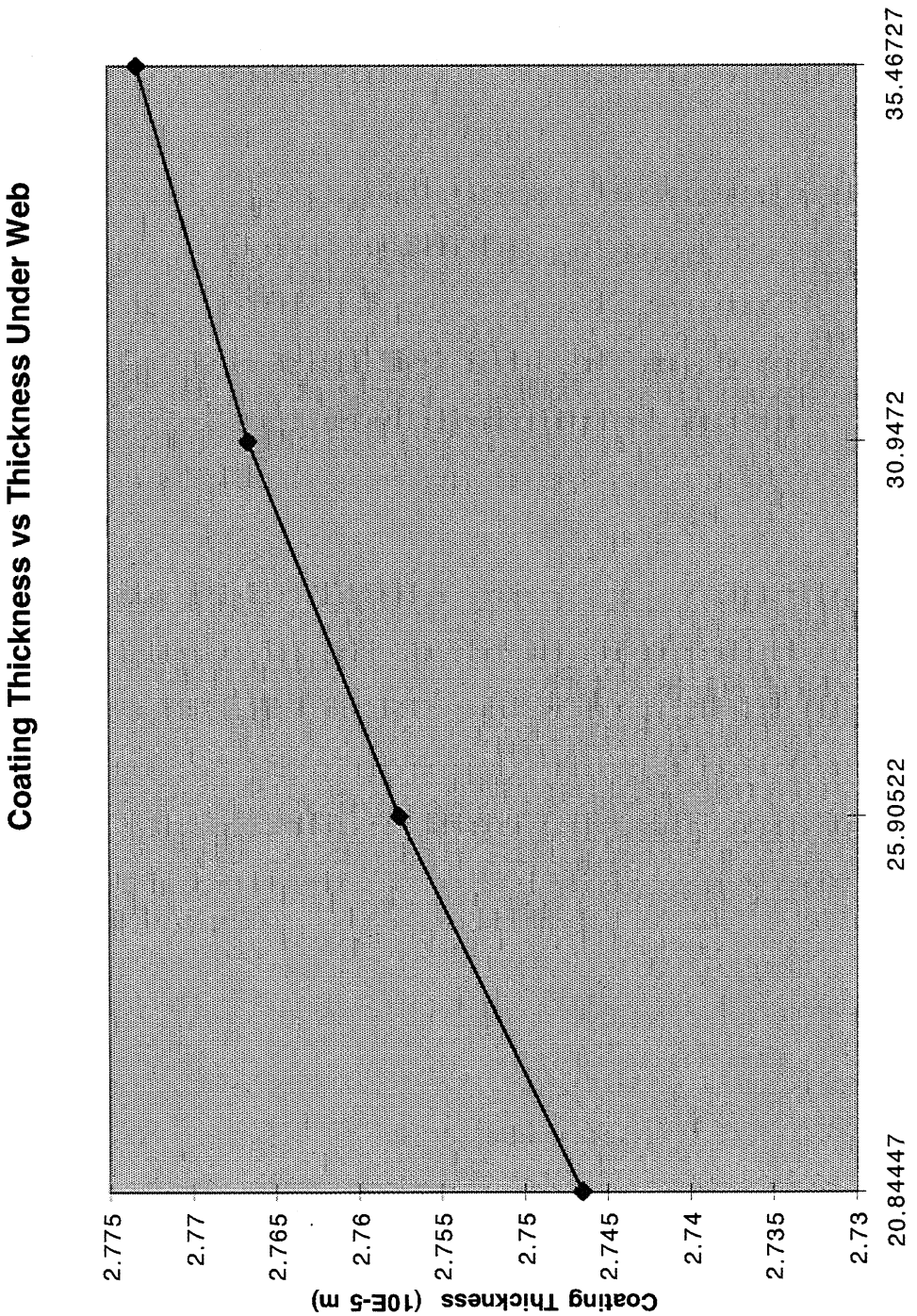
Coating Thickness vs Thickness Under Web
Coating Thickness (10E-5 m)
2.775
2.77
2.765
2.76
2.755
2.75
2.745
2.74
2.735
2.73
20.84447
25.90522
30.9472
35.46727
Thickness Under Web (10E-5 m)

Figure 24

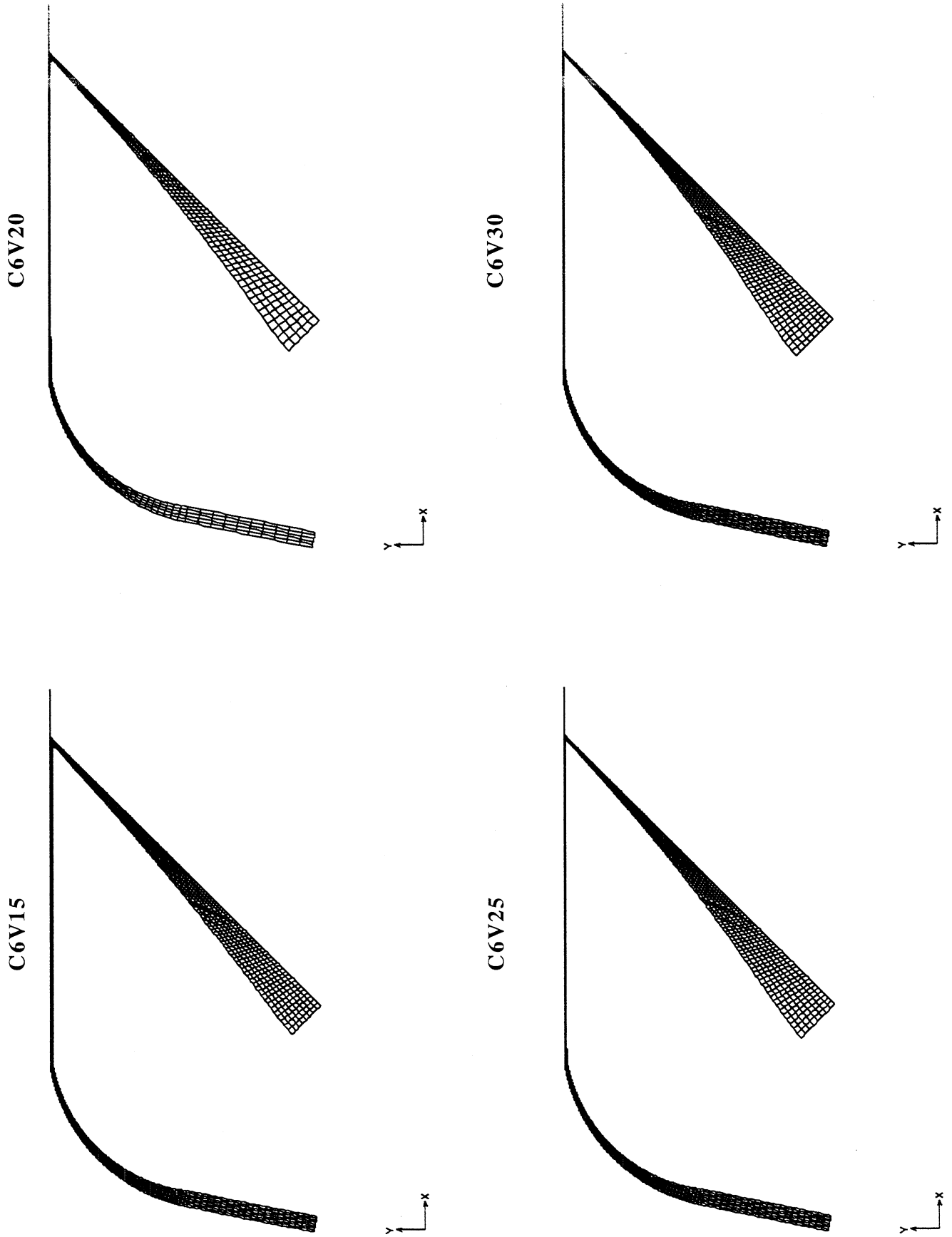

Figure 25

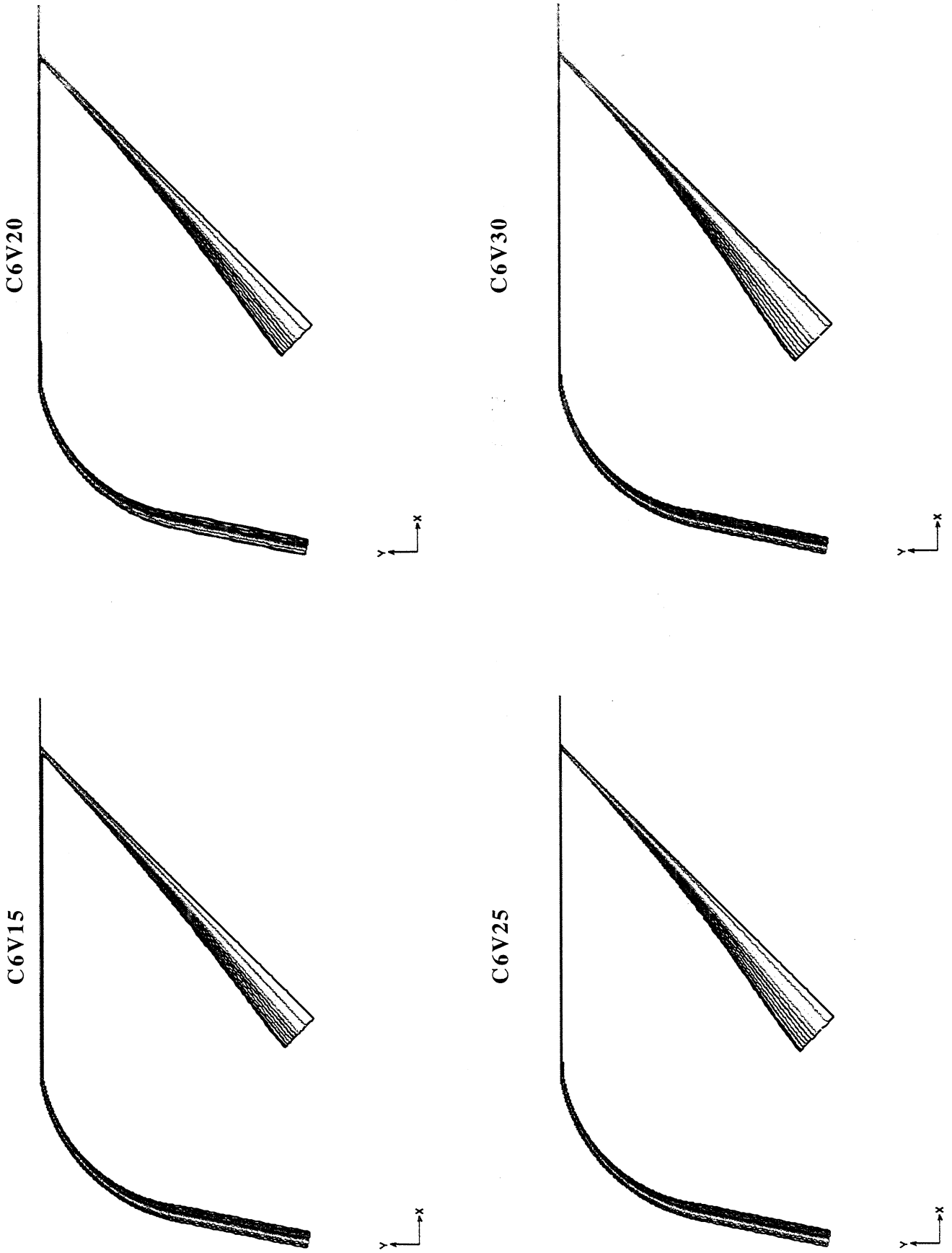

Figure 26

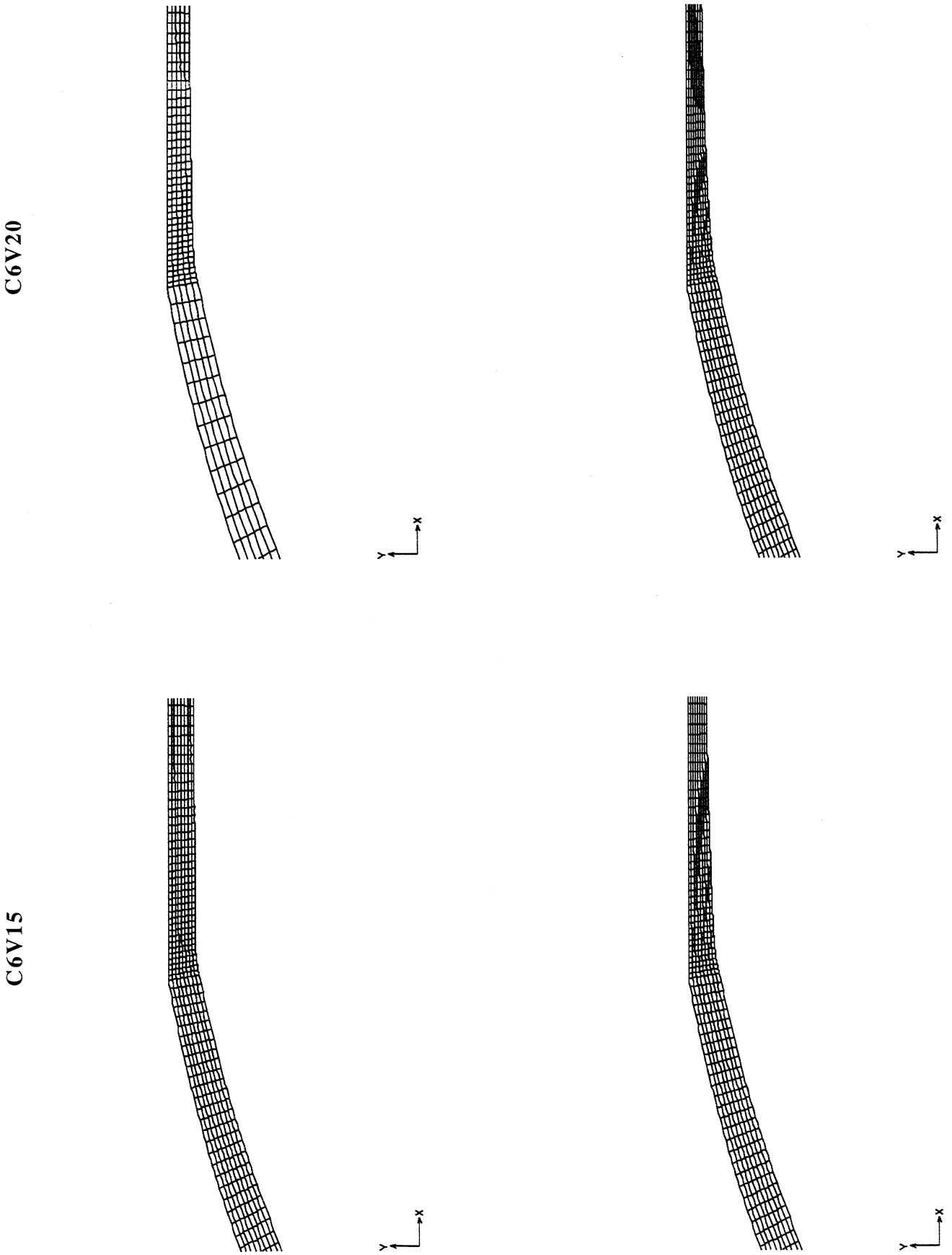

Figure 27

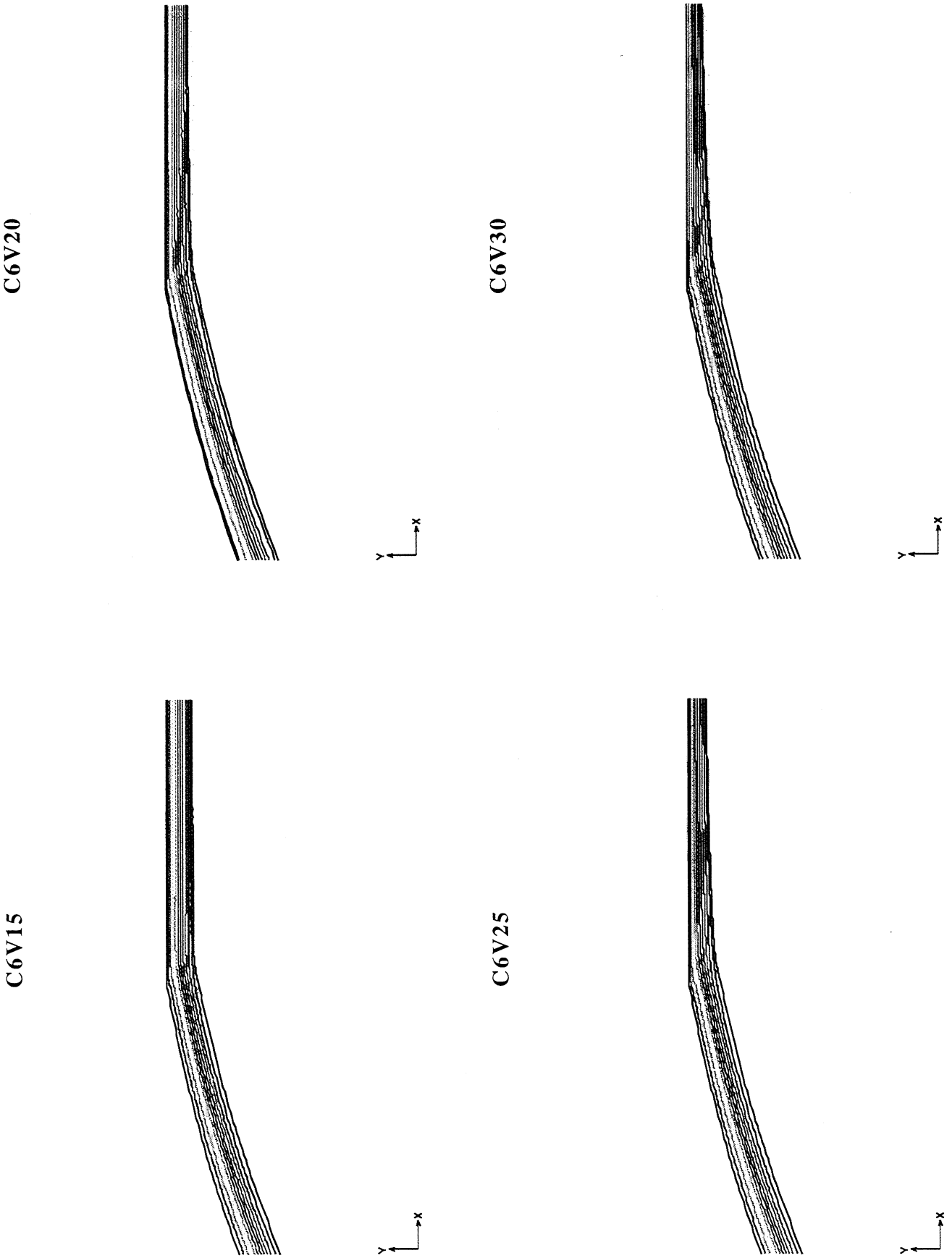

Figure 28

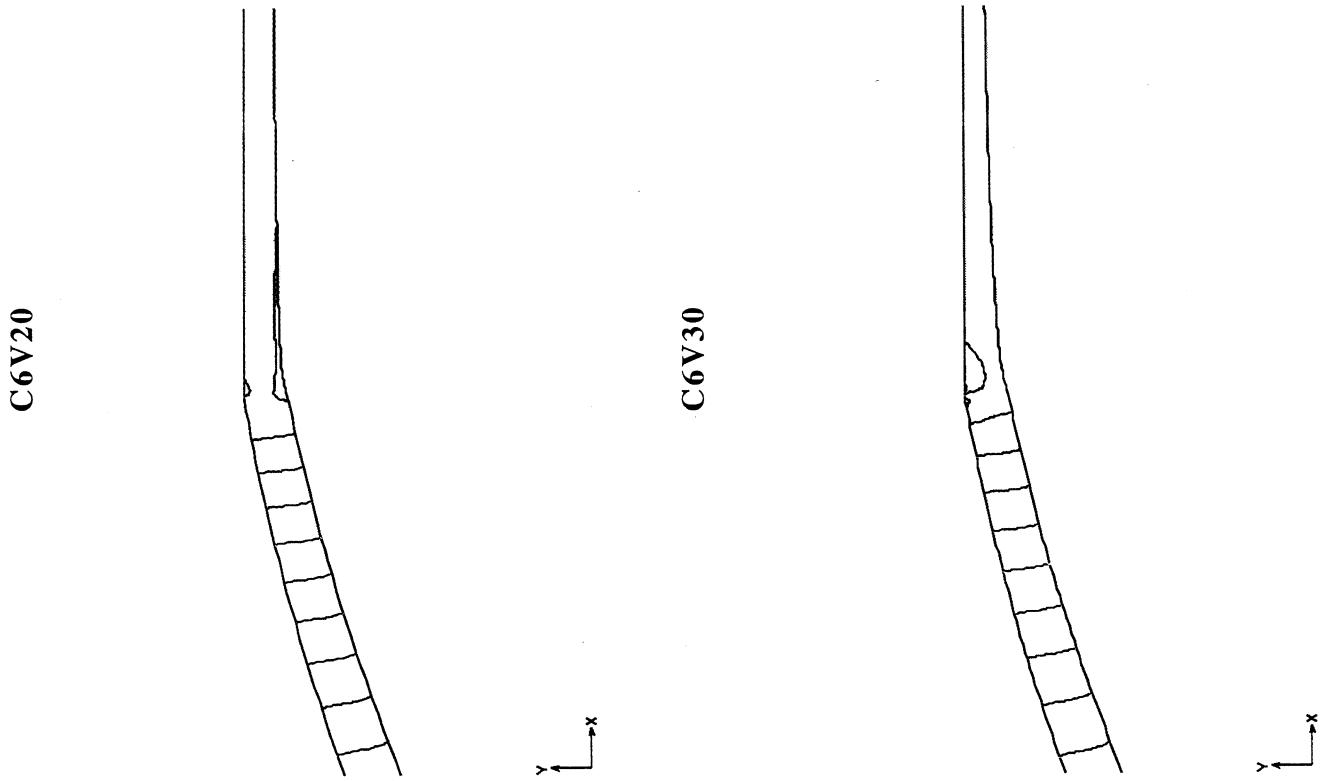

Figure 29

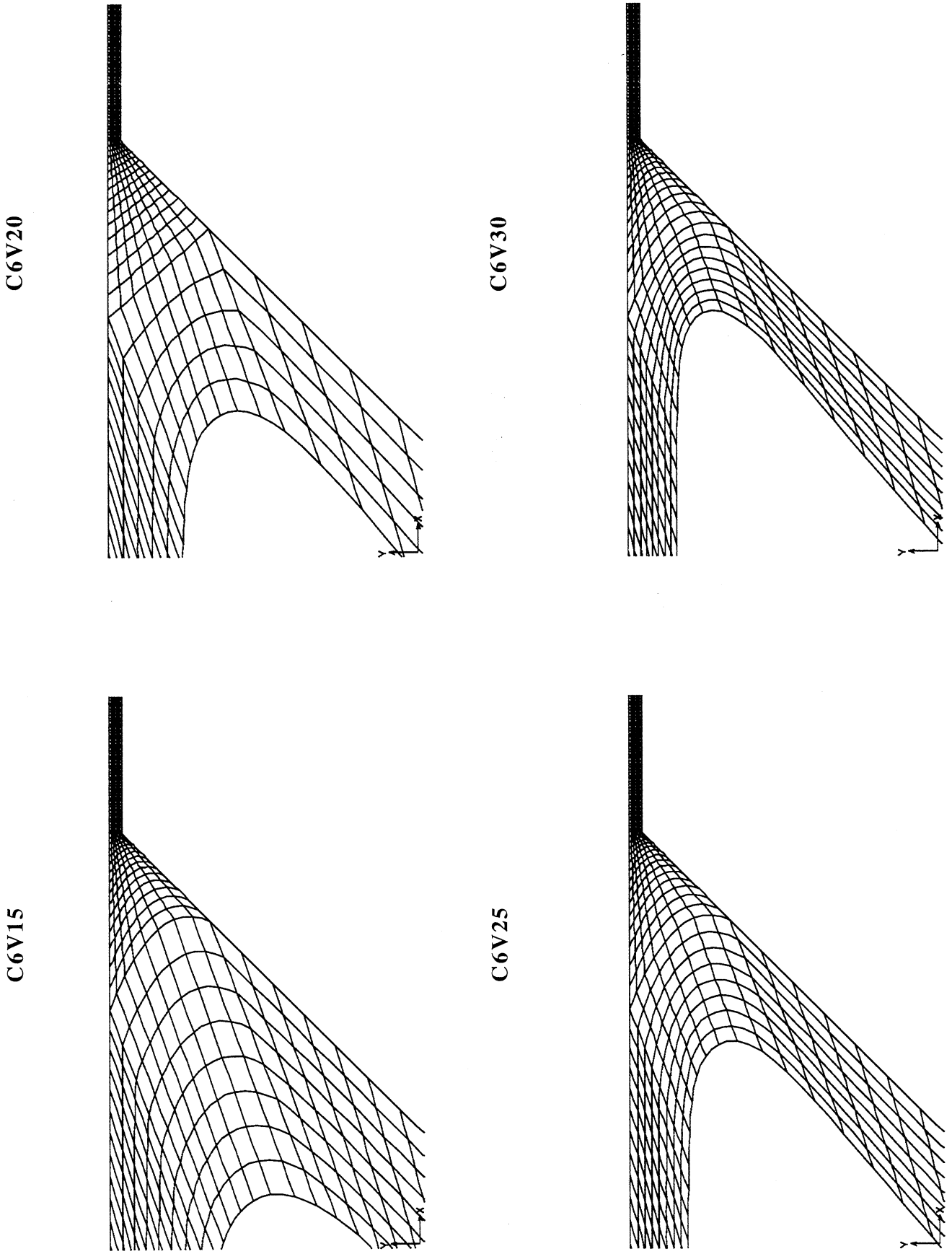

Figure 30

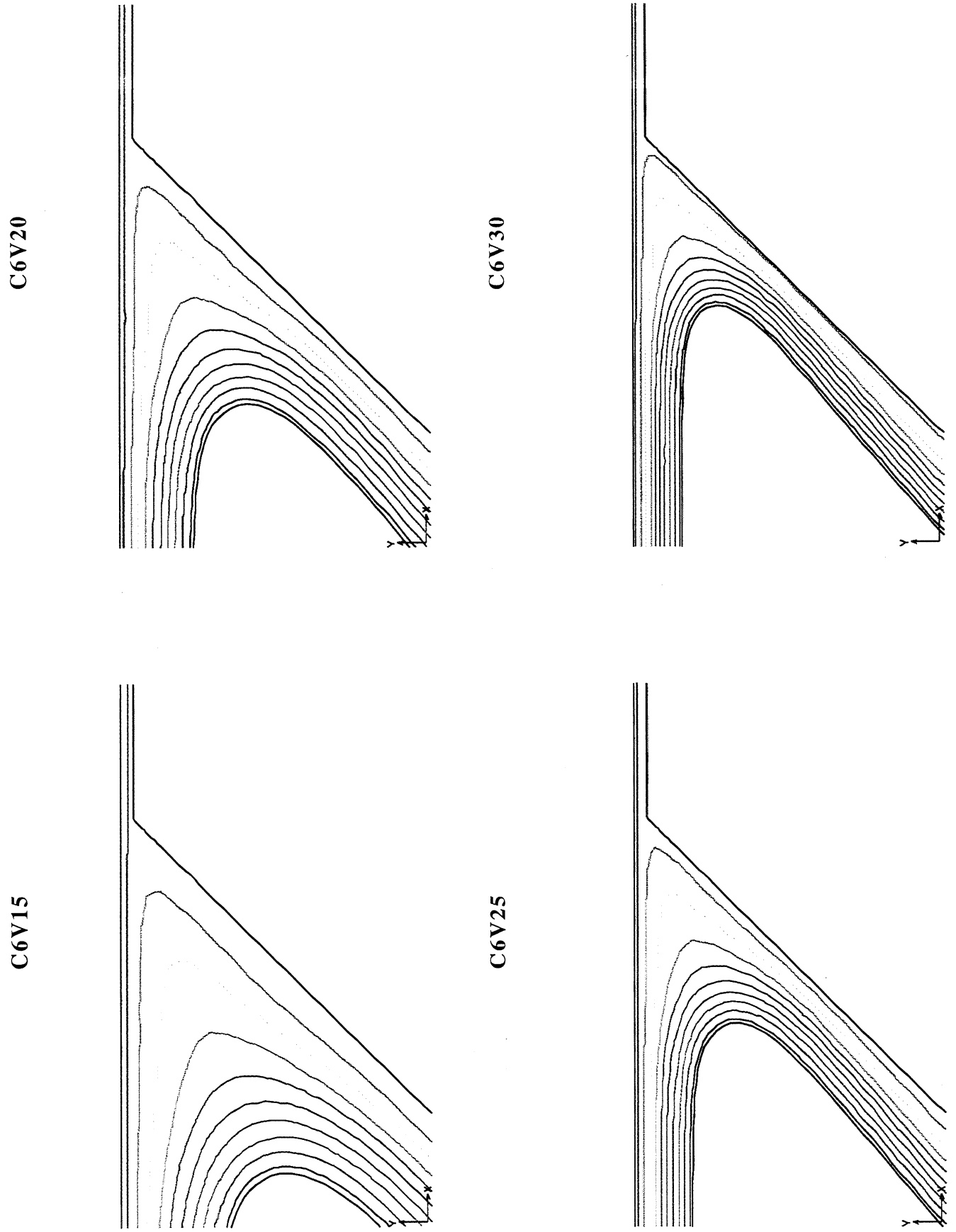

Figure 31

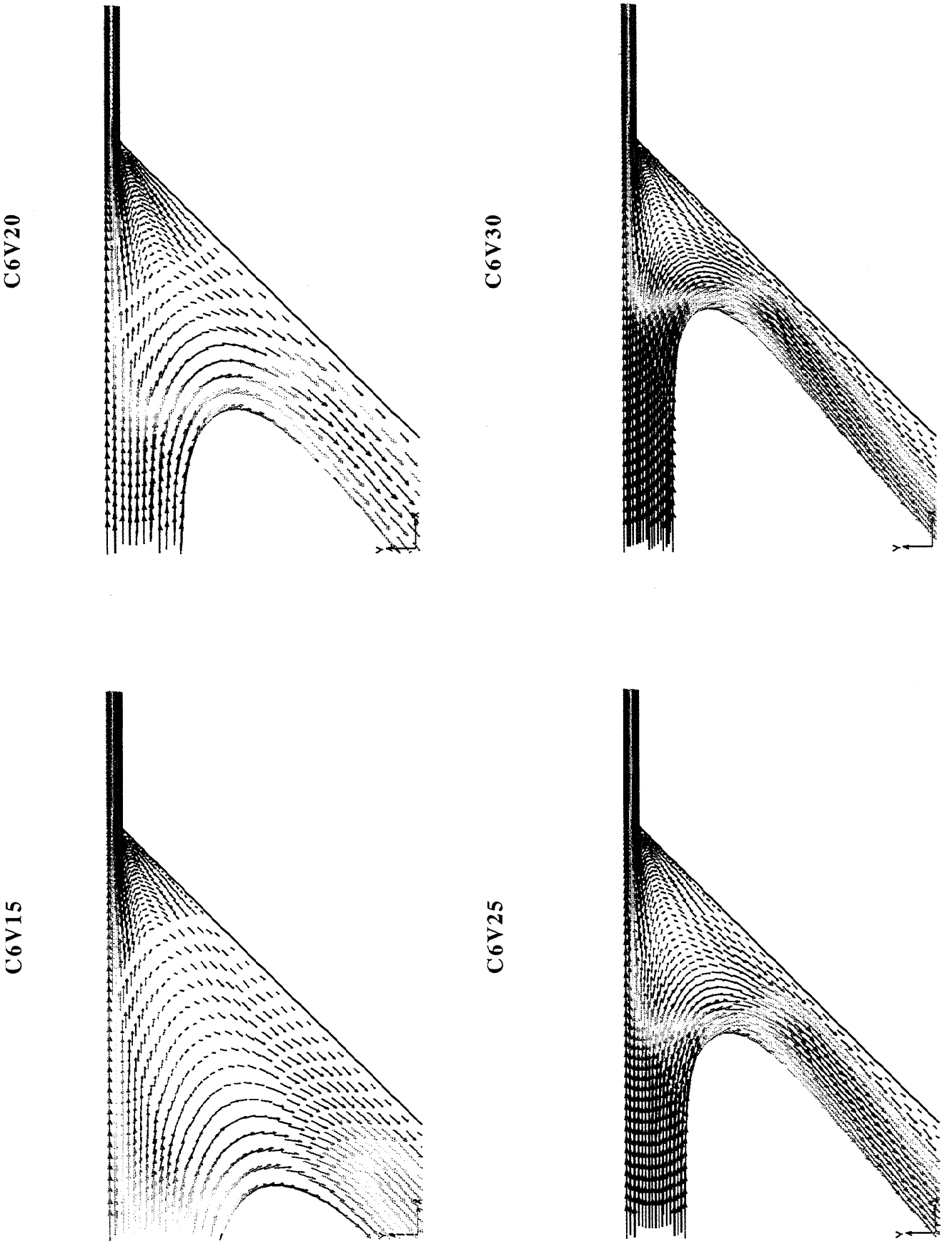

Figure 32

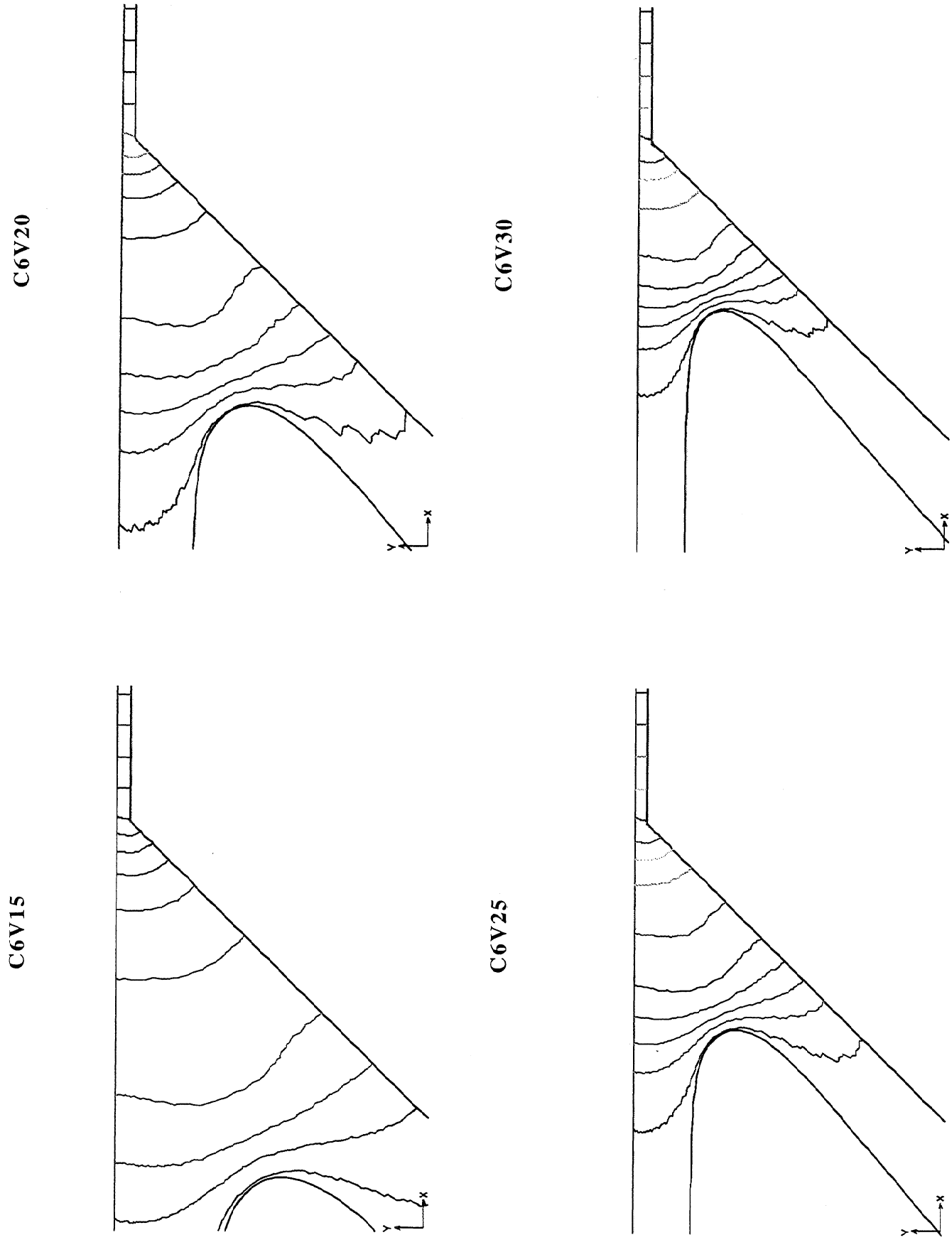

Figure 33

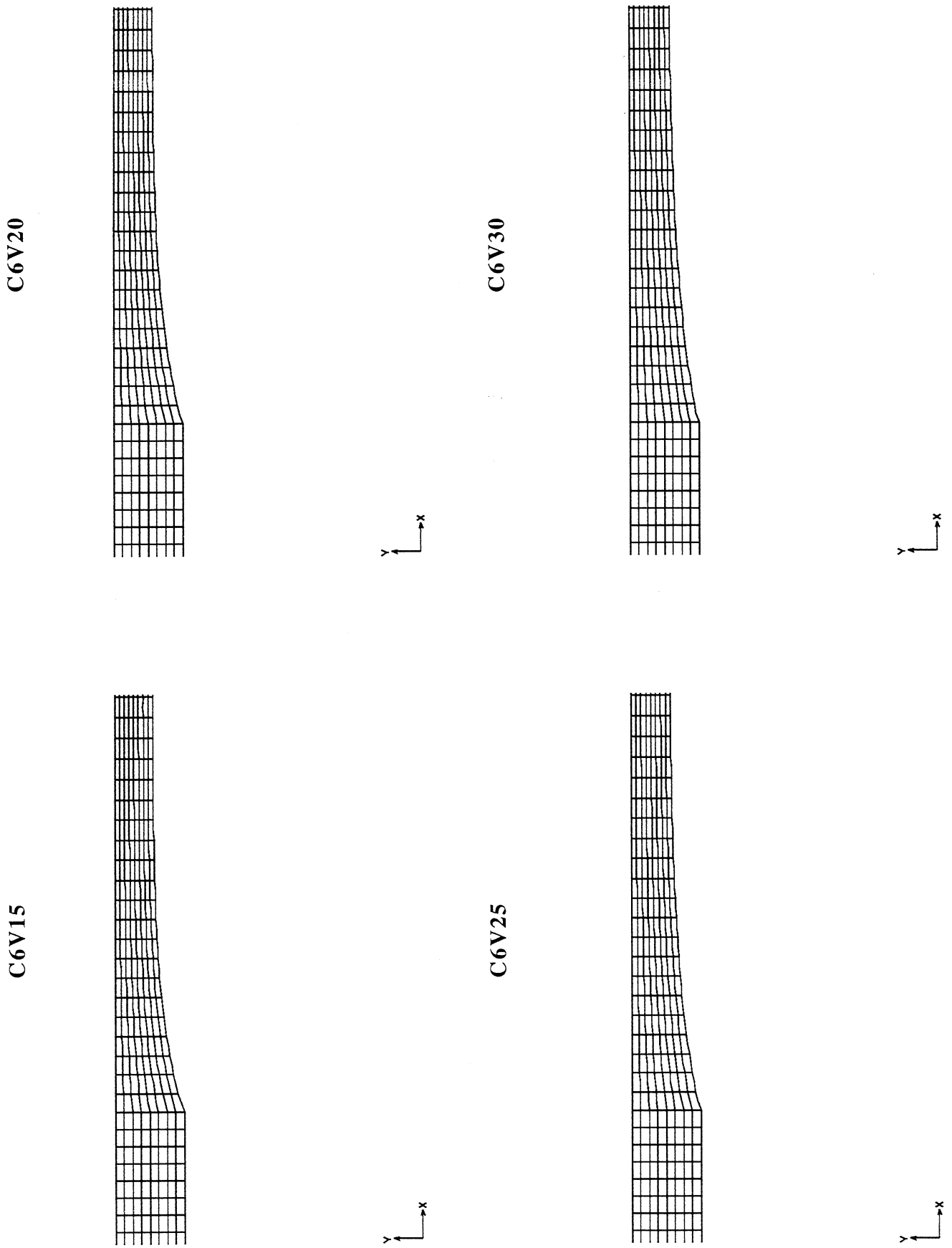

Figure 34

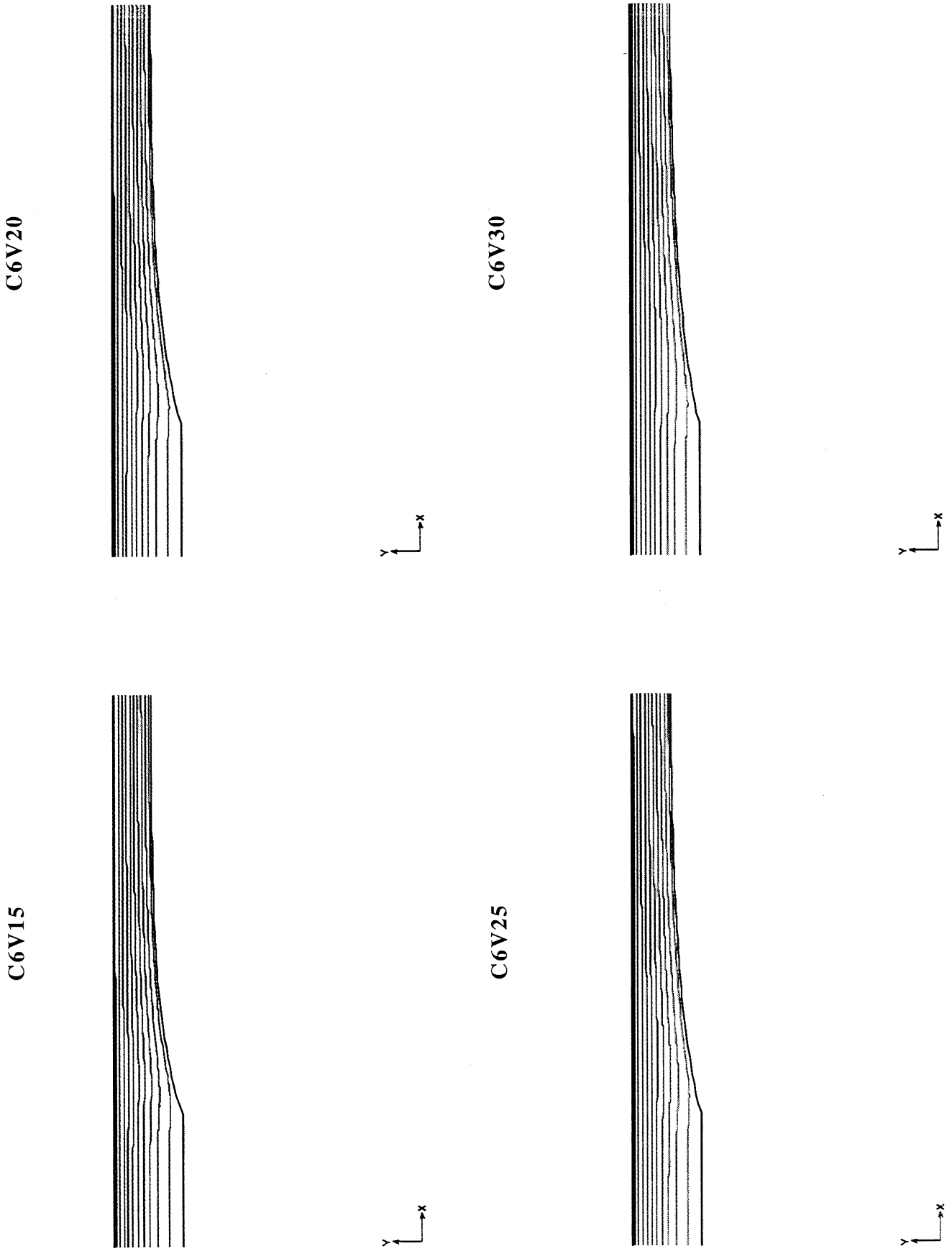

Figure 35

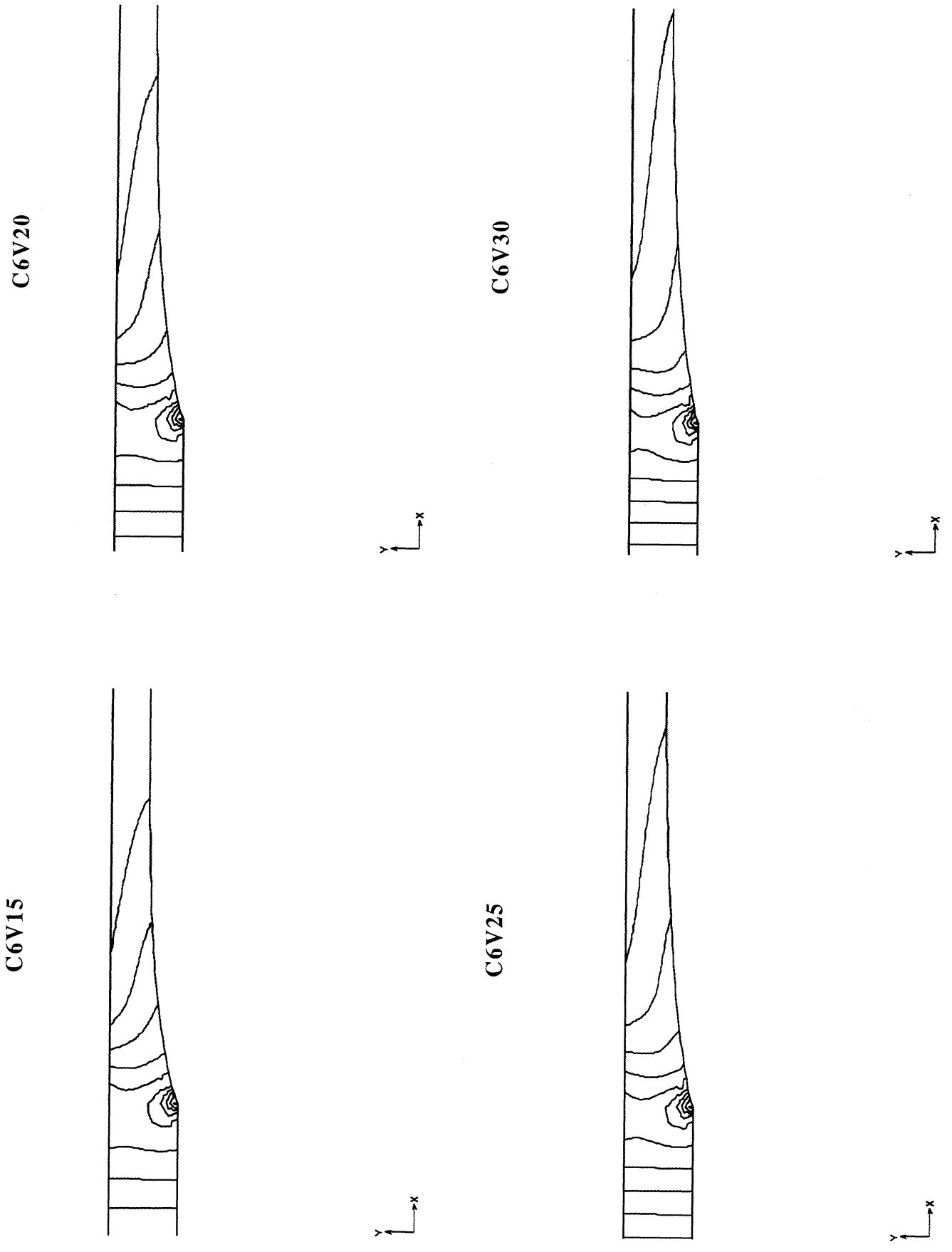

Figure 36

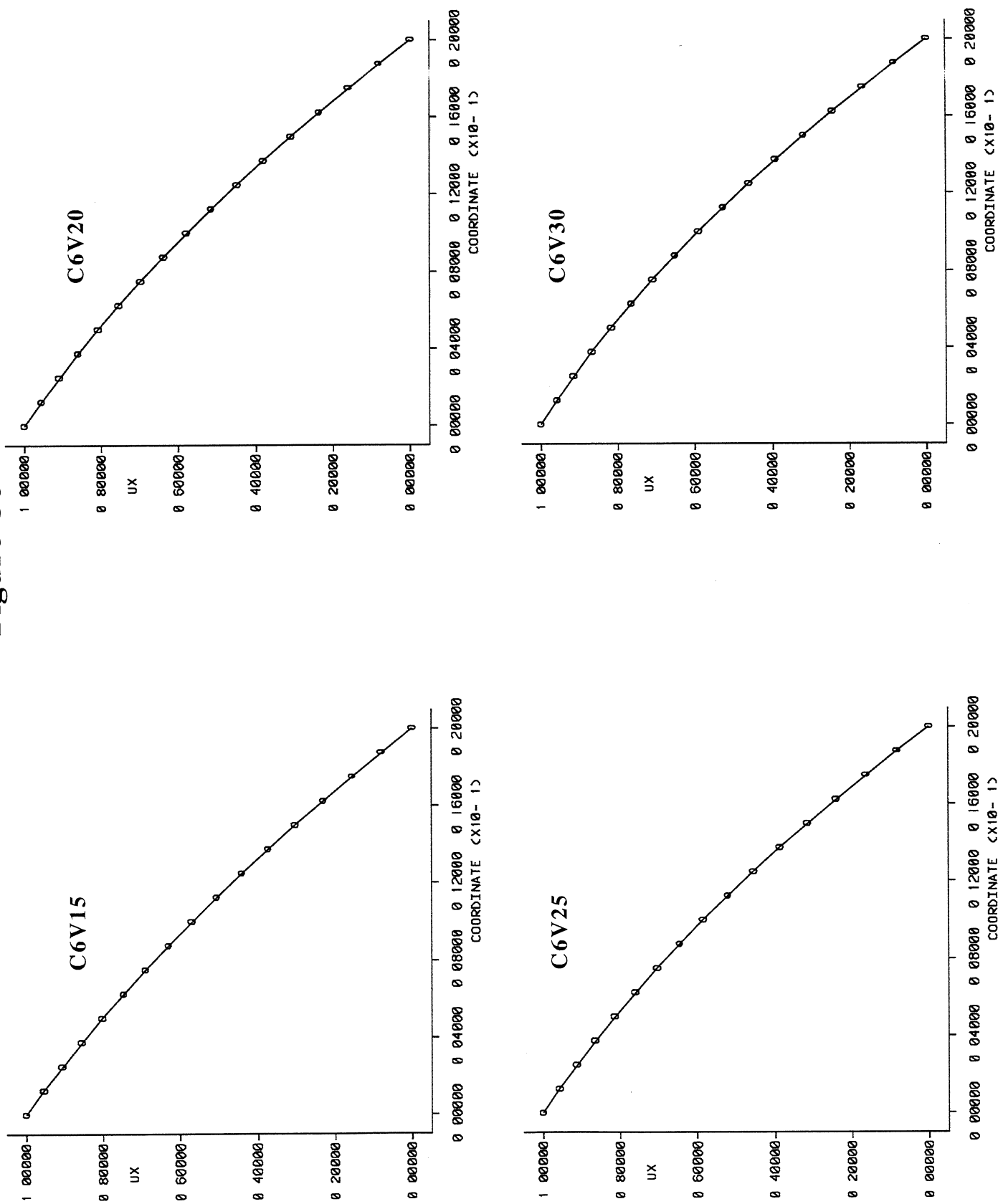
C6V20
C6V30
C6V15
C6V25
UX
COORDINATE (X10- 1)
1 00000
0 80000
0 60000
0 40000
0 20000
0 00000
0 00000
0 04000
0 08000
0 12000
0 16000
0 20000

Figure 37

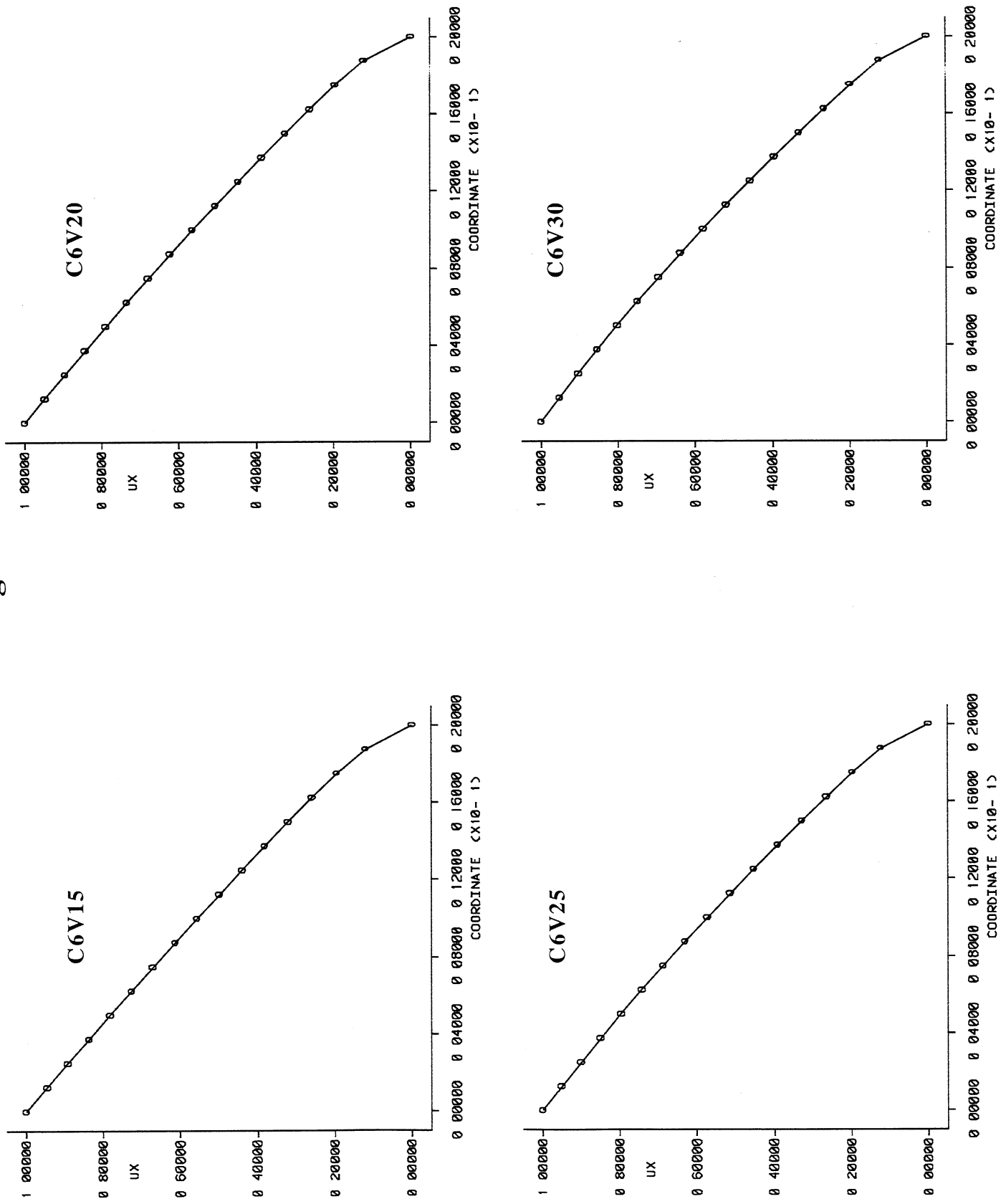
C6V20
C6V30
C6V15
C6V25
UX
COORDINATE (X10- 1)
1 00000
0 80000
0 60000
0 40000
0 20000
0 00000
0 00000
0 04000
0 08000
0 12000
0 16000
0 20000

Figure 38

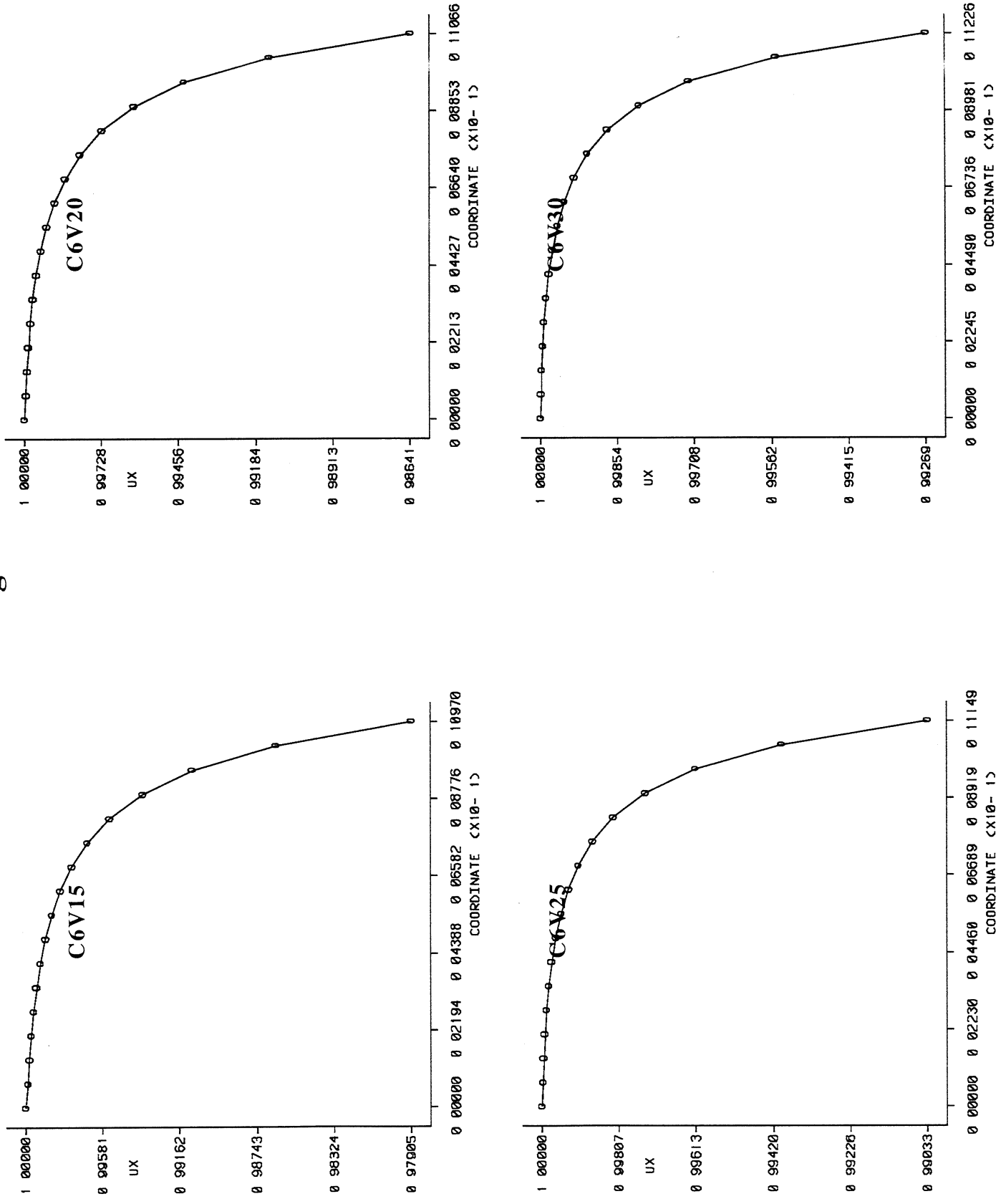

Figure 39

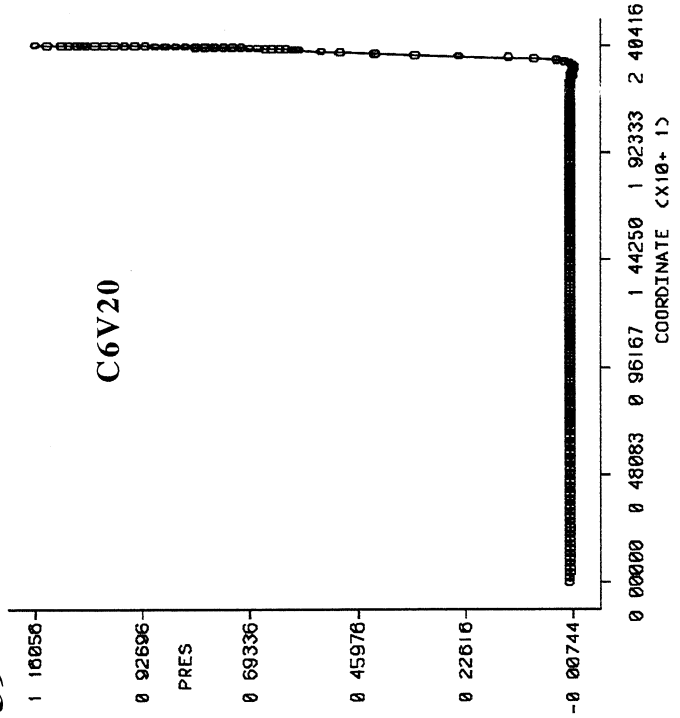
C6V20
1 16056
0 92696
PRES
0 69336
0 45976
0 22616
-0 00744
0 00000 0 48083 0 96167 1 44250 1 92333 2 40416
COORDINATE (X10+ 1)

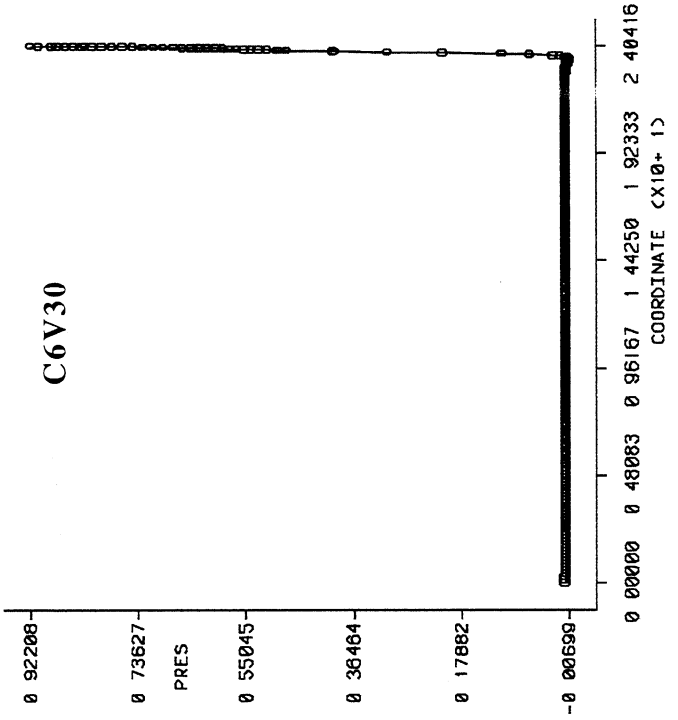
C6V30
0 92208
0 73627
PRES
0 55045
0 36464
0 17882
-0 00699
0 00000 0 48083 0 96167 1 44250 1 92333 2 40416
COORDINATE (X10+ 1)

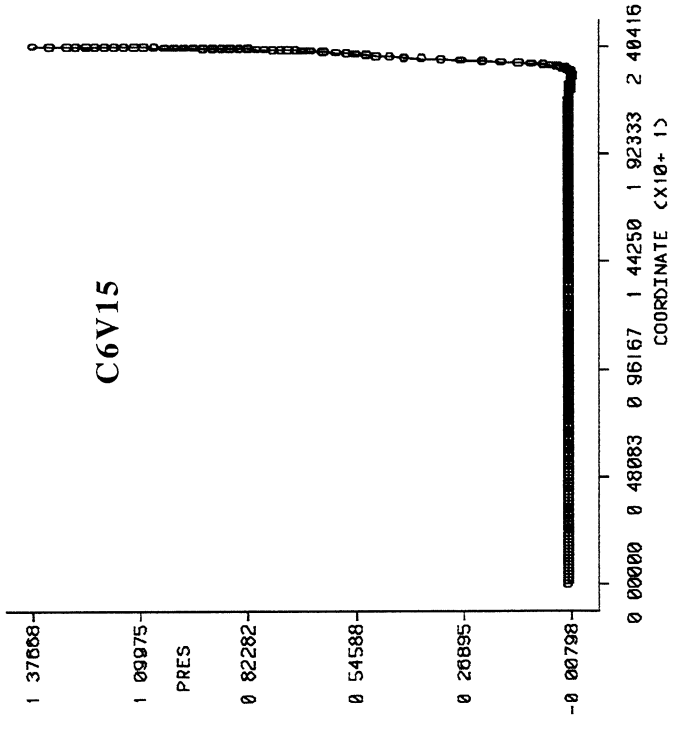
C6V15
1 37668
1 09975
PRES
0 82282
0 54588
0 26895
-0 00798
0 00000 0 48083 0 96167 1 44250 1 92333 2 40416
COORDINATE (X10+ 1)

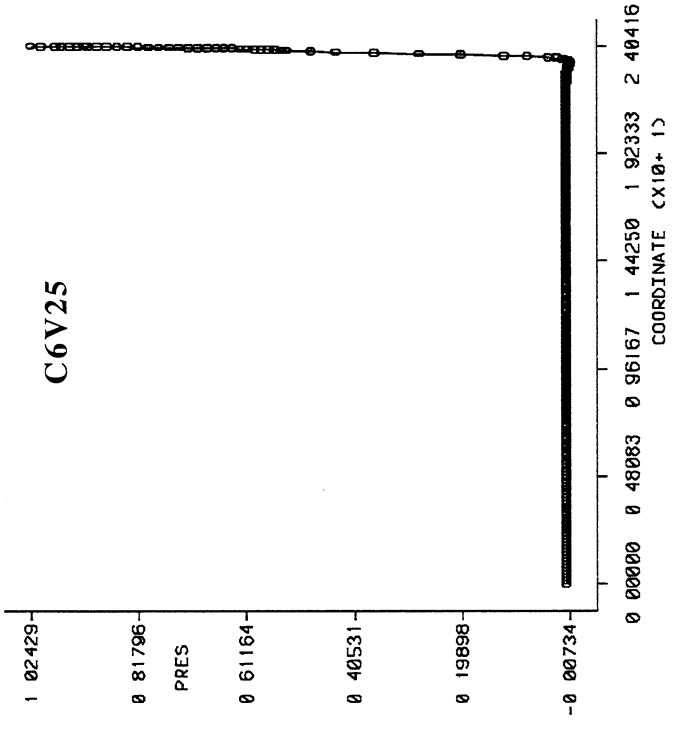
C6V25
1 02429
0 81796
PRES
0 61164
0 40531
0 19898
-0 00734
0 00000 0 48083 0 96167 1 44250 1 92333 2 40416
COORDINATE (X10+ 1)

Figure 40

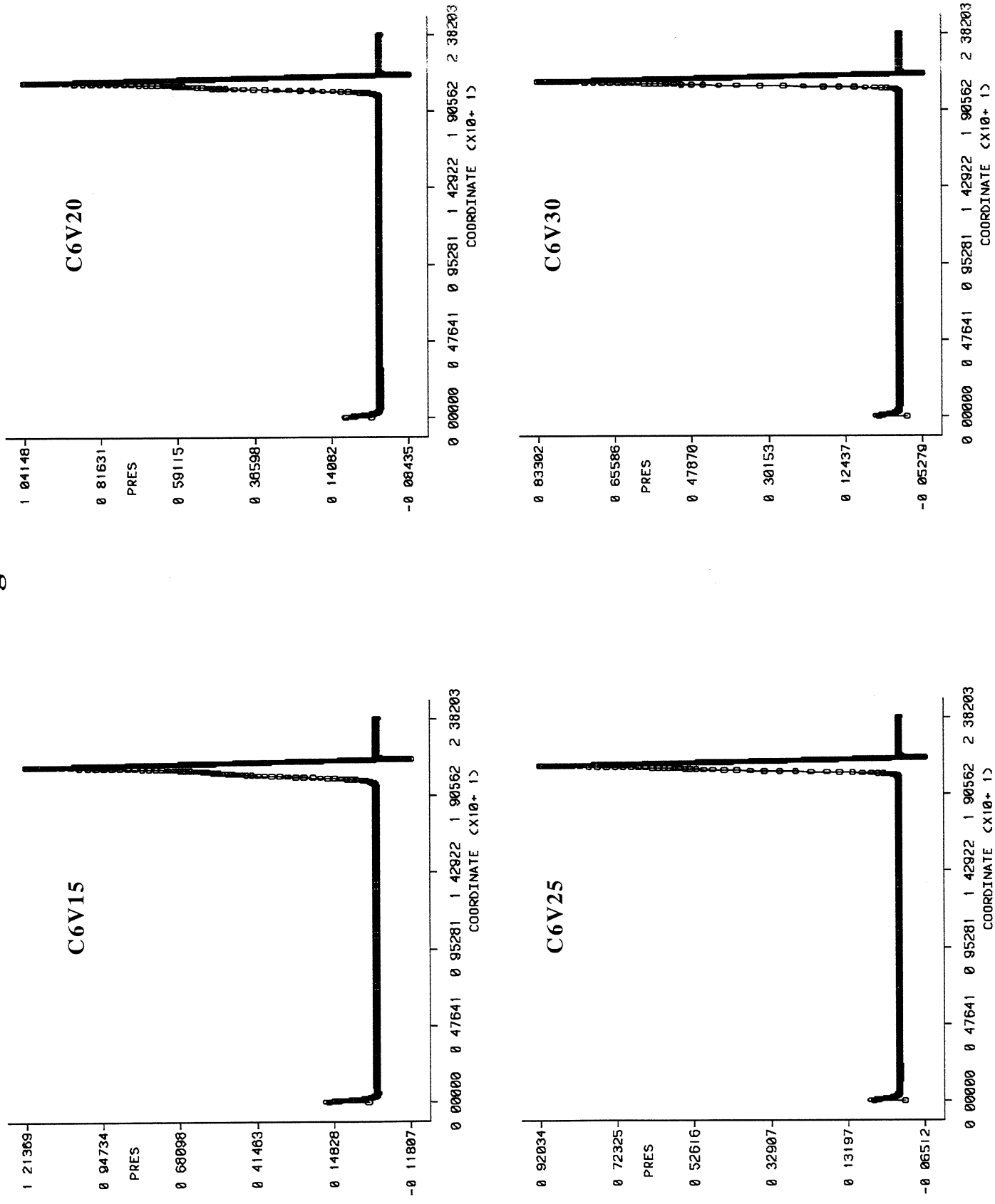
C6V20
1 04148
0 81631
PRES
0 59115
0 36598
0 14082
-0 08435
0 00000 0 47641 0 95281 1 42922 1 90562 2 38203
COORDINATE (X10+ 1)
C6V30
0 83302
0 65586
PRES
0 47870
0 30153
0 12437
-0 05279
0 00000 0 47641 0 95281 1 42922 1 90562 2 38203
COORDINATE (X10+ 1)
C6V15
1 21369
0 94734
PRES
0 68098
0 41463
0 14828
-0 11807
0 00000 0 47641 0 95281 1 42922 1 90562 2 38203
COORDINATE (X10+ 1)
C6V25
0 92034
0 72325
PRES
0 52616
0 32907
0 13197
-0 06512
0 00000 0 47641 0 95281 1 42922 1 90562 2 38203
COORDINATE (X10+ 1)

Figure 41

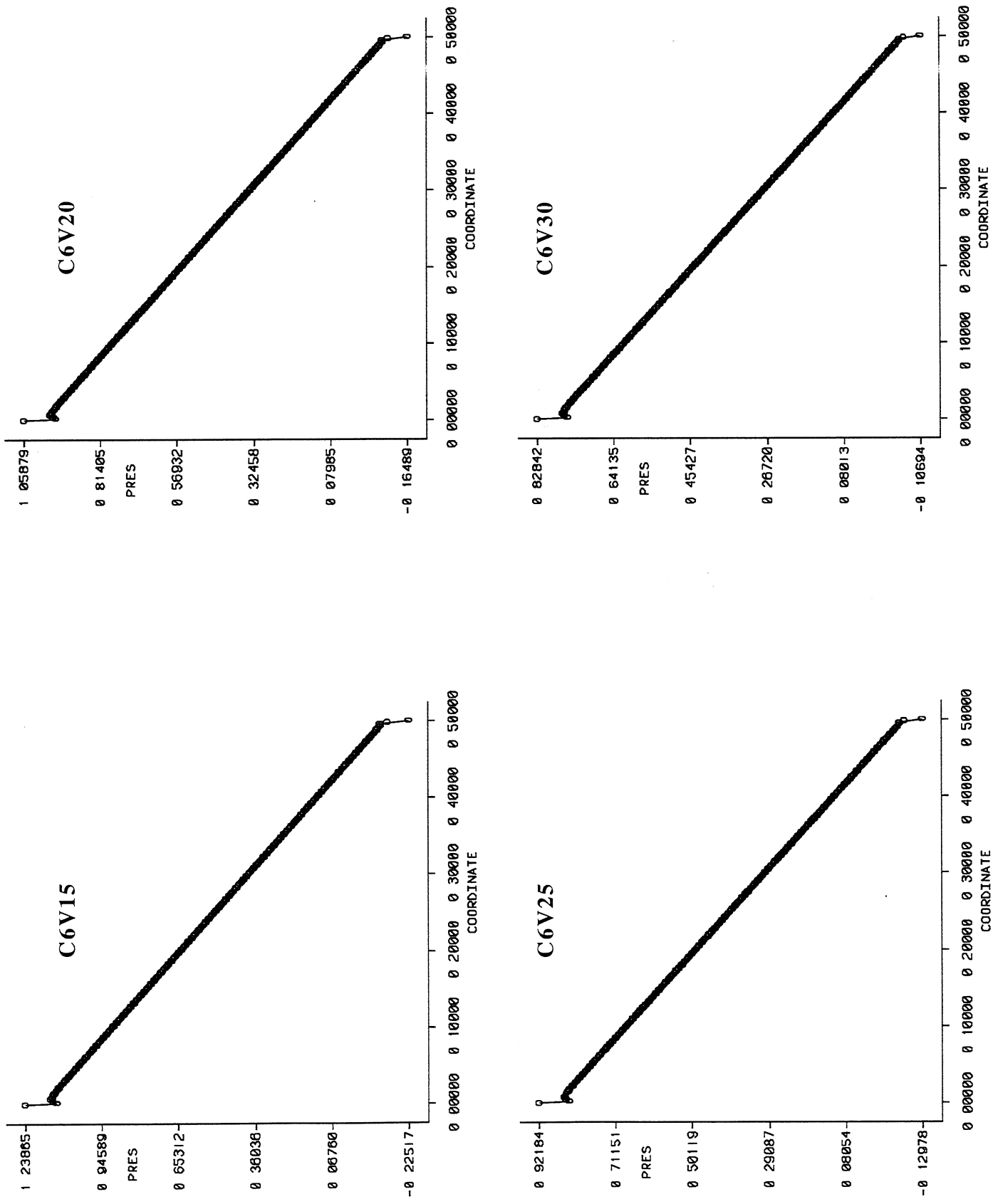
C6V20
1 05879
0 81405
PRES
0 56932
0 32458
0 07985
-0 16489
0 00000 0 10000 0 20000 0 30000 0 40000 0 50000
COORDINATE
C6V30
0 82842
0 64135
PRES
0 45427
0 26720
0 08013
-0 10694
0 00000 0 10000 0 20000 0 30000 0 40000 0 50000
COORDINATE
C6V15
1 23865
0 94589
PRES
0 65312
0 36036
0 06760
-0 22517
0 00000 0 10000 0 20000 0 30000 0 40000 0 50000
COORDINATE
C6V25
0 92184
0 71151
PRES
0 50119
0 29087
0 08054
-0 12978
0 00000 0 10000 0 20000 0 30000 0 40000 0 50000
COORDINATE

Figure 42

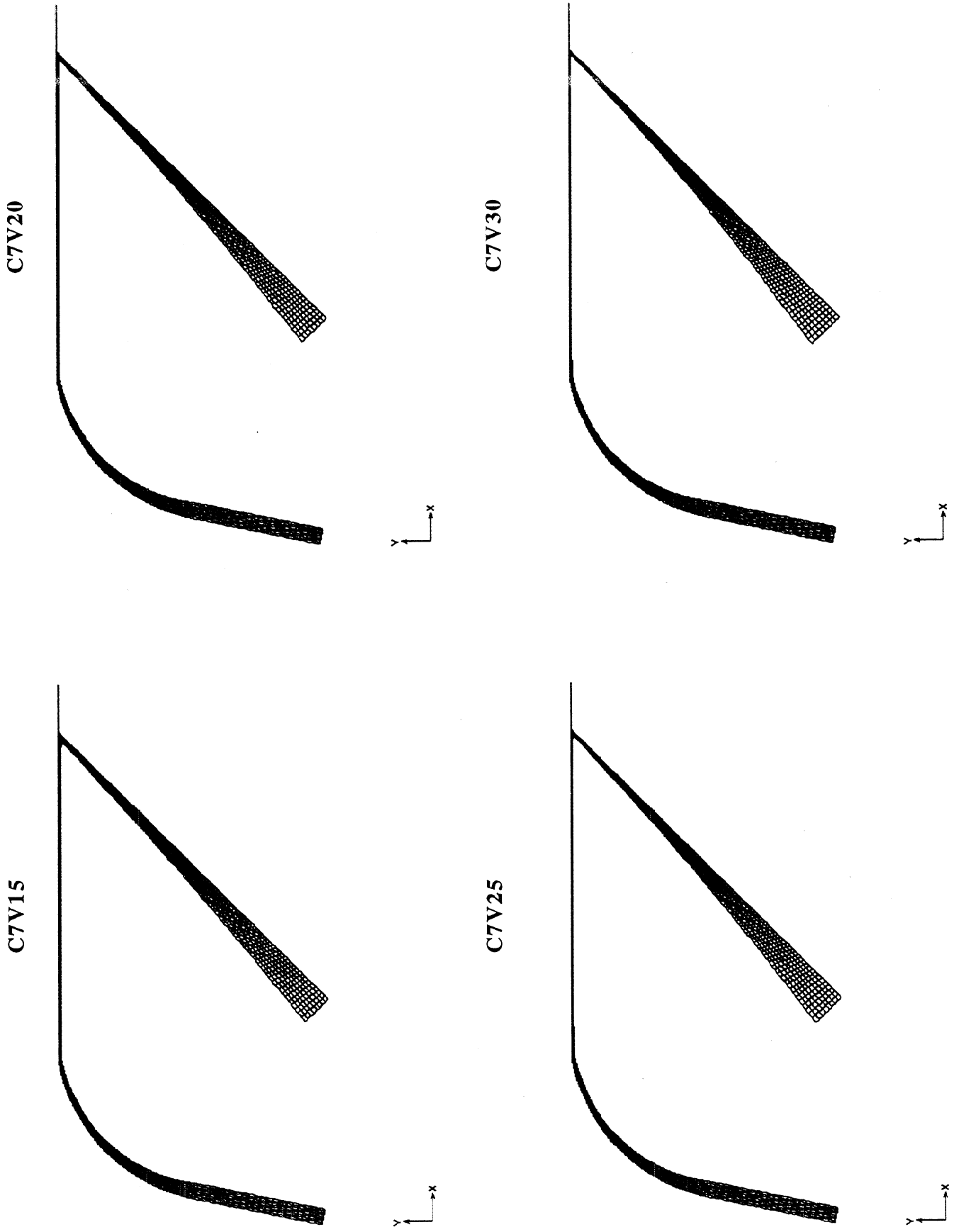

Figure 43

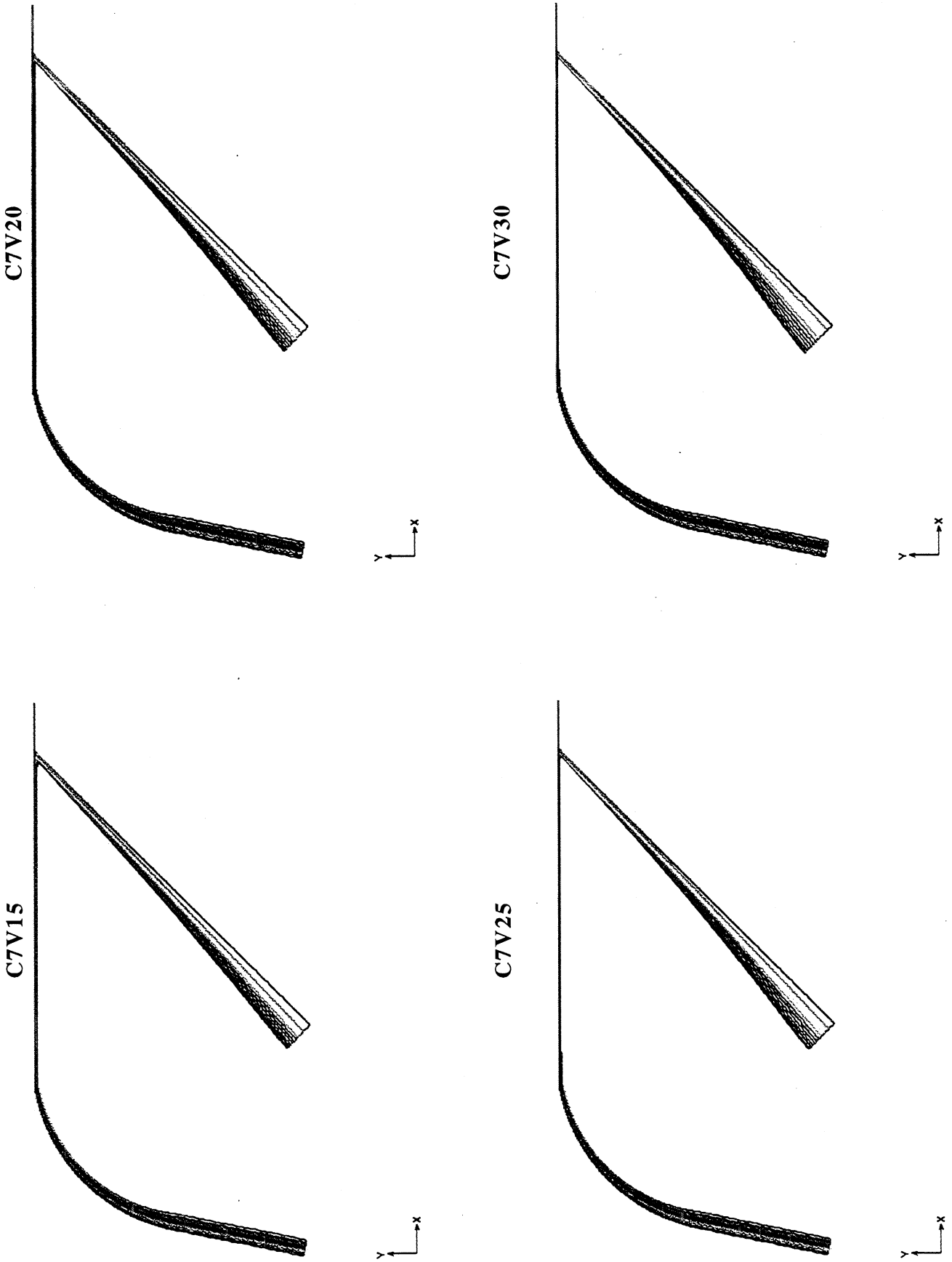

Figure 44

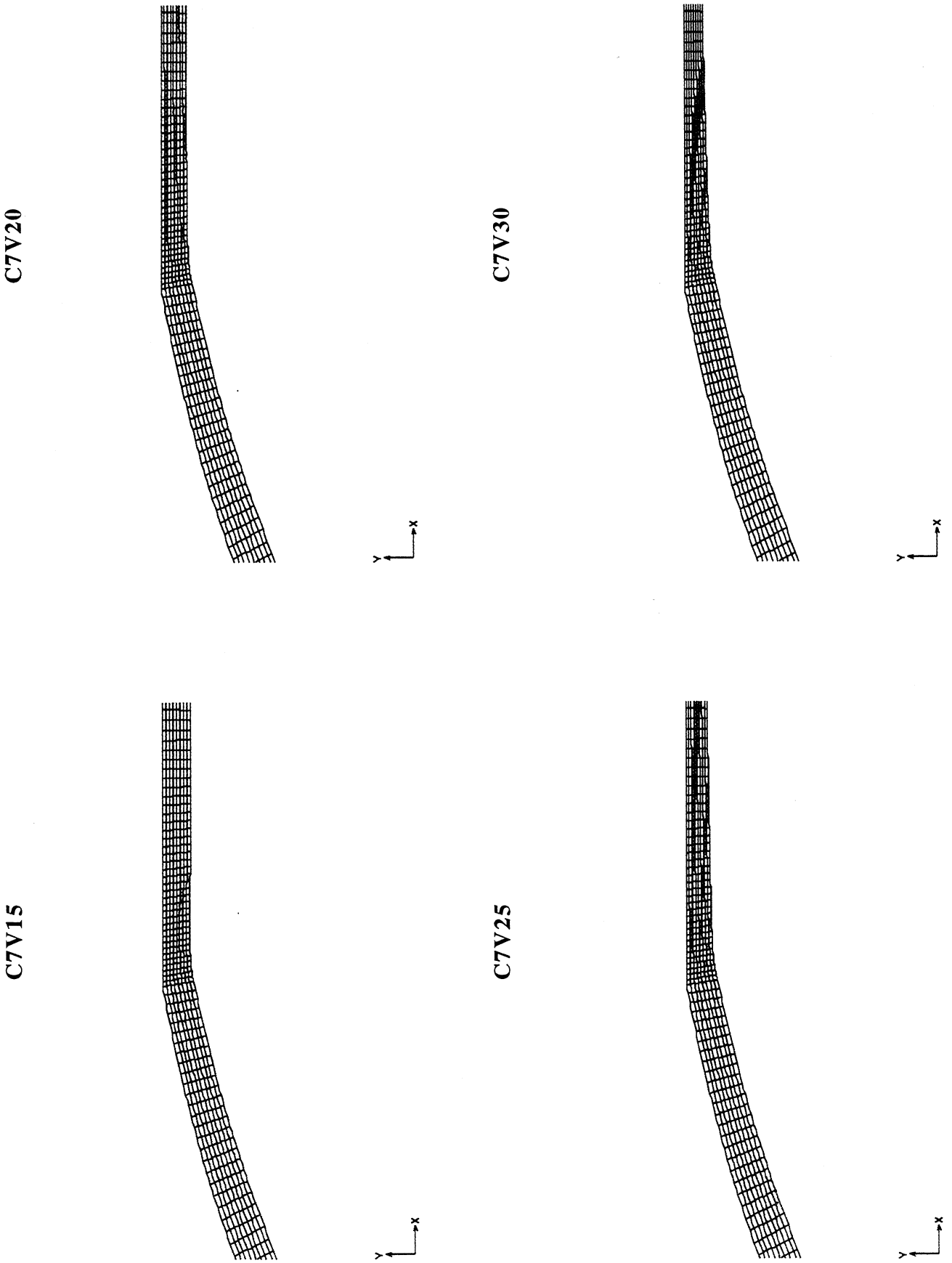

Figure 45

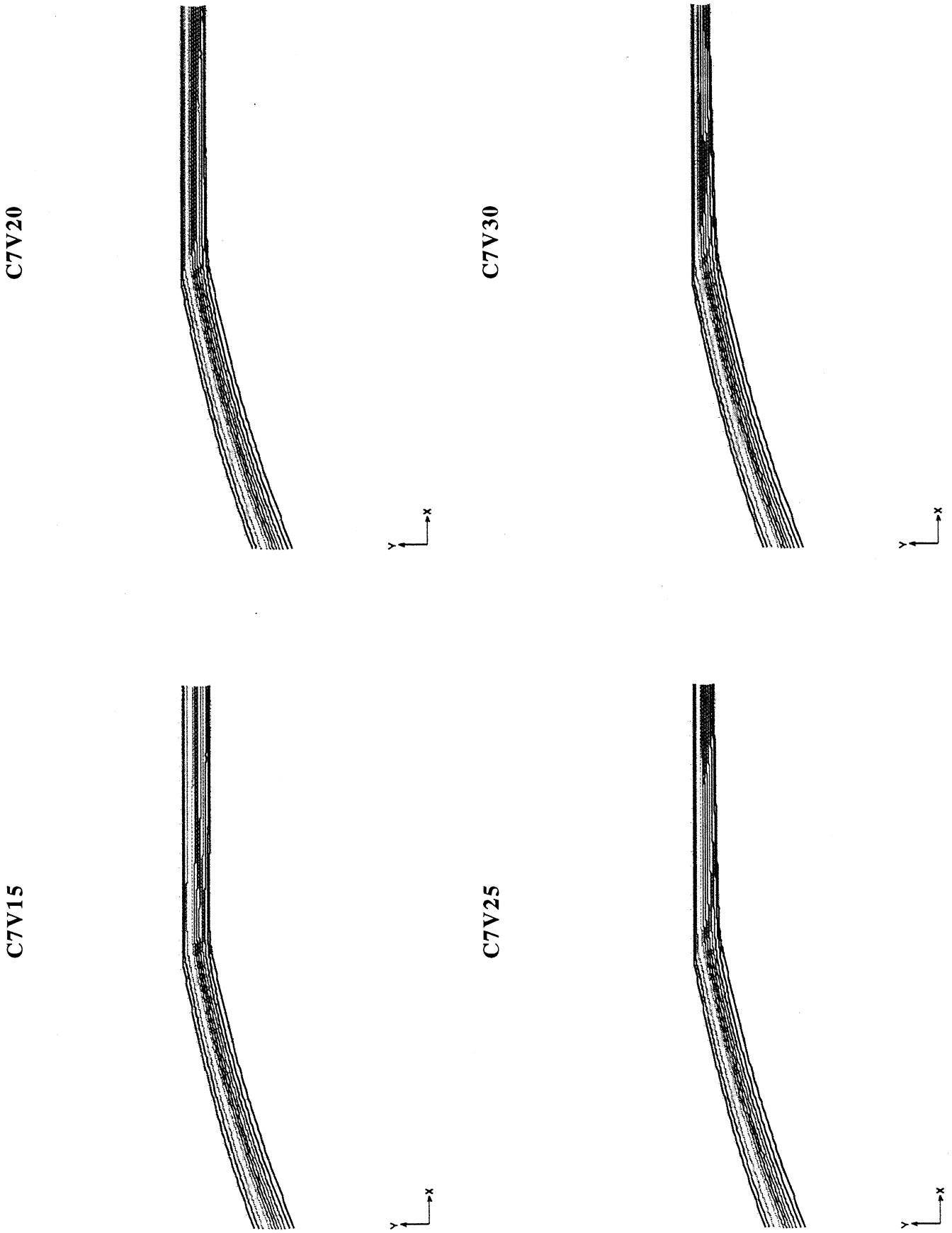

Figure 46

C7V20

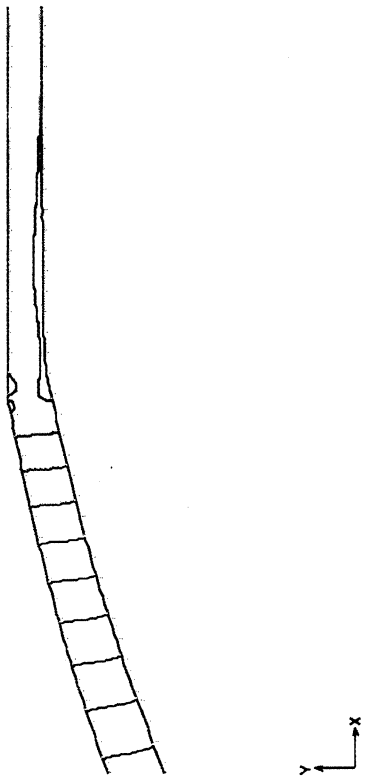

C7V30

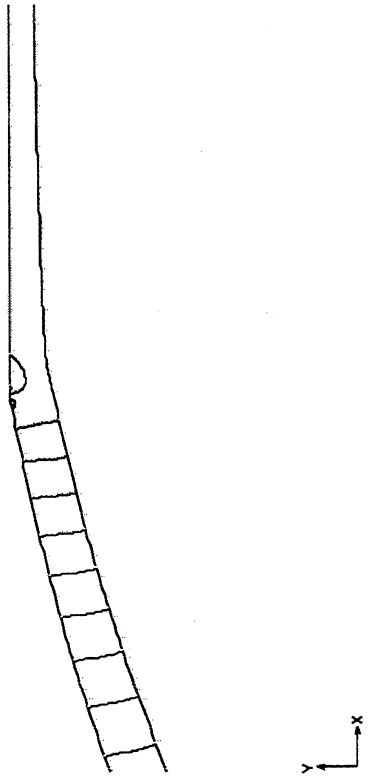

C7V15

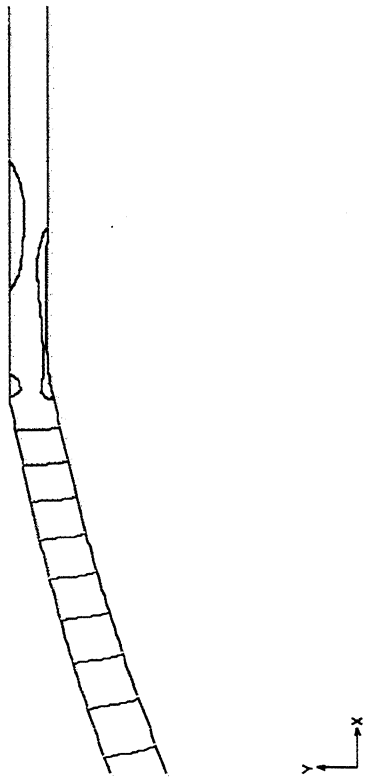

C7V25

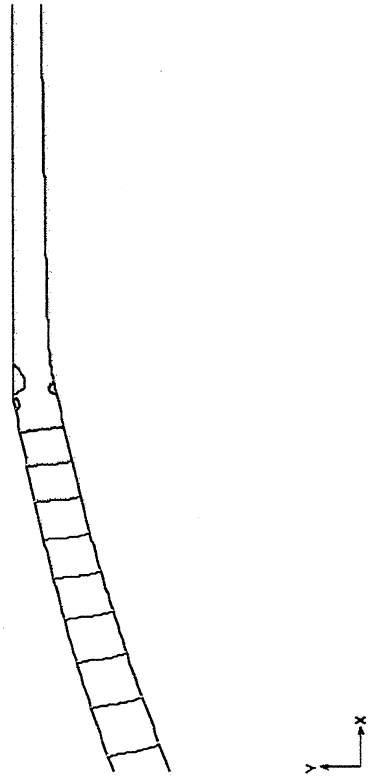

Figure 47

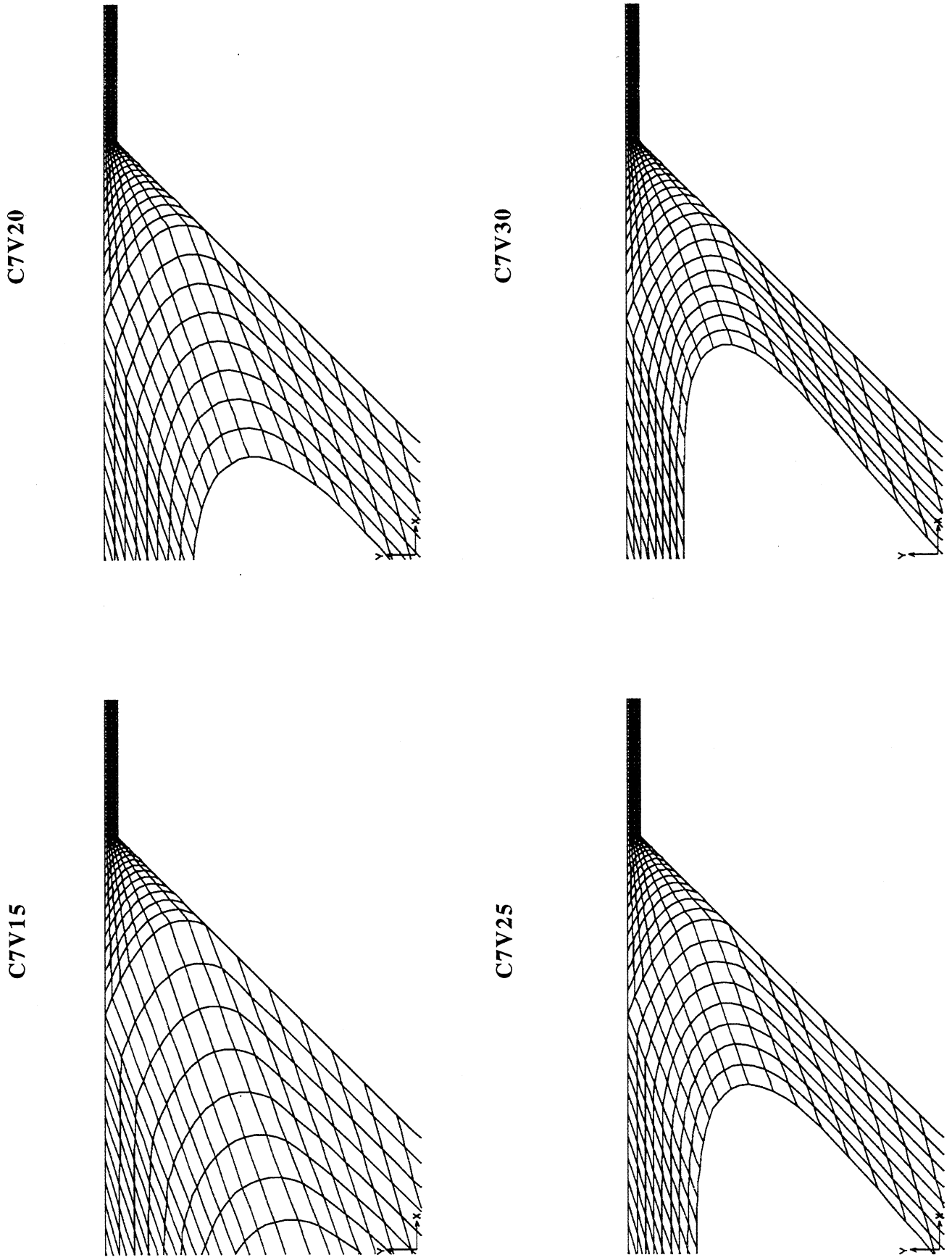

Figure 48

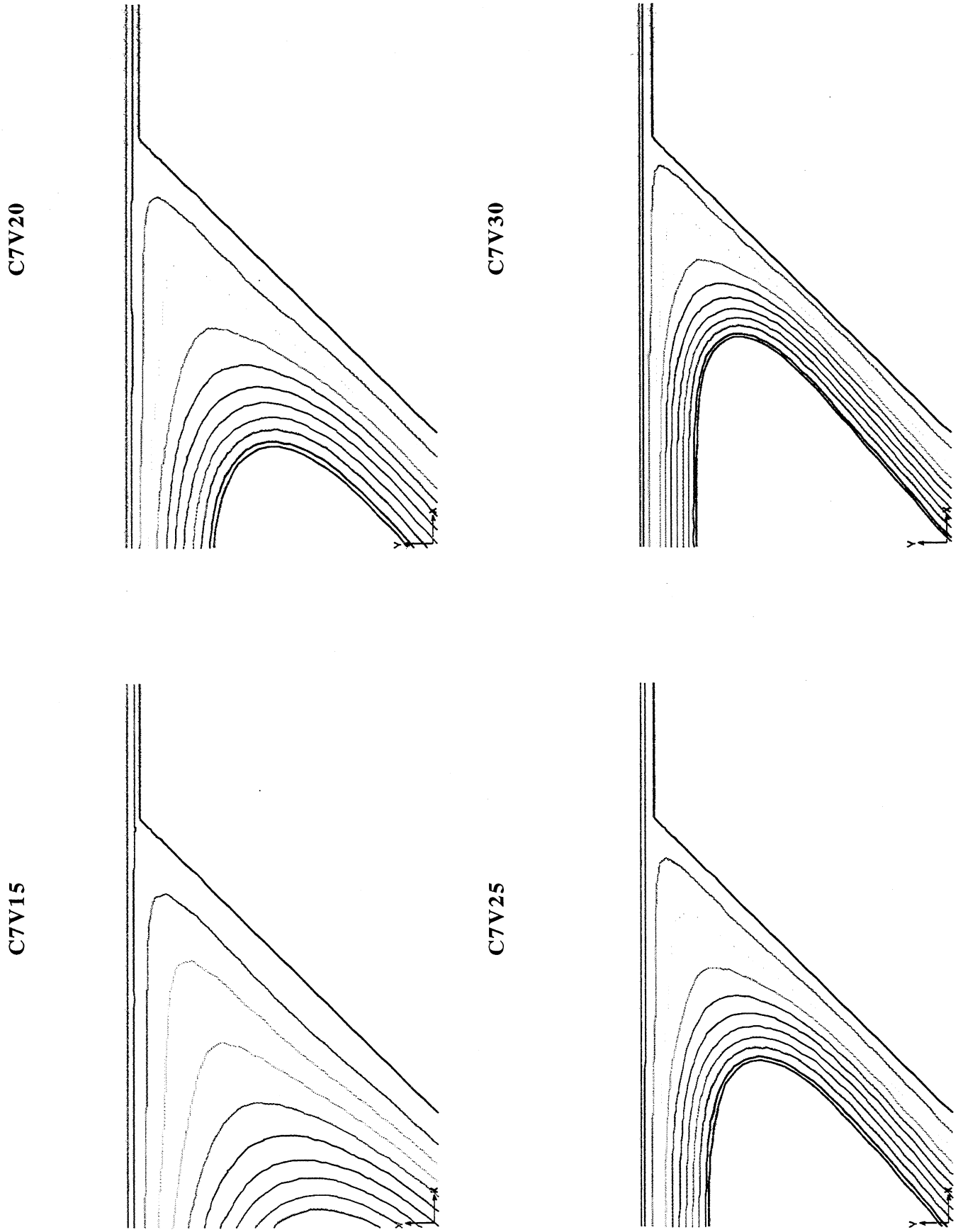

Figure 49

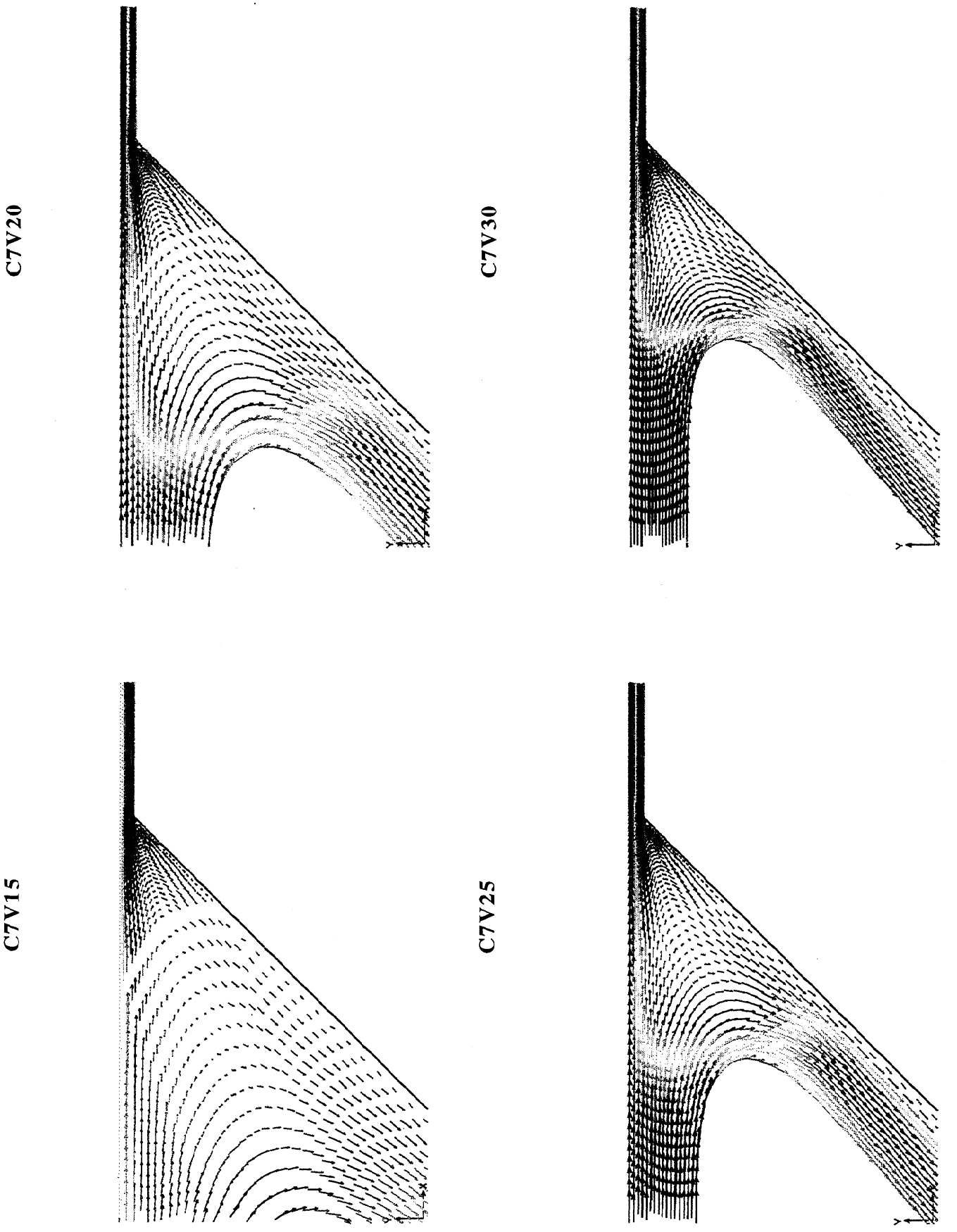

Figure 50

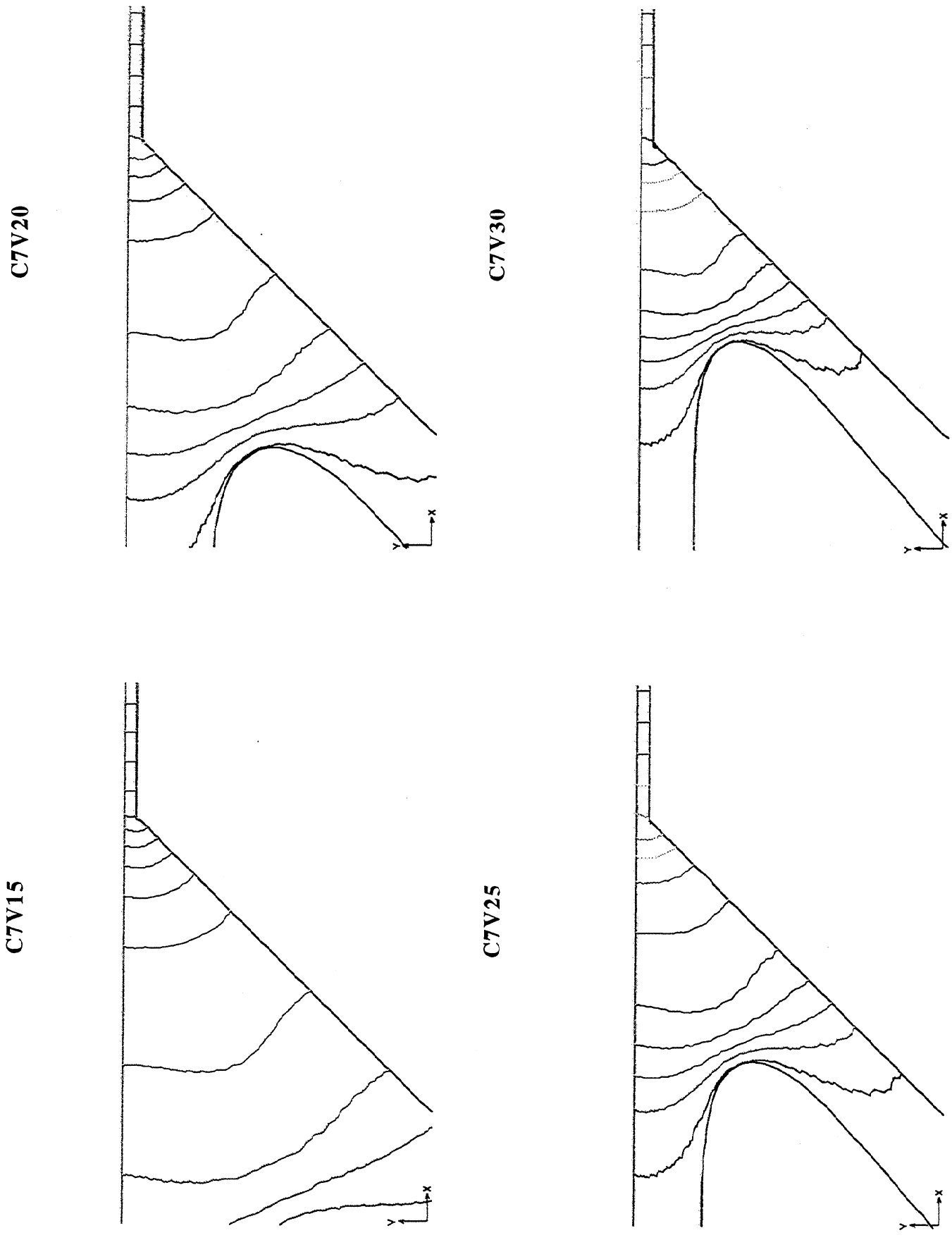

Figure 51

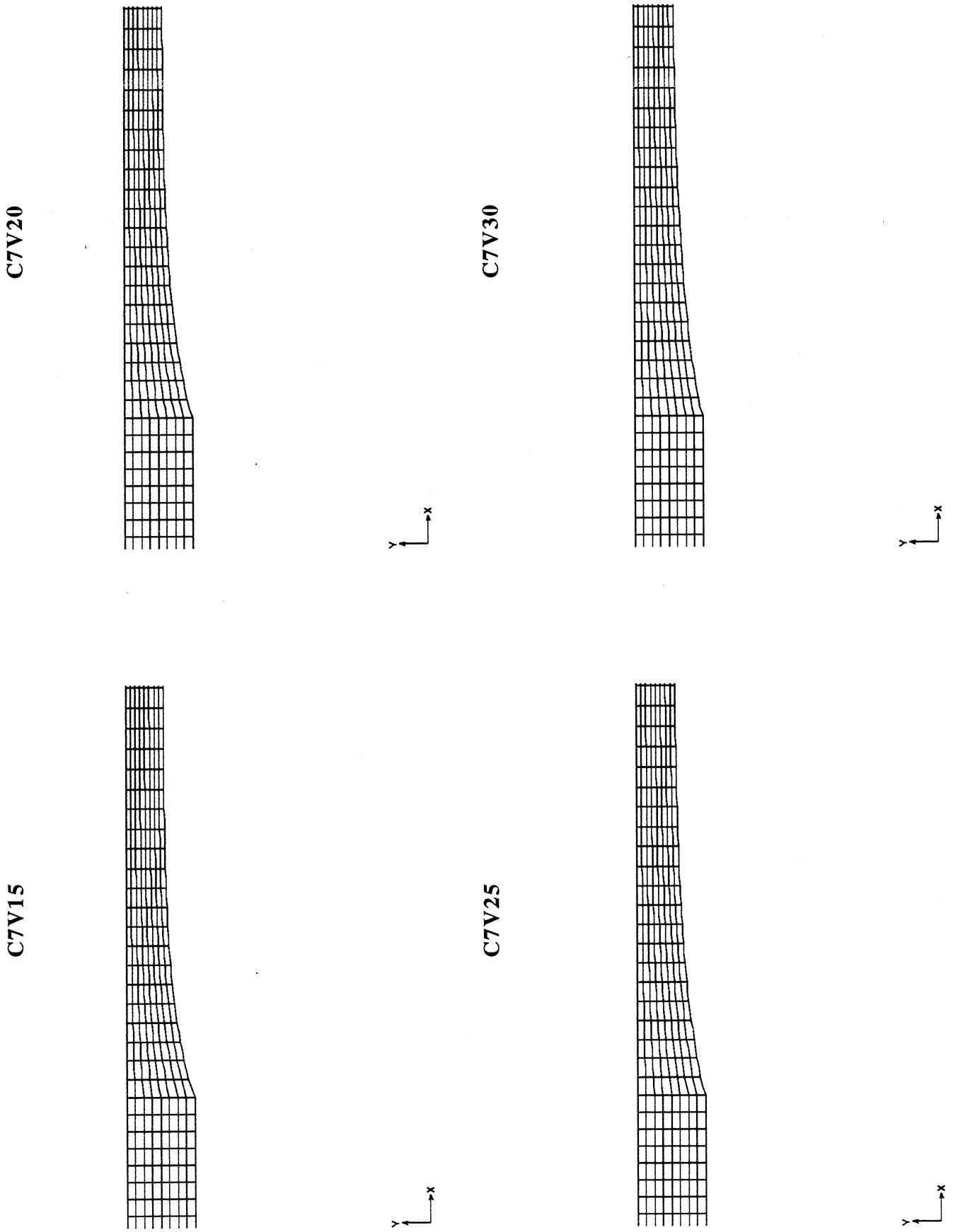

3595 Accomplishments:

- Negotiated agreements with Beloit on commercialization of IPST impulse drying technology for board grades.
- Obtained DOE funding and Beloit involvement and contributions for a two-year continuous high-speed pilot impulse drying development and evaluation project.

Figure 53

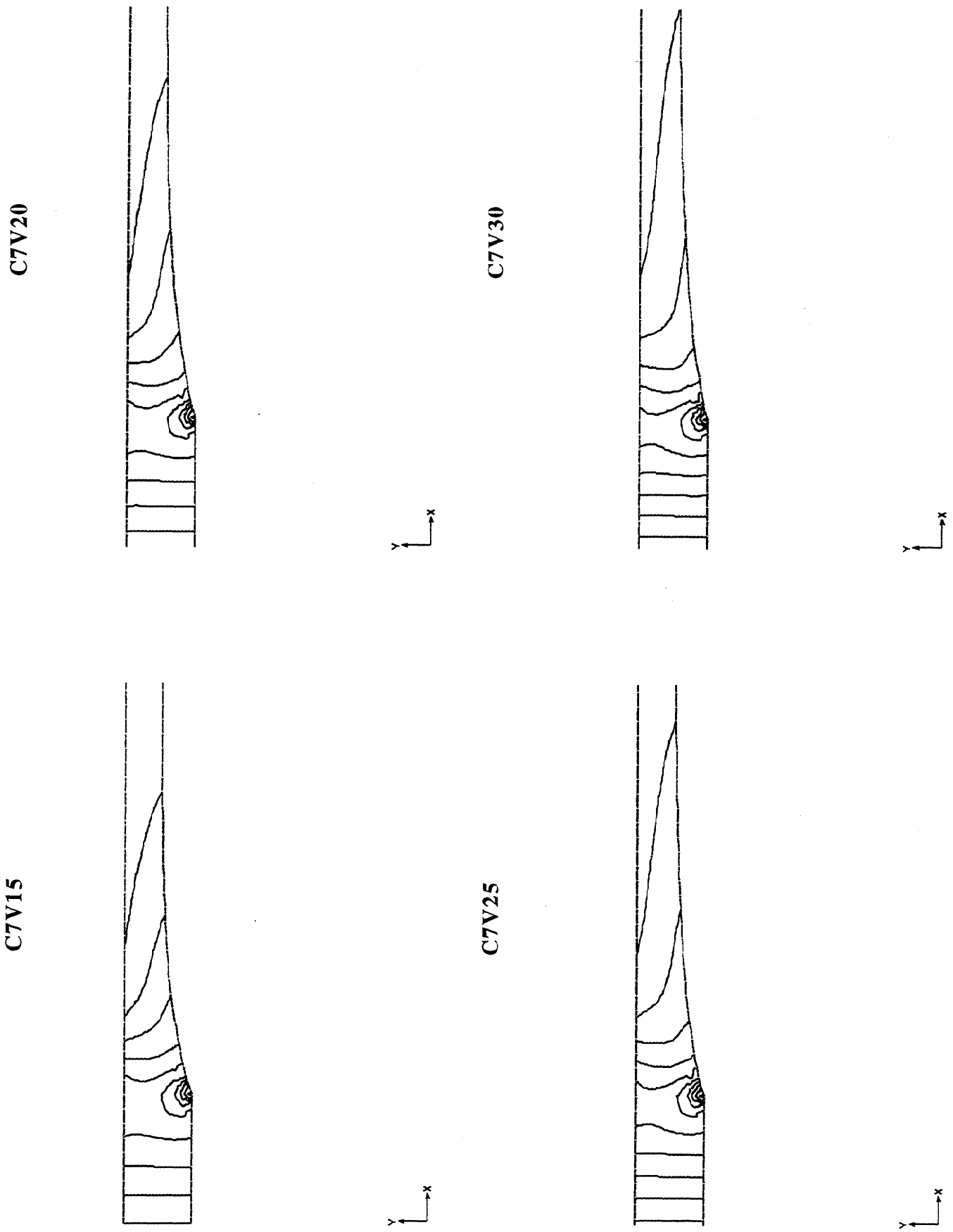

Figure 54

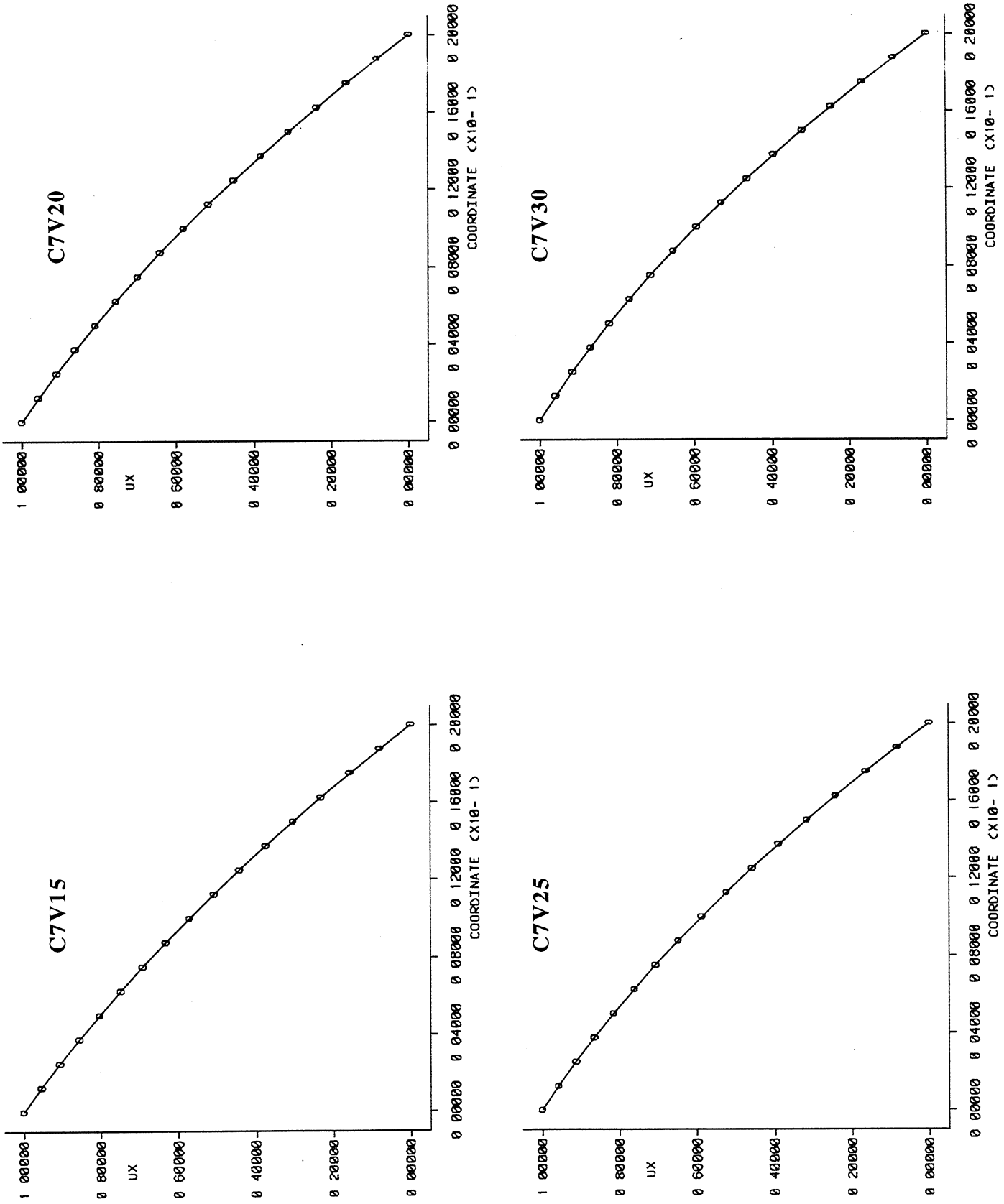
C7V20
C7V30
C7V15
C7V25
UX
COORDINATE (X10- 1)
1 00000
0 80000
0 60000
0 40000
0 20000
0 00000
0 00000
0 04000
0 08000
0 12000
0 16000
0 20000

Figure 55

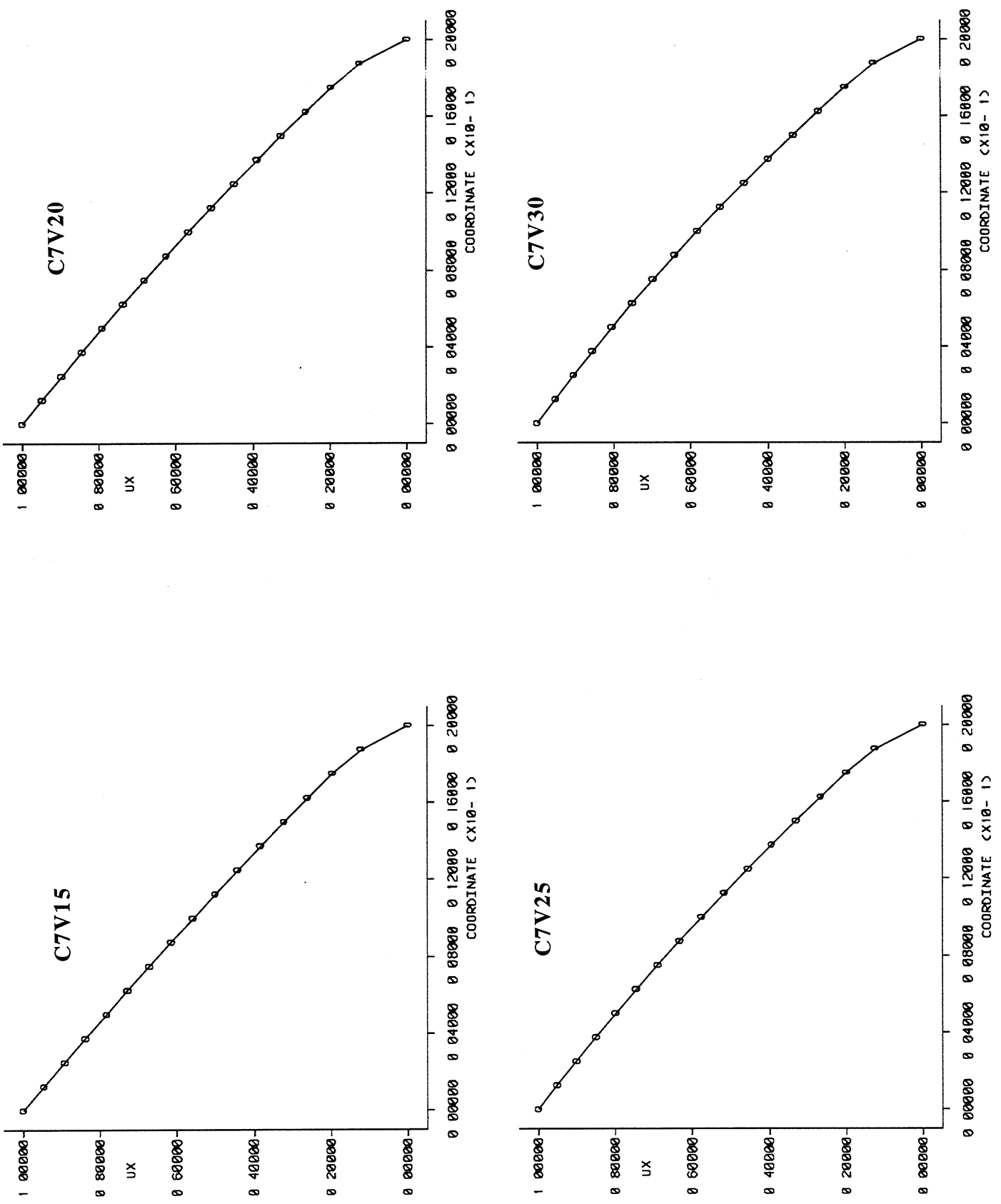

Figure 56

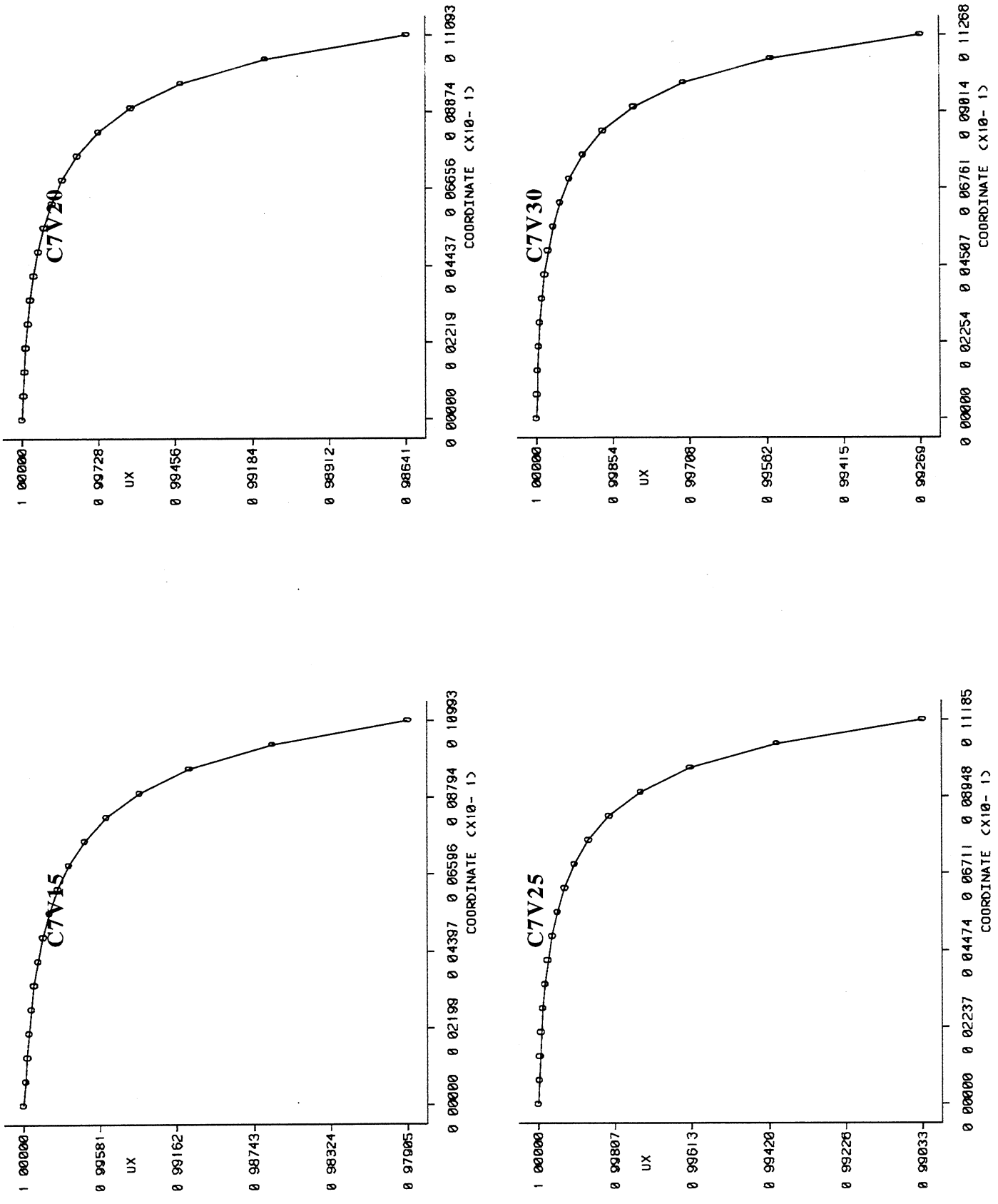

Figure 57

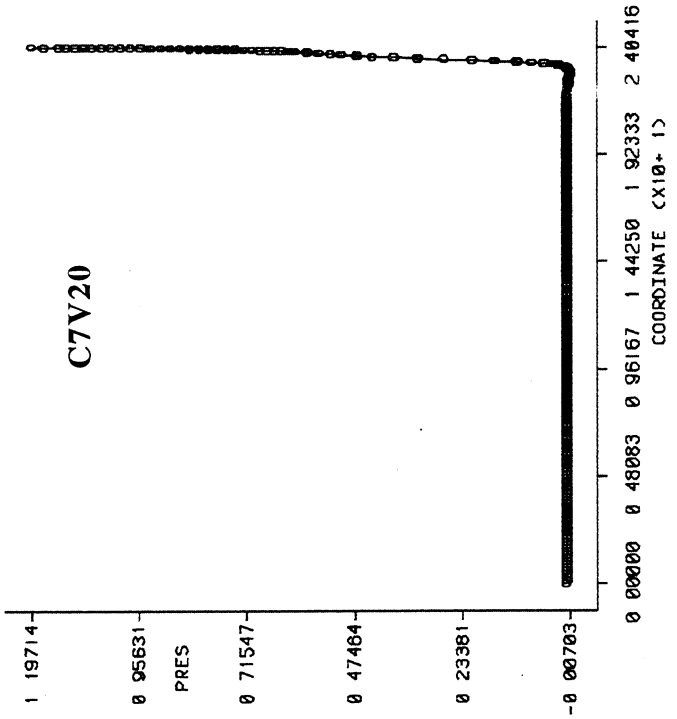
C7V20
1 19714
0 95631
PRES
0 71547
0 47464
0 23381
-0 00703
0 00000 0 48083 0 96167 1 44250 1 92333 2 40416
COORDINATE (X10+ 1)

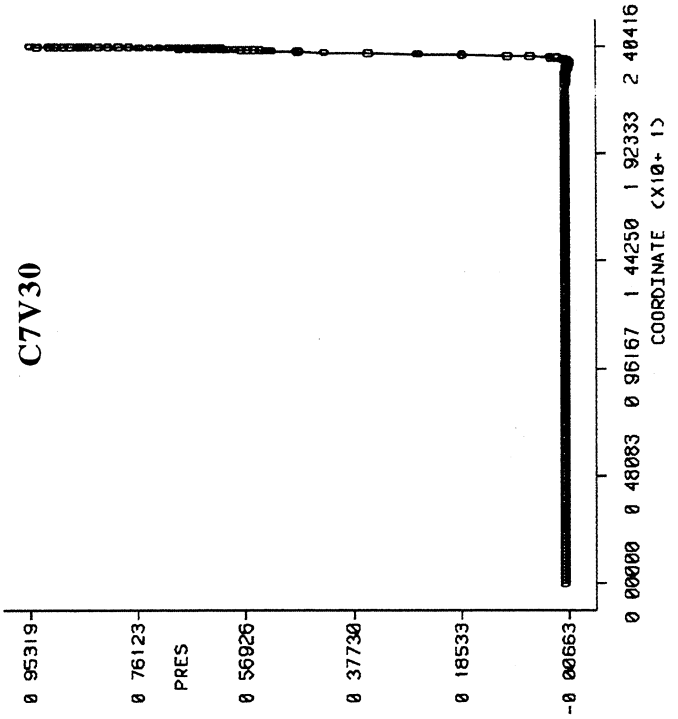
C7V30
0 95319
0 76123
PRES
0 56926
0 37730
0 18533
-0 00663
0 00000 0 48083 0 96167 1 44250 1 92333 2 40416
COORDINATE (X10+ 1)

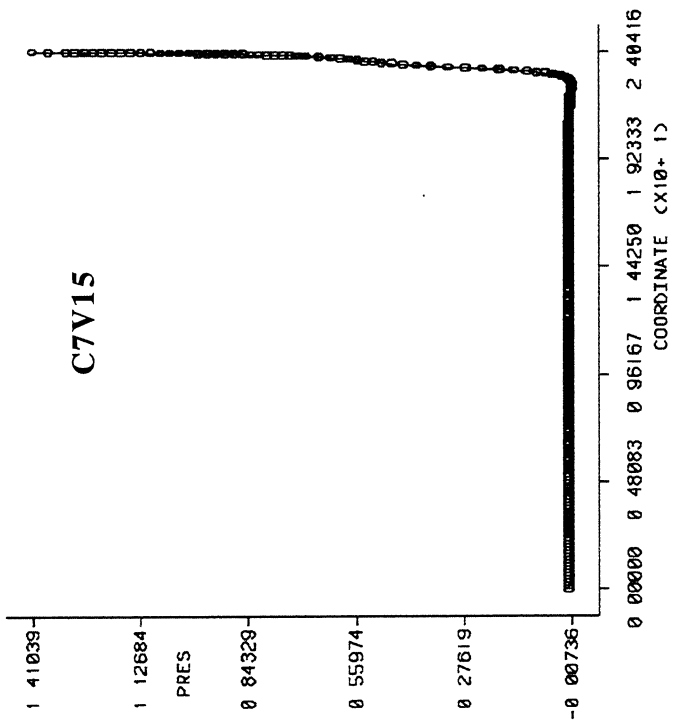
C7V15
1 41039
1 12684
PRES
0 84329
0 55974
0 27619
-0 00736
0 00000 0 48083 0 96167 1 44250 1 92333 2 40416
COORDINATE (X10+ 1)

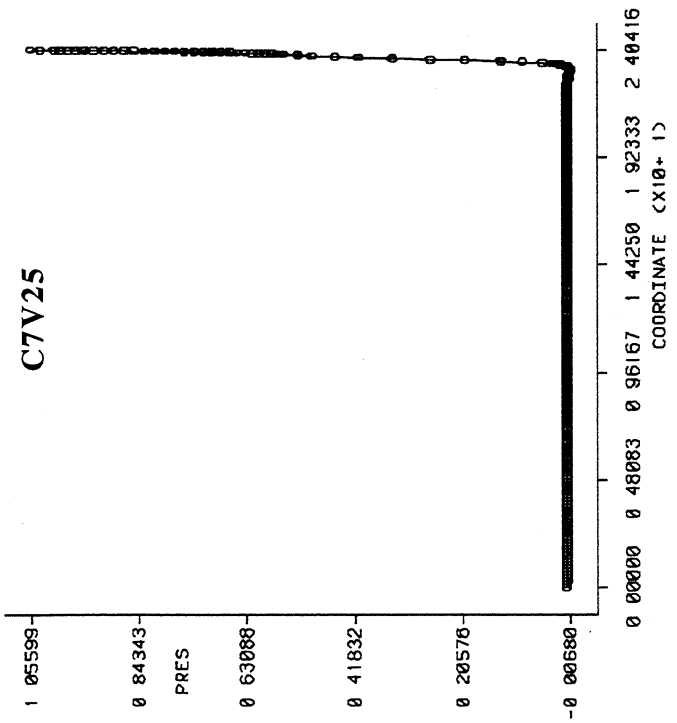
C7V25
1 05599
0 84343
PRES
0 63088
0 41832
0 20576
-0 00680
0 00000 0 48083 0 96167 1 44250 1 92333 2 40416
COORDINATE (X10+ 1)

Figure 58

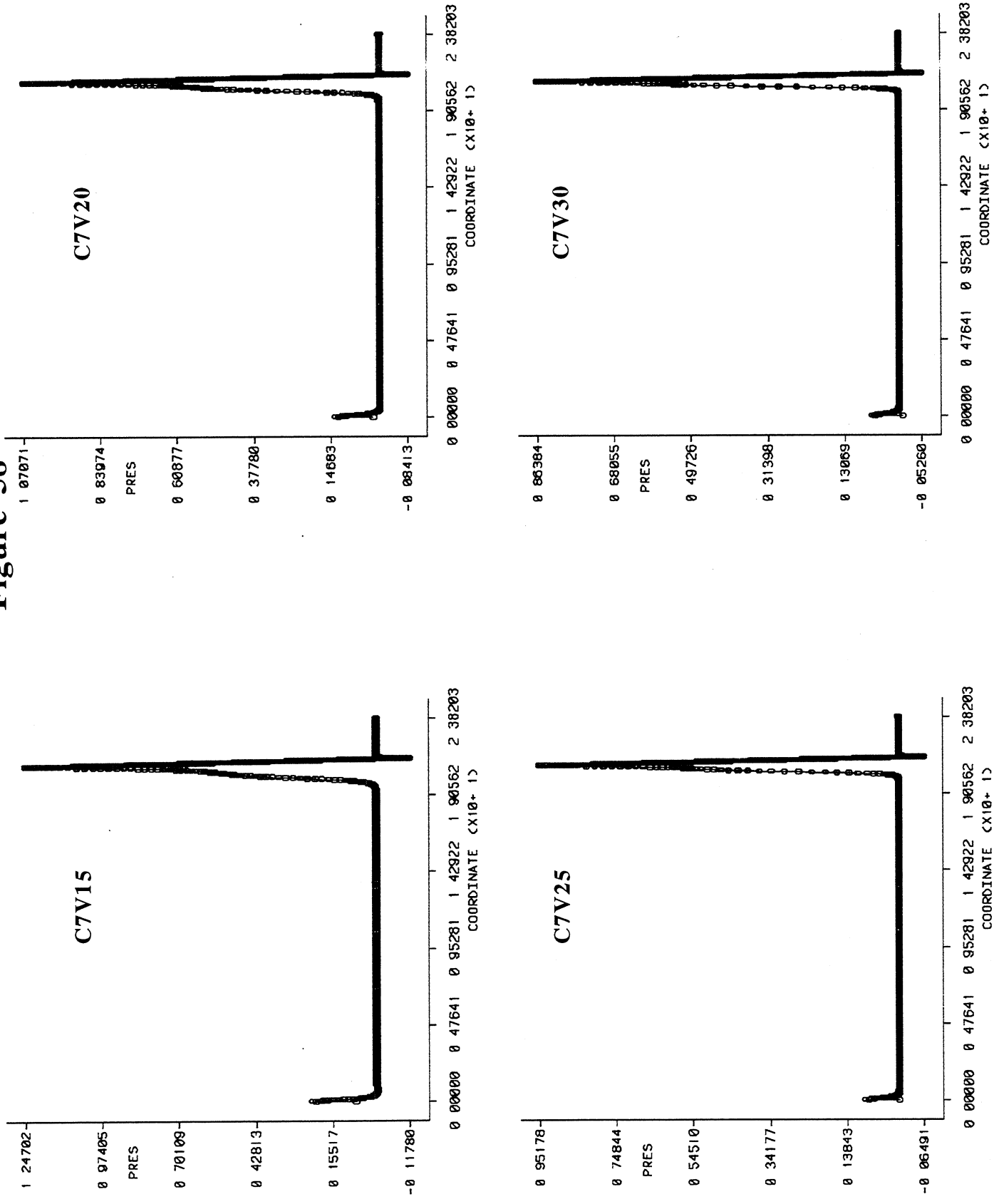

Figure 59

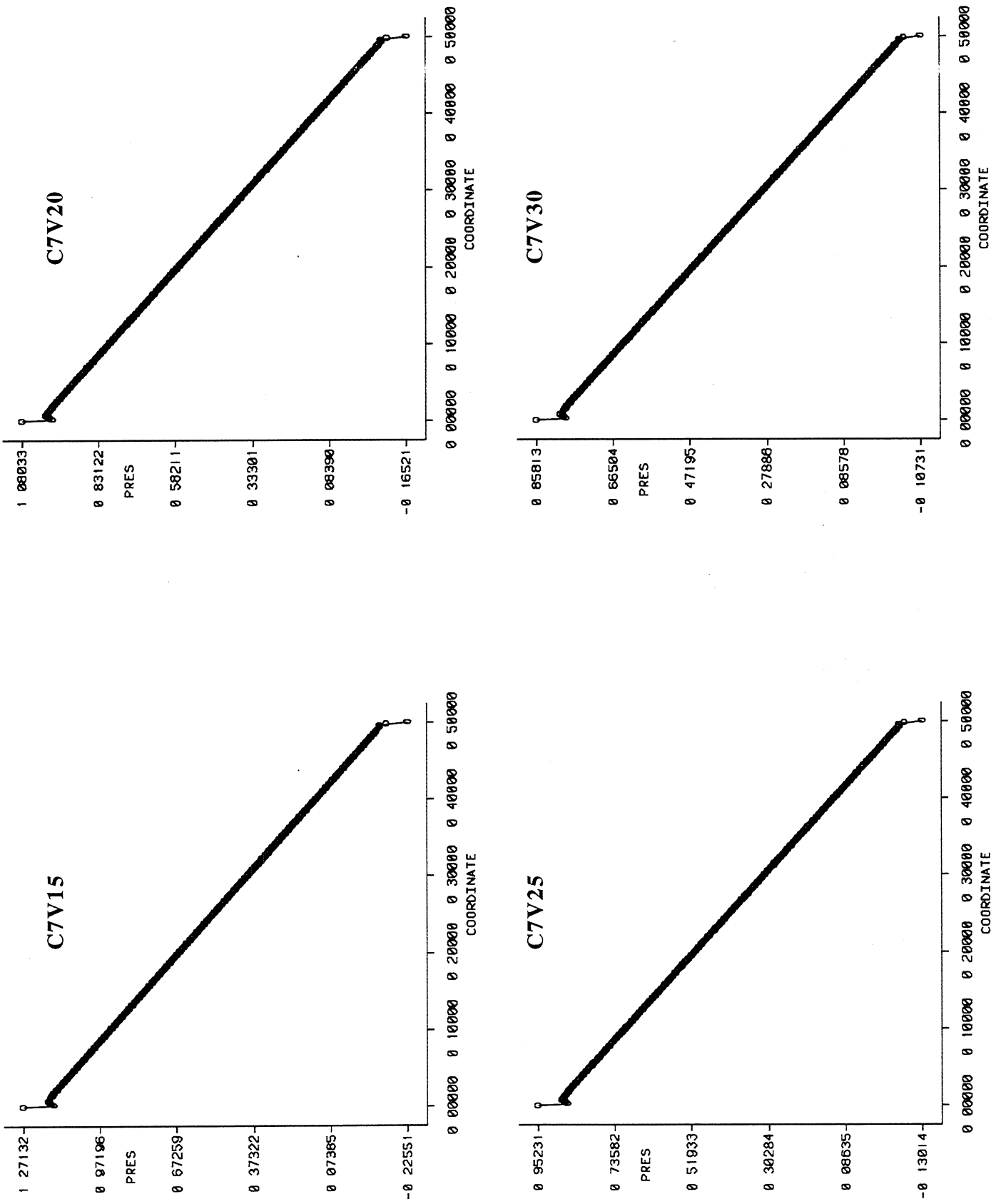
C7V15
C7V20
C7V25
C7V30
PRES
COORDINATE
1 27132
0 97196
0 67259
0 37322
0 07385
-0 22551
1 08033
0 83122
0 58211
0 33301
0 08390
-0 16521
0 95231
0 73582
0 51933
0 30284
0 08635
-0 13014
0 85813
0 66504
0 47195
0 27886
0 08578
-0 10731
0 000000
0 100000
0 200000
0 300000
0 400000
0 500000

Figure 60

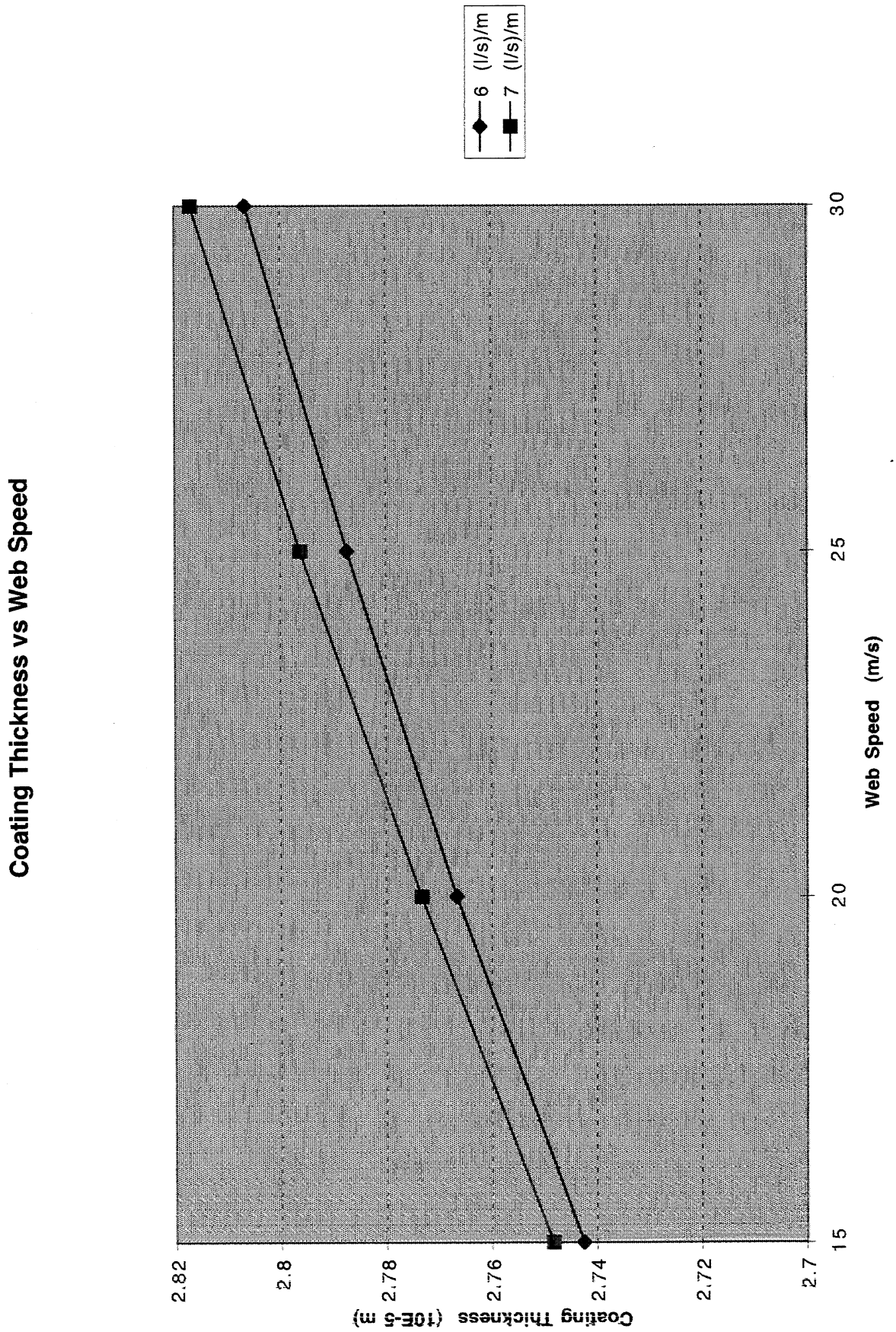
Coating Thickness vs Web Speed
6 (l/s)/m
7 (l/s)/m
Coating Thickness (10E-5 m)
2.82
2.8
2.78
2.76
2.74
2.72
2.7
15
20
25
30
Web Speed (m/s)

Figure 61

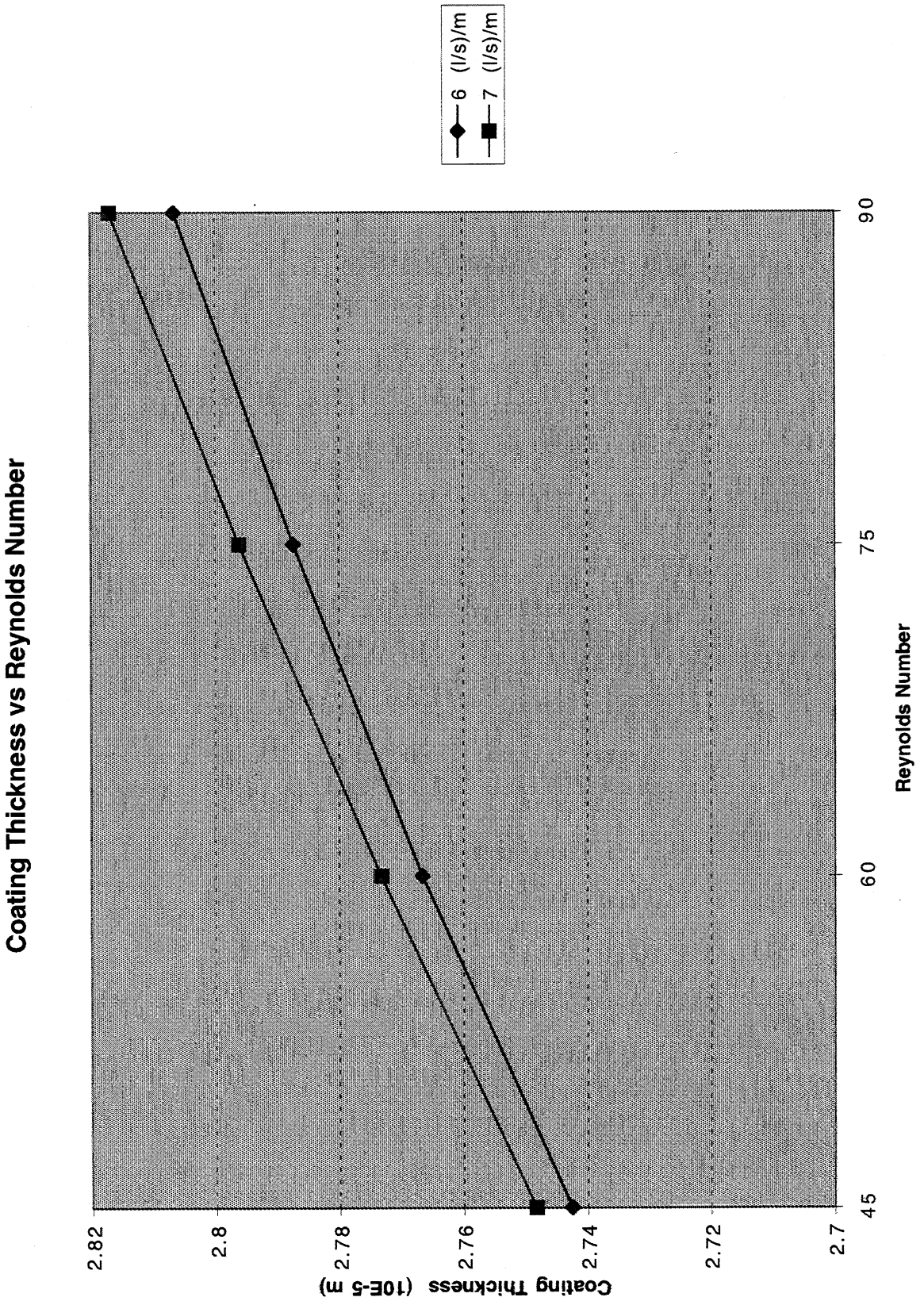
Coating Thickness vs Reynolds Number
6 (l/s)/m
7 (l/s)/m
Coating Thickness (10E-5 m)
2.82
2.8
2.78
2.76
2.74
2.72
2.7
45
60
75
90
Reynolds Number

Figure 62

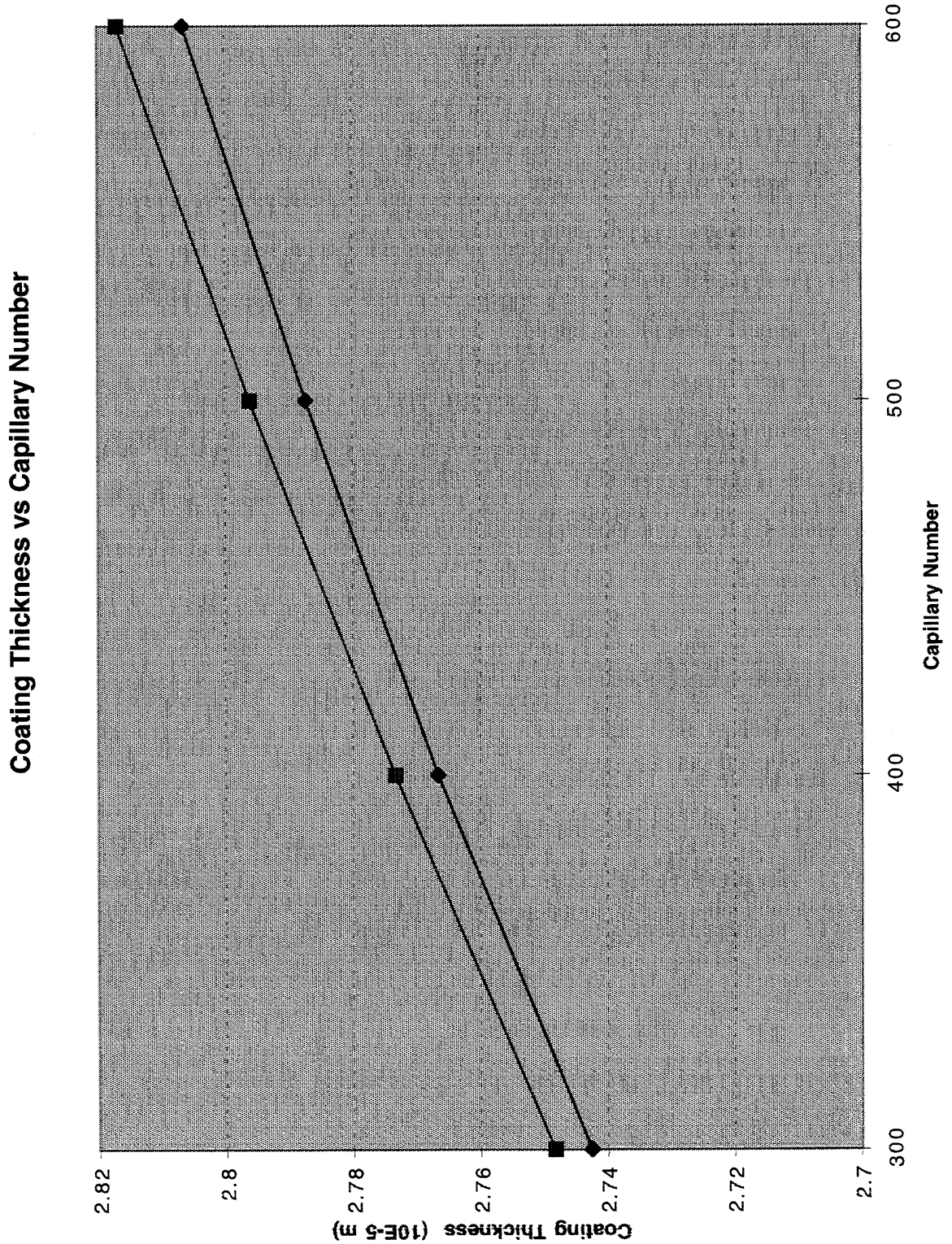
Coating Thickness vs Capillary Number
6 (l/s)/m
7 (l/s)/m
Coating Thickness (10E-5 m)
2.82
2.8
2.78
2.76
2.74
2.72
2.7
300
400
500
600
Capillary Number

AIR-SHEET INTERACTIONS

STATUS REPORT

FOR

PROJECT F006 (3730)

Xiaodong Wang

March 18 - 19, 1996

Institute of Paper Science and Technology
500 10th Street, N.W.
Atlanta, Georgia 30318

Project F006 Status Report

AIR-SHEET INTERACTION PROJECT

by

Xiaodong Wang, Assistant Professor of Engineering

Submitted to the Institute of Paper Science and Technology
on March 18, 1996

Abstract

In this status report, the progress made during the period from October 7, 1995, to March 17, 1996, are presented.

To predict accurately the natural frequencies and modeshapes of the coupled system between a traveling pretensioned web and its surrounding air, a reliable mixed displacement/pressure finite element procedure is applied to the complete surrounding air domain. It is shown analytically that the previous coupled natural frequency prediction based on the computational model with only the added mass effects shall be noticeably higher than the experimental measurements.

In order to suppress the out-of-plane displacement of the moving web and consequently reduce the likelihood of wrinkling and sheet breakage, a two-sided sheet flutter suppression device was proposed at the Fall 95 PAC meeting. The formulations based on the lubrication theory are presented in this report. It is expected that the suppression device will provide both the middle support and damping effects on the traveling web. In addition, this type of device can be used along with certain control systems as the mounting stage for online sensors.

From the comparison of different dynamical behaviors with and without the suppression device, the effectiveness of such devices is highly anticipated.

Acknowledgments

I would like to thank Professor Cyrus Aidun for helping me to start working on this challenging project and providing valuable comments. I would also like to acknowledge Dr. Maclin Hall for pointing out important references, and to George Renner, one of my graduate students.

Introduction

With the increase of the machine speed in paper, thin film, and textile manufacturing processes, the vibration and instability of the traveling web have received much attention. In addition, the development of online nondestructive sensors requires better understanding of the dynamical effects of the air-sheet interactions.

Air-Sheet Interaction Project at IPST was initiated by Prof. C. Aidun and Prof. P. Neitzel two years ago. During the past two years, they have made a good start and published two papers related to their research work [1] [2]. During the last PAC meeting (Oct. 5–6, 1995), it was agreed that I will continue the work of this project. Naturally, there might be some slight modifications of the planning and the time tables to be followed; however, the main objectives of this project stay the same:

- to gain a better understanding of the fluid dynamics and its interaction with sheet fluttering;
- to correlate the traveling sheet dynamical behavior with the paper physical properties (such as CD and MD basis weight) variation, roll eccentricity, and tension variations;
- to develop and to analyze sheet flutter suppression devices; and

- to extend the results to the analysis of blade deformation and vibration effects in coating processes.

Some statistics of this project are listed below:

Project Title:	**Air-Sheet Interaction**
Project Code:	**AIRPA**
Project Number:	**3730 (F006)**
PAC:	**Papermaking**
Division:	**Engineering and Paper Materials**
Project Leader:	**Xiaodong Wang**
Budget (FY94-FY95):	**$149,600.00**
Budget (FY95-FY96):	**$164,200.00**

This status report contains the progress made during the research period between Fall 95 and Spring 96 PAC meetings.

In order to analytically explain why the previously computed frequencies are always higher than the experimental results, in chapter 2, a fully coupled 2D model of a traveling pretensioned web interacting with its surrounding air (assumed isentropic, inviscid, and slightly compressible) has been analyzed with both the mixed displacement/pressure finite element formulation and the pressure formulation. It is shown analytically that both the added mass and added stiffness effects are introduced from the surrounding air. Therefore, the discrepancy between the previous computational and experimental results can be explained on a mathematical basis.

For the traveling pretensioned web, the web vibration may be induced by aerodynamics of the surrounding air, roll eccentricity, basis weight variations, and the tension variation; and it causes problems such as wrinkling, sheet breakage, and other runnability problems. This phenomenon is often called sheet flutter. To avoid the modification of the existing machine design, an easily installable and retrievable suppression device was presented in the last PAC meeting. In chapter 3, nonlinear

finite element formulations are developed for the mathematical model including the paper porosity. Although the analysis is only in the theoretical stage, it is anticipated that further research will continue towards the actual design. Of course, if during the detail design process, the lubrication theory becomes invalid for some geometrical restrictions, the full Navier-Stokes equations should be applied. In chapter 4, the computational simulation of the traveling pretensioned web with the expected damping effects from the sheet flutter suppression device is obtained and compared with those results without the suppression device.

Surrounding Air Effects

2.1 Introduction

The natural frequencies of axially moving material in vacuum have been studied by Sack [3], Archibald and Emslie [4], Mote [5], Wickert and Mote [6] and others researchers both analytically and numerically. Furthermore, the change of the unique behaviors of two additional inertia terms (gyroscopic and centrifugal) with the added mass effects are discussed in refs [7] [8] [9]. Their results of the critical velocities and the eigen frequencies are only 15-30% of the earlier predictions in vacuum [10]; however, an experimental discrepancy was discovered, i.e., the experimental frequency measurements are always lower than the numerical predictions with the added mass effects. It is also noticed that the added mass effects introduced previously are based on the assumption that the surrounding air domain is infinite, which in actuality is very different from the air pockets on paper machines. In this chapter, we will show analytically the fundamental reason for the observed discrepancy and discuss the numerical procedures to accurately predict the coupled natural frequencies.

To fully predict the dynamic coupling behavior between a structure and surrounding flows, a number of finite element formulations have been proposed; namely, the displacement formulation (see Bathe and Hahn [11], Akkas et al [12], Hamdi et al [13],

Belytschko and Kennedy [14], Belytschko [15], Olson and Bathe [16]), the displacement potential and pressure formulation (Morand and Ohayon [17]), and the velocity potential formulation (Everstine [18], Olson and Bathe [19], Felippa and Ohayon [20]). For the inviscid and irrotational fluids, the displacement (or the velocity) potential and pressure are often used instead of the displacement or velocity unknowns. Recently, the primitive variable formulations have received considerable attention because they do not require any special interface conditions or new solution strategies (for example, in frequency calculations and response spectrum analysis). Moreover, the true mass and stiffness matrices generated from these formulations provide convenience in solving general coupled problems. With the ever-increasing availability of high-speed and large-capacity computers, this approach shows great promise in general applications to the solution of a broad range of problems (specifically nonlinear problems).

To demonstrate the fundamental reason for the observed discrepancy, in this chapter, we will use both the mixed displacement/pressure formulation and the pressure formulation. As should be noted, the mixed displacement/pressure formulation with the mixed elements satisfying the inf-sup condition is highly recommended in practice [21] [22] [23].

From the analytical derivation, it is found that the surrounding air contributes not only added mass effects but also added stiffness effects. Since the traditional added mass concept is based on the incompressibility assumptions, i.e., the bulk modulus $\kappa = \infty$, naturally, the predicted frequencies will be higher than the physical ones with the actual finite compressibility of the surrounding air [24].

2.2 Governing Equations

Our ultimate interest in this project is to understand the edge effects of the sheet fluttering as well as the uniform transverse motion, therefore, we need to analyze

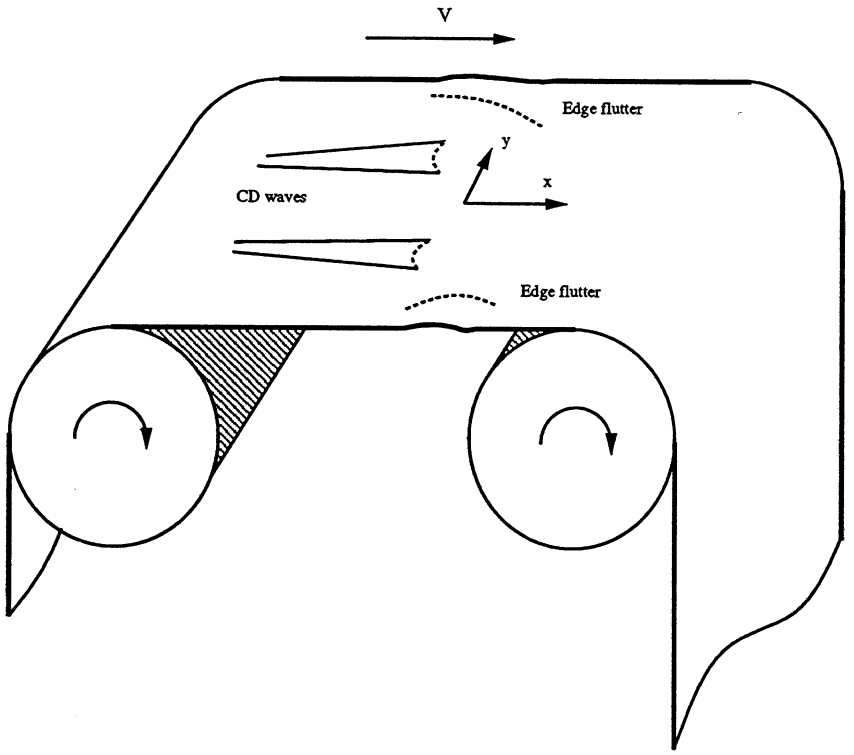

Figure 2-1: Three-dimensional traveling pretensioned thin wide material.

the complete 3D coupled problem which involves the 3D aerodynamic effects and a traveling pretenioned thin structure shown in Fig. 2-1. At this early stage of the project, we will consider the 2D model as shown in Fig. 2-2. The justification of this model is that in a common web handling machine, the paper is considerably wide, therefore, to understand the transverse dynamical behavior, this 2D model is applicable. In addition, this 2D model will provide a good starting point for us to focus on the dynamic aspects of air-sheet interaction and development of flutter suppression devices. Although vibrations of this 2D axially moving model in vacuum has been extensively studied, many nonlinear dynamic aspects, such as the introduction of second order tension variation and viscoelastic material, still remain unsolved [25] [26]. Therefore, the complication of including the surrounding air effects needs to be understood before we study the more realistic 3D model.

Ignoring the stiffness contribution from the bending effects, the traveling pretensioned web is governed by

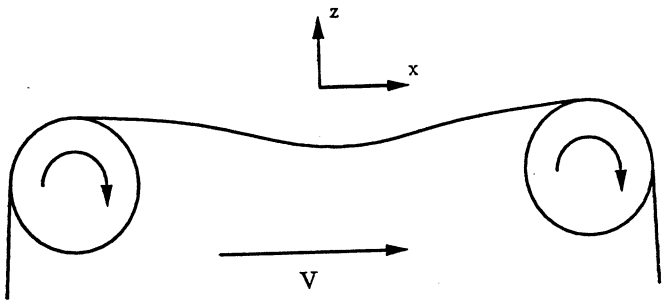

Figure 2-2: The simplified 2D model of a traveling pretensioned web.

$$m\frac{\partial^2 w}{\partial t^2} + 2mV\frac{\partial^2 w}{\partial x \partial t} + (mV^2 - T)\frac{\partial^2 w}{\partial x^2} = f(x,t) \tag{2.1}$$

with the boundary and initial conditions

$$\begin{aligned} w(x,t)|_{x=0} &= w(x,t)|_{x=L} = 0 \\ w(x,t)|_{t=0} &= w(x,0) \\ \frac{\partial w(x,t)}{\partial t}|_{t=0} &= \frac{\partial w(x,0)}{\partial t} \end{aligned} \tag{2.2}$$

where $w(x,t), m, L, f$, and V denote the out-of-plane displacement, mass per unit length, open draw length, excitation force distribution and traveling velocity, respectively. To include the surrounding air effects explicitly, in refs [8] [27], different added mass effects, $m1, m2$, and $m3$ are introduced to the inertia, gyroscopic, and centrifugal terms. Consequently, Eq. (2.2) is changed to

$$(m+m1)\frac{\partial^2 w}{\partial t^2} + 2(m+m2)V\frac{\partial^2 w}{\partial x \partial t} + ((m+m3)V^2 - T)\frac{\partial^2 w}{\partial x^2} = f_1(x,t). \tag{2.3}$$

To confirm the added mass effects, some experimental natural frequency measurements were taken and compared with the analytical predictions [7] [8] [9]. It was

found that the measured frequencies are much closer to the analytical solutions with the added mass effects than to the predictions without added mass effects [10]. However, the measured frequencies are always noticeably lower than the numerical predictions. This suggests that the mathematical mode of the surrounding air with only the consideration of added mass effects, i.e., assuming incompressible and inviscid, is inadequate. In the next section, we will introduce an isentropic, inviscid acoustic fluid model for the surrounding air and apply both the mixed displacement/pressure formulation and the pressure formulation [22] [23] [28] [29].

2.3 Displacement/Pressure (u/p) Formulation

The variational approaches for potential-based formulations are discussed in [30], in this section, for our mixed displacement/pressure formulation, we define a variational indicator

$$\Pi = \int_{\Omega} \{\frac{p^2}{2\beta} - \mathbf{u} \cdot \boldsymbol{f}^B - \lambda_p(\frac{p}{\beta} + \nabla \cdot \mathbf{u})\} d\Omega + \int_{S_f} \bar{p}\, u_n^s \, dS$$

where the variables are p, $\mathbf{u}$, and the Lagrange multiplier λ_p. We note that the first two terms correspond to the usual strain energy (given in terms of the pressure) and the potential of the externally applied body forces. The third term implies the mass conservation equation. The last term is the potential due to any applied boundary pressure on the surface S_f. Ω and S stand for the fluid domain and its boundary as shown in Fig. 2-3.

Invoking the stationarity of Π, we identify the Lagrange multiplier λ_p to be the pressure p and obtain the governing equations

$$\nabla p - \boldsymbol{f}^B = 0 \tag{2.4}$$

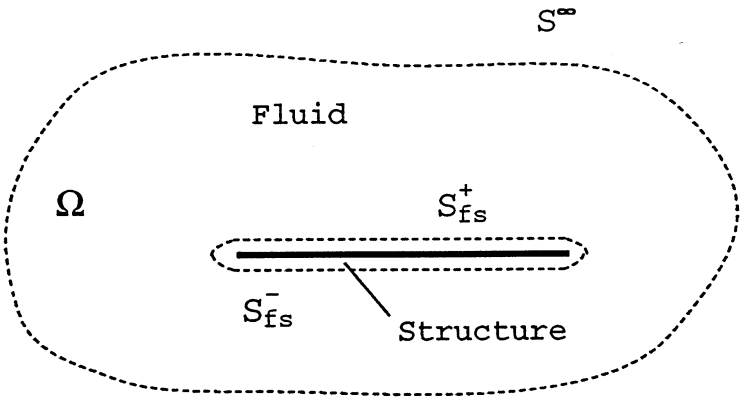

Figure 2-3: The mathematical model of the fluid-structure coupled system.

$$\nabla \cdot \mathbf{u} + \frac{p}{\beta} = 0 \tag{2.5}$$

with the boundary conditions

$$\begin{aligned} \mathbf{u} \cdot \mathbf{n} &= \bar{u}_n \quad \text{on } S_u \\ p &= \bar{p} \quad \text{on } S_f. \end{aligned} \tag{2.6}$$

Applying the standard Galerkin discretization procedure, and hence for a typical finite element, we have

$$\begin{aligned} \mathbf{u} &= \mathbf{H}\widehat{\mathbf{U}} \\ p &= \mathbf{H}_p\widehat{\mathbf{P}} \\ \nabla \cdot \mathbf{u} &= (\nabla \cdot \mathbf{H})\widehat{\mathbf{U}} = \mathbf{B}\widehat{\mathbf{U}} \end{aligned}$$

where $\mathbf{H}$ and $\mathbf{H}_p$ are the interpolation matrices, and $\widehat{\mathbf{U}}$ and $\widehat{\mathbf{P}}$ are the vectors of solution variables.

The matrix equations of the u/p formulation are

$$\begin{bmatrix} \mathbf{M} & \mathbf{0} \\ \mathbf{0} & \mathbf{0} \end{bmatrix} \begin{Bmatrix} \ddot{\widehat{\mathbf{U}}} \\ \ddot{\widehat{\mathbf{P}}} \end{Bmatrix} + \begin{bmatrix} \mathbf{0} & \mathbf{L} \\ \mathbf{L}^T & \mathbf{A} \end{bmatrix} \begin{Bmatrix} \widehat{\mathbf{U}} \\ \widehat{\mathbf{P}} \end{Bmatrix} = \begin{Bmatrix} \mathbf{R} \\ \mathbf{0} \end{Bmatrix} \tag{2.7}$$

where

$$\mathbf{M} = \int_{\Omega} \rho \mathbf{H}^T \mathbf{H} d\Omega, \qquad \mathbf{L} = -\int_{\Omega} \mathbf{B}^T \mathbf{H}_p d\Omega;$$
$$\mathbf{A} = -\int_{\Omega} \frac{1}{\beta} \mathbf{H}_p^T \mathbf{H}_p d\Omega, \qquad \mathbf{R} = -\int_{S_f} \mathbf{H}_n^{S^T} \bar{p}\, dS.$$

The variational equation for the traveling web with the consideration of surrounding air can be written as

$$\int_0^L \{\delta w m \frac{\partial^2 w}{\partial t^2} + 2mV\delta w \frac{\partial^2 w}{\partial x \partial t} - (mV^2 - T)\frac{\partial \delta w}{\partial x}\frac{\partial w}{\partial x} + \delta w(p^+ - p^-)\} dl = 0 \qquad (2.8)$$

where p^+ and p^- are the pressures on the upper and lower surfaces S_{fs}^+ and S_{fs}^- shown in Fig 2-3. Combine Eqs. (2.8) and (2.7) during the matrix assemblage, and condense out the pressure unknowns, we automatically achieve the coupling between the web and its surrounding air

$$\mathbf{M}_h \ddot{\widehat{\mathbf{U}}} + \mathbf{C}_h \dot{\widehat{\mathbf{U}}} + \mathbf{K}_h \widehat{\mathbf{U}} = \mathbf{R}_h \qquad (2.9)$$

where the effects of compressibility $-\mathbf{L}\mathbf{A}^{-1}\mathbf{L}^T$ is included in $\mathbf{K}_h$ and the added mass $\mathbf{M}$ is included in $\mathbf{M}_h$. Neglect the thickness of the traveling web, we have

$$w^+ = w^- = w \qquad (2.10)$$

where w^+ and w^- are the out-of-plane displacements on S_{fs}^+ and S_{fs}^-. Note that the tangential (or horizontal) displacements on S_{fs}^+ and S_{fs}^- are different.

It is obvious that as the bulk modulus increases, the added stiffness increases. Since the actual surrounding air introduces less added stiffness than the assumed incompressible air model, the corresponding computational predictions shall be higher than the experimental measurements.

2.4 Pressure Formulation

In the pressure formulation, we introduce the pressure as the primary unknowns for the surrounding air with the bulk modulus β, i.e., $c^2 = \frac{\beta}{\rho}$. The governing equation is then given as

$$\nabla^2 p = \frac{1}{c^2}\frac{\partial^2 p}{\partial t^2} \quad \text{on } \Omega \tag{2.11}$$

with the boundary conditions

$$\frac{\partial p}{\partial z} = -\rho\ddot{w} \quad \text{on } S_{fs}^{+} \tag{2.12}$$

$$\frac{\partial p}{\partial z} = \rho\ddot{w} \quad \text{on } S_{fs}^{-} \tag{2.13}$$

$$\frac{\partial p}{\partial n} = 0 \quad \text{on } S^{\infty}. \tag{2.14}$$

Therefore, from the variational equation

$$\int_{\Omega} \{\delta p \frac{1}{c^2}\frac{\partial^2 p}{\partial t^2} - \delta p \nabla^2 p\} d\Omega \tag{2.15}$$

with the divergence's theory and $S = S^{\infty} + S_f s^{+} + S_f s^{-}$, the following discretized equations can be derived

$$\begin{bmatrix} \mathbf{M}_{ww} & \mathbf{0} \\ \mathbf{S}_{wp}^{T} & \mathbf{M}_{pp} \end{bmatrix} \begin{Bmatrix} \ddot{\mathbf{W}} \\ \ddot{\mathbf{P}} \end{Bmatrix} + \begin{bmatrix} \mathbf{C}_{ww} & \mathbf{0} \\ \mathbf{0} & \mathbf{0} \end{bmatrix} \begin{Bmatrix} \dot{\mathbf{W}} \\ \dot{\mathbf{P}} \end{Bmatrix} + \begin{bmatrix} \mathbf{K}_{ww} & -\frac{1}{\rho}\mathbf{S}_{wp} \\ \mathbf{0} & \mathbf{K}_{pp} \end{bmatrix} \begin{Bmatrix} \mathbf{W} \\ \mathbf{P} \end{Bmatrix} = \begin{Bmatrix} \mathbf{R}_s \\ \mathbf{0} \end{Bmatrix}$$

with

$$\mathbf{M}_{ww} = \int_0^L m\mathbf{H}^T\mathbf{H}dl, \qquad \mathbf{C}_{ww} = \int_0^L 2mV\mathbf{B}^T\mathbf{H}dl;$$

$$\mathbf{K}_{ww} = -\int_0^L (mV^2 - T)\mathbf{B}^T\mathbf{B}dl, \qquad \mathbf{S}_{wp} = -\int_{S_{fs}} \rho\mathbf{H}^T\mathbf{H}_p dS;$$

$$\mathbf{M}_{pp} = \int_\Omega \frac{1}{c^2}\mathbf{H}^T\mathbf{H}d\Omega, \qquad \mathbf{K}_{pp} = \int_\Omega \mathbf{B}^T\mathbf{B}d\Omega.$$

Condense out the pressure unknowns, and apply the characteristic solution $\mathbf{W} = e^{\lambda t}\widehat{\mathbf{W}}$, along with

$$\widehat{\mathbf{P}} = -(\mathbf{K}_{pp} + \lambda^2\mathbf{M}_{pp})^{-1}\lambda^2\mathbf{S}_{wp}^T\widehat{\mathbf{W}} \tag{2.16}$$

$$(\mathbf{K}_{pp} + \lambda^2\mathbf{M}_{pp})^{-1} = \mathbf{K}_{pp}^{-1}(\mathbf{I} - \lambda^2\mathbf{M}_{pp}\mathbf{K}_{pp}^{-1} + \lambda^4(\mathbf{M}_{pp}\mathbf{K}_{pp}^{-1})^2 - ...) \tag{2.17}$$

we finally get

$$\lambda^2(\mathbf{M}_{ww} + \mathbf{M}_{ww}^a)\widehat{\mathbf{W}} + \lambda\mathbf{C}_{ww}\widehat{\mathbf{W}} + (\mathbf{K}_{ww} + \mathbf{K}_{ww}^a)\widehat{\mathbf{W}} = 0. \tag{2.18}$$

Therefore, it is clear that the added mass $\mathbf{M}_{ww}^a$ is the term $\frac{1}{\rho}\mathbf{S}_{wp}\mathbf{K}_{pp}^{-1}\mathbf{S}_{wp}^T$, and the added stiffness $\mathbf{K}_{ww}^a$ is the term $-\lambda^4\frac{1}{\rho}\mathbf{S}_{wp}\mathbf{K}_{pp}^{-1}\mathbf{M}_{pp}\mathbf{K}_{pp}^{-1}\mathbf{S}_{wp}^T$.

Notice that with the incompressible assumption, $\mathbf{M}_{pp} = 0$; and obviously for finite bulk modulus, the added stiffness effect will reduce the natural frequency compared with the incompressible case.

2.5 Conclusion

For the first approximation, some empirical added mass effects can be used to estimate the coupled system natural frequencies. However, it must be exercised with care. To accurately predict the coupled system natural frequency, and moreover, to take into

consideration the geometry of the drying pocket, the mixed displacement/pressure finite element formulation is recommended.

It is concluded that if only the added mass effects are introduced, the prediction of the coupled system natural frequency will be higher than the experimental results.

Flutter Suppression Device

3.1 Introduction

Air lubrication theory has been widely used to analyze and to design various mechanical devices where slipping bearing surfaces exist [31]. The lubrication mechanism is characterized by conformal surfaces, where relative motion introduces the desired pressure and prevents the opposing surfaces from coming into contact situation.

Some preliminary research has been done to extend the air-bearing concepts to the transportation of paper webs [32] [33]. In ref [33], Müftü and Benson proposed a device to transport paper webs (illustrated in Fig. 3-1), however, it was stated in ref [33] that "our theoretical study showed no evidence of flying for highly permeable paper webs", and the paper's porosity was concluded to be the primary cause of the total pressure leak. In addition, the idea proposed in refs [32] [33] has two other drawbacks:

- The rigid cylindrical guide is of significant size and almost block one side of the paper web; therefore, the dry pocket heat transfer is expected to be greatly reduced.

- The original setting of paper web transportation and, more importantly, the

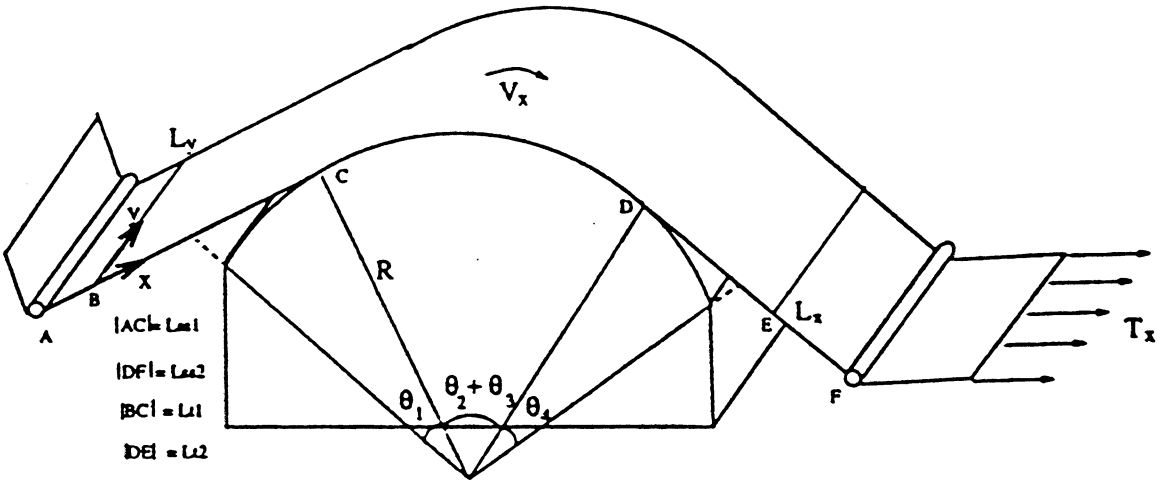

Figure 3-1: The Müftü and Benson's idea of transporting paper web over a rigid cylindrical guide.

tension distribution over the whole paper machine can be significantly changed due to the existence of the rigid cylindrical guide.

In order to overcome the above stated drawbacks, in this chapter, we propose a two-sided flutter suppression device (of course, the clearance h shall be small compared with the characteristic length L_o, i.e., the aspect ratio h/L_o and $Re(h/L_o)^2$ shall be much smaller than $O(1)$ for the lubrication theory to hold). We believe that in the best interest of minimizing the change within the dry pockets of the existing old machines and other machine designs, this type of small adaptable device is practical. In addition, certain online sensors can be also mounted on these suppression devices.

3.2 Governing Equations

The mathematical model of the 2D flutter suppression device is shown in Fig 3-2.

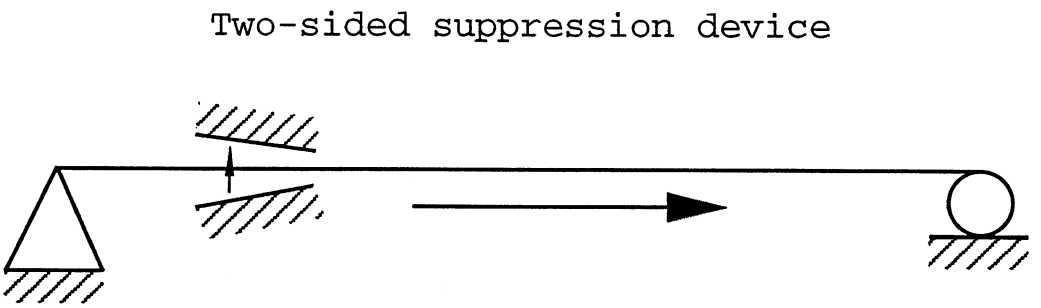

Figure 3-2: The two-sided suppression device.

The device is sited between the interval $a \leq x \leq b$, where a and b are less than L. In practice, the distance between a and b should be small compared with L so that the device will be acting as a support point with damping. We define h_1 and h_2 as the two-sided air-bearing film thicknesses, $H(x)$ as the clearance profile between the two rigid device surfaces, p_1 and p_2 as the corresponding pressures within two air lubrication regions, and v_d as the net outward velocity of a diffusion flow through porous boundary surface (the traveling paper sheet). From the Darcy's law, we can derive the following approximation

$$v_d = B(p_1 - p_2)/d \tag{3.1}$$

where d denotes the web thickness and B is the paper porosity.

The governing Reynolds equations are written as

$$-\frac{\partial}{\partial x}(\frac{1}{12\mu}\frac{\partial p_1}{\partial x}h_1^3) + \frac{\partial h_1}{\partial t} + \frac{V}{2}\frac{\partial h_1}{\partial x} + v_d = 0 \tag{3.2}$$

$$-\frac{\partial}{\partial x}(\frac{1}{12\mu}\frac{\partial p_2}{\partial x}h_2^3) + \frac{\partial h_2}{\partial t} + \frac{V}{2}\frac{\partial h_2}{\partial x} - v_d = 0 \tag{3.3}$$

with the kinematic relation

$$h_1 = \frac{H(x)}{2} - w \tag{3.4}$$

$$h_2 = \frac{H(x)}{2} + w \tag{3.5}$$

where μ stands for the viscosity of air-steam mixture.

The boundary conditions for the Reynolds equations are assumed to be

$$p_{1,2} = p_o \quad \text{at } x = 0 \tag{3.6}$$

$$p_{1,2} = p_o \quad \text{at } x = L. \tag{3.7}$$

Notice that the above boundary conditions are only true on the vicinity of the suppression device, and for the other region of the traveling pretensioned web, we have to introduce the added mass and added stiffness effects from the surrounding air.

In Eqs. (2.1), (3.2), and (3.3), we have three unknowns w, p_1 and p_2. Since the pressures and displacement unknowns relate to each other nonlinearly, we will implement the Newton-Raphson iteration scheme.

The variational forms of the governing equations are derived as

$$\begin{aligned}\delta W_w = & \int_0^L \{\delta w(m\frac{\partial^2 w}{\partial t^2} + 2mV\frac{\partial^2 w}{\partial x \partial t}) - \frac{\partial \delta w}{\partial x}(mV^2 - T)\frac{\partial w}{\partial x} \\ & -\delta w(p_1 - p_2 + mg)\}dl \end{aligned} \tag{3.8}$$

$$\begin{aligned}\delta W_{p_1} = & \int_a^b \{\frac{\partial \delta p_1}{\partial x}\frac{1}{12\mu}(\frac{H}{2} - w)^3\frac{\partial p_1}{\partial x} - \delta p_1\frac{\partial w}{\partial t} \\ & +\delta p_1 B\frac{(p_1 - p_2)}{d} - \delta p_1\frac{V}{2}\frac{\partial w}{\partial x}\}dl \end{aligned} \tag{3.9}$$

$$\delta W_{p_2} = \int_a^b \{\frac{\partial \delta p_2}{\partial x}\frac{1}{12\mu}(\frac{H}{2}+w)^3\frac{\partial p_2}{\partial x} + \delta p_2\frac{\partial w}{\partial t} + \delta p_2 B\frac{(p_2-p_1)}{d} + \delta p_2\frac{V}{2}\frac{\partial w}{\partial x}\}dl \tag{3.10}$$

where the displacement variation δw is the arbitrary admissible out-of-plane displacement, i.e., $\delta w = 0$, on $x = 0, L$, and the pressure variations $\delta p1$ and $\delta p2$ are commonly assigned to be zero on $x = 0, L$.

Denote $\delta\mathbf{W}$ and $\delta\mathbf{R}$ as the left and right sides of equilibrium equations in variational forms. In the incremental analysis, at any time t, the equilibrium equations must be satisfied [28]

$$\delta^t\mathbf{W} = \delta^t\mathbf{R} \tag{3.11}$$

where $\delta\mathbf{W} = (\delta W_w, \delta W_{p_1}, \delta W_{p_2})^T$, moveover, from the Taylor's expansion, we have

$$\delta^t\dot{\mathbf{W}}\Delta t \simeq \delta^{t+\Delta t}\mathbf{R} - \delta^t\mathbf{W}. \tag{3.12}$$

Assume the increment of a is defined as $\Delta a = \dot{a}\Delta t$, consequently, we have

$$\delta\dot{W}_w\Delta t = \int_0^L \{\delta w(m\frac{\partial^2\Delta w}{\partial t^2} + 2mV\frac{\partial^2\Delta w}{\partial x\partial t}) - \frac{\partial\delta w}{\partial x}(mV^2 - T)\frac{\partial\Delta w}{\partial x} + \delta w(\Delta p_1 - \Delta p_2)\}dl \tag{3.13}$$

$$\delta\dot{W}_{p_1}\Delta t = \int_a^b \{\frac{\partial\delta p_1}{\partial x}\frac{1}{12\mu}(\frac{H}{2}-w)^3\frac{\partial\Delta p_1}{\partial x} - \frac{\partial\delta p_1}{\partial x}\frac{1}{4\mu}(\frac{H}{2}-w)^2\Delta w\frac{\partial p_1}{\partial x} - \delta p_1\frac{\partial\Delta w}{\partial t} + \delta p_1 B\frac{(\Delta p_1 - \Delta p_2)}{d} - \delta p_1\frac{V}{2}\frac{\partial\Delta w}{\partial x}\}dl \tag{3.14}$$

$$\delta\dot{W}_{p_2}\Delta t = \int_a^b \{\frac{\partial\delta p_2}{\partial x}\frac{1}{12\mu}(\frac{H}{2}+w)^3\frac{\partial\Delta p_2}{\partial x} + \frac{\partial\delta p_2}{\partial x}\frac{1}{4\mu}(\frac{H}{2}+w)^2\Delta w\frac{\partial p_2}{\partial x} + \delta p_2\frac{\partial\Delta w}{\partial t} + \delta p_2 B\frac{(\Delta p_2 - \Delta p_1)}{d} + \delta p_2\frac{V}{2}\frac{\partial\Delta w}{\partial x}\}dl. \tag{3.15}$$

3.3 Finite Element Discretization

Introduce the nodal unknowns $\widehat{\mathbf{W}}$, $\widehat{\mathbf{P}}_1$, and $\widehat{\mathbf{P}}_2$, and apply the standard Galerkin finite element procedure to

$$\Delta^t\mathbf{W} = \frac{\partial^t\mathbf{W}}{\partial\Theta}\Delta\Theta + \frac{\partial^t\mathbf{W}}{\partial\dot{\Theta}}\Delta\dot{\Theta} + \frac{\partial^t\mathbf{W}}{\partial\ddot{\Theta}}\Delta\ddot{\Theta} \tag{3.16}$$

we finally get

$$\mathbf{M}\Delta\ddot{\Theta} + \mathbf{C}\Delta\dot{\Theta} + \mathbf{K}\Delta\Theta = \Delta\mathbf{R} \tag{3.17}$$

where

$$\mathbf{M} = \begin{bmatrix} \mathbf{M}_{ww} & \mathbf{0} & \mathbf{0} \\ \mathbf{0} & \mathbf{0} & \mathbf{0} \\ \mathbf{0} & \mathbf{0} & \mathbf{0} \end{bmatrix}, \qquad \mathbf{C} = \begin{bmatrix} \mathbf{C}_{ww} & \mathbf{0} & \mathbf{0} \\ \mathbf{C}_{p_1w} & \mathbf{0} & \mathbf{0} \\ \mathbf{C}_{p_2w} & \mathbf{0} & \mathbf{0} \end{bmatrix};$$

$$\mathbf{K} = \begin{bmatrix} \mathbf{K}_{ww} & \mathbf{K}_{wp_1} & \mathbf{K}_{wp_2} \\ \mathbf{K}_{p_1w} & \mathbf{K}_{p_1p_1} & \mathbf{K}_{p_1p_2} \\ \mathbf{K}_{p_2w} & \mathbf{K}_{p_2p_1} & \mathbf{K}_{p_2p_2} \end{bmatrix}, \quad \Delta\mathbf{R} = \begin{Bmatrix} \mathbf{R}_w \\ \mathbf{0} \\ \mathbf{0} \end{Bmatrix} - \begin{Bmatrix} \mathbf{F}_w \\ \mathbf{F}_{p_1} \\ \mathbf{F}_{p_2} \end{Bmatrix};$$

$$\delta\mathbf{W}^T\mathbf{F}_w = \delta W_w, \quad \delta\mathbf{P}_1{}^T\mathbf{F}_{p_1} = \delta W_{p_1}, \quad \delta\mathbf{P}_2{}^T\mathbf{F}_{p_2} = \delta W_{p_2};$$

and

$$
\begin{aligned}
\delta \mathbf{W}^T \mathbf{K}_{wp_1} \Delta \widehat{\mathbf{P}}_1 &= \int_a^b \delta w \Delta p_1 dl, & \delta \mathbf{W}^T \mathbf{C}_{ww} \Delta \dot{\widehat{\mathbf{W}}} &= \int_0^L 2mV \delta w \frac{\partial^2 \Delta w}{\partial x \partial t} dl; \\
\delta \mathbf{P}_1{}^T \mathbf{K}_{p_1 p_2} \Delta \widehat{\mathbf{P}}_2 &= -\int_a^b \delta p_1 B \frac{\Delta p_2}{d} dl, & \delta \mathbf{W}^T \mathbf{M}_{ww} \Delta \ddot{\widehat{\mathbf{W}}} &= \int_0^L m \delta w \frac{\partial^2 \Delta w}{\partial t^2} dl; \\
\delta \mathbf{W}^T \mathbf{K}_{wp_2} \Delta \widehat{\mathbf{P}}_2 &= -\int_a^b \delta w \Delta p_2 dl, & \delta \mathbf{P}_1{}^T \mathbf{C}_{p_1 w} \Delta \dot{\widehat{\mathbf{W}}} &= -\int_a^b \delta p_1 \frac{\partial \Delta w}{\partial t} dl; \\
\delta \mathbf{P}_2{}^T \mathbf{K}_{p_2 p_1} \Delta \widehat{\mathbf{P}}_1 &= -\int_a^b \delta p_2 B \frac{\Delta p_1}{d} dl, & \delta \mathbf{P}_2{}^T \mathbf{C}_{p_2 w} \Delta \dot{\widehat{\mathbf{W}}} &= \int_a^b \delta p_2 \frac{\partial \Delta w}{\partial t} dl;
\end{aligned}
$$

$$
\begin{aligned}
\delta \mathbf{W}^T \mathbf{K}_{ww} \Delta \widehat{\mathbf{W}} &= -\int_0^L \frac{\partial \delta w}{\partial x} (mV^2 - T) \frac{\partial \Delta w}{\partial x} dl; \\
\delta \mathbf{P}_1{}^T \mathbf{K}_{p_1 p_1} \Delta \widehat{\mathbf{P}}_1 &= \int_a^b \{ \frac{\partial \delta p_1}{\partial x} \frac{1}{12\mu} (\frac{H}{2} - w)^3 \frac{\partial \Delta p_1}{\partial x} + \delta p_1 B \frac{\Delta p_1}{d} \} dl; \\
\delta \mathbf{P}_1{}^T \mathbf{K}_{p_1 w} \Delta \widehat{\mathbf{W}} &= -\int_a^b \{ \frac{\partial \delta p_1}{\partial x} \frac{1}{4\mu} (\frac{H}{2} - w)^2 \Delta w \frac{\partial p_1}{\partial x} + \delta p_1 \frac{V}{2} \frac{\partial \Delta w}{\partial x} \} dl; \\
\delta \mathbf{P}_2{}^T \mathbf{K}_{p_2 p_2} \Delta \widehat{\mathbf{P}}_2 &= \int_a^b \{ \frac{\partial \delta p_2}{\partial x} \frac{1}{12\mu} (\frac{H}{2} + w)^3 \frac{\partial \Delta p_2}{\partial x} + \delta p_2 B \frac{\Delta p_2}{d} \} dl; \\
\delta \mathbf{P}_2{}^T \mathbf{K}_{p_2 w} \Delta \widehat{\mathbf{W}} &= \int_a^b \{ \frac{\partial \delta p_2}{\partial x} \frac{1}{4\mu} (\frac{H}{2} + w)^2 \Delta w \frac{\partial p_2}{\partial x} + \delta p_2 \frac{V}{2} \frac{\partial \Delta w}{\partial x} \} dl.
\end{aligned}
$$

The trapezoidal temporal discretization is as follows [34]:

$$
\begin{aligned}
{}^{t+\Delta t}\mathbf{b} &= {}^t\mathbf{b} + \frac{\Delta t}{2} ({}^t\dot{\mathbf{b}} + {}^{t+\Delta t}\dot{\mathbf{b}}) \\
{}^{t+\Delta t}\dot{\mathbf{b}} &= {}^t\dot{\mathbf{b}} + \frac{\Delta t}{2} ({}^t\ddot{\mathbf{b}} + {}^{t+\Delta t}\ddot{\mathbf{b}})
\end{aligned}
\tag{3.18}
$$

and further more

$${}^{t+\Delta t}\mathbf{b} = {}^t\mathbf{b} + {}^t\dot{\mathbf{b}} \Delta t + \frac{\Delta t^2}{4} ({}^t\ddot{\mathbf{b}} + {}^{t+\Delta t}\ddot{\mathbf{b}}) \tag{3.19}$$

where $\mathbf{b}$ stands for the nodal unknown vectors.

3.4 Conclusion and Discussion

In this chapter we have discussed further the proposed two-sided sheet suppression device and one nonlinear finite element procedure for the analysis of the coupled system between two Reynolds equations and a traveling pretensioned web. The fast moving web is expected to travel between the air-steam mixture which also prevents the web from contacting the two rigid suppression device surfaces.

To reiterate, three benefits of using this type of flutter suppression device are listed below:

- The fluid (air-steam mixture) is entrained between two surfaces, therefore, even for highly permeable paper webs, there is no mechanism for the fluid to leave the lubrication zones.
- The device is small and can be easily installed on the existing web transporting system without modifying the tension distributions within paper machines; in addition, the device is retrievable and can also be connected to fluidics control systems.
- The device can be used as the mounting platform for certain online sensors.

Dynamical Aspects

4.1 Introduction

Axially moving continua, such as the pretensioned traveling paper web, experience a Coriolis acceleration component which renders such system gyroscopic as well as the surrounding air effects. The combination of these effects will create problems such as sheet fluttering and dynamic instability. The characteristics of the vibration and dynamic stability of such systems in vacuum have been studied by Wickert and Mote [35], and other researchers. However, the surrounding air effects have only been investigated recently, with the application of empirical added mass estimation, by Pramila [8] [9], Chang and Moretti [7], and others in the interest of the paper industry. In chapter 2, we discussed an accurate prediction of both the added mass and added stiffness effects; while the effective damping and stiffness of the proposed two-sided flutter suppression device can be calculated through the formulation discussed in chapter 3. In this chapter, we will use the information provided in the previous two chapters and analyze the effects on the dynamical behavior of the traveling web.

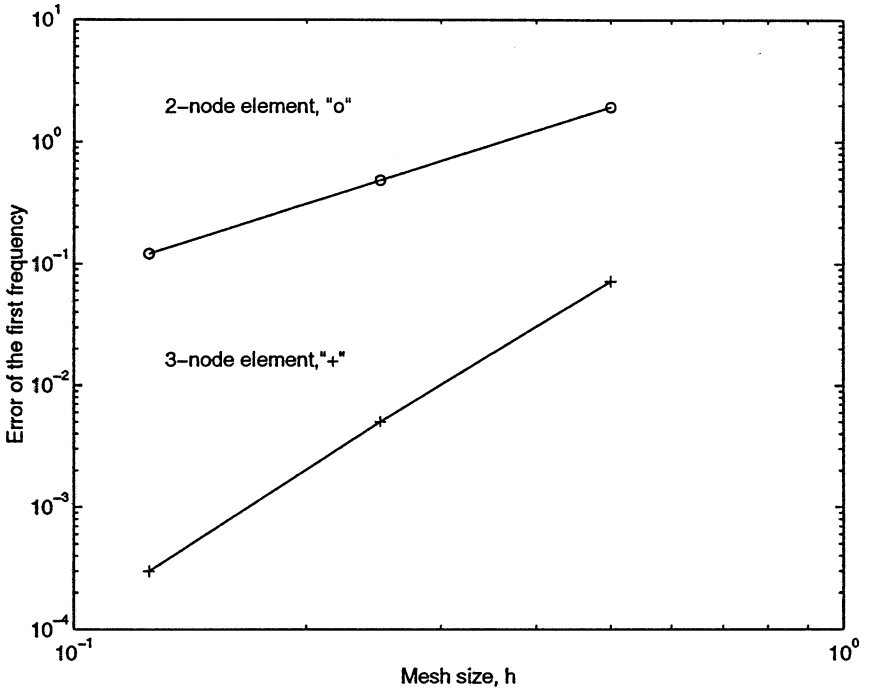

Figure 4-1: The convergence study of the pretensioned web without traveling speed.

4.2 Simulation Results

For fully 3D coupled system, the out-of-plane displacement w is a function of time t, as well as MD and CD coordinates x and y, i.e., $w = w(x, y, t)$; while for the simplified 2D model, $w = w(x, t)$.

The convergence results using 2-node and 3-node elements for traveling and stationary pretensioned web are shown in Figs. 4-1 and 4-2. The first and second modeshapes for the cases with and without traveling velocity are shown in Figs. 4-3 and 4-4. The differences of modeshapes with and without added mass effects are also noticeable. One interesting observation from Figure 10 in ref [7] confirms that it is necessary to introduce the added mass effects (shown in Fig. 4-5). The computed frequencies of a convergence study are listed in Table 4-1.

If the average positive and negative out-of-plane displacement amplitudes are defined as

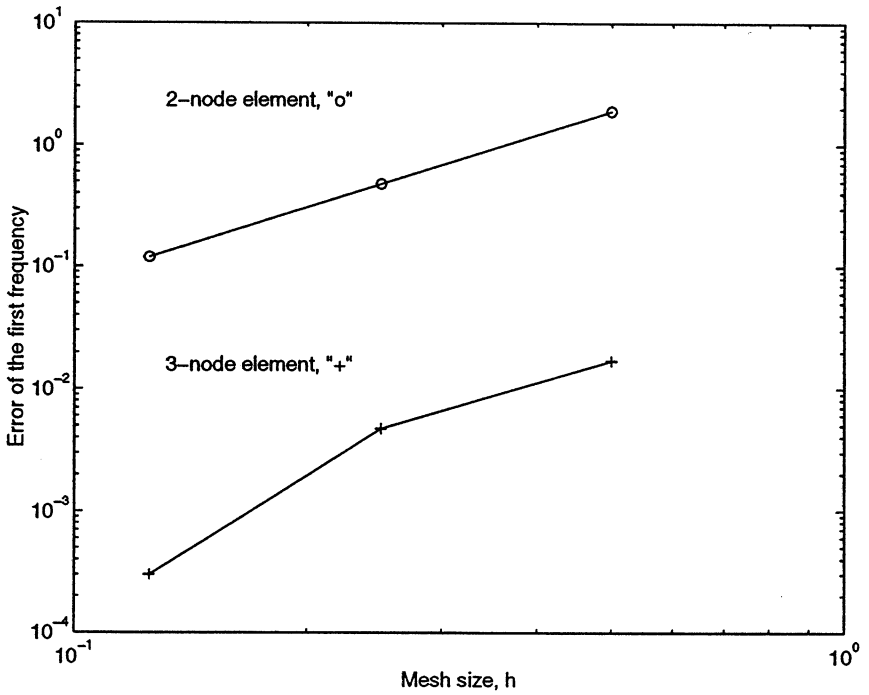

Figure 4-2: The convergence study of the pretensioned web with traveling speed.

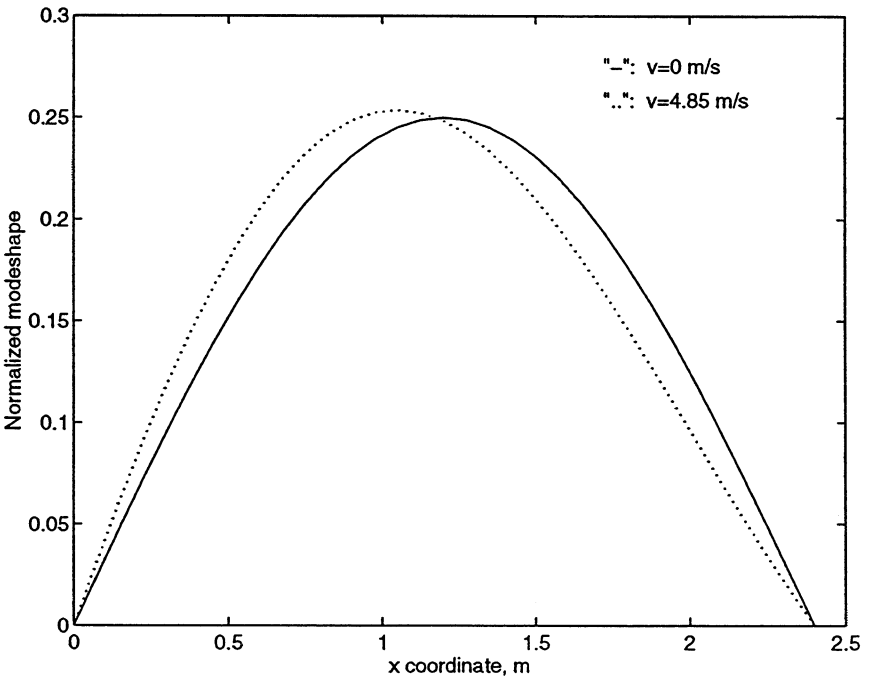

Figure 4-3: The first modeshape of the web with and without traveling speed.

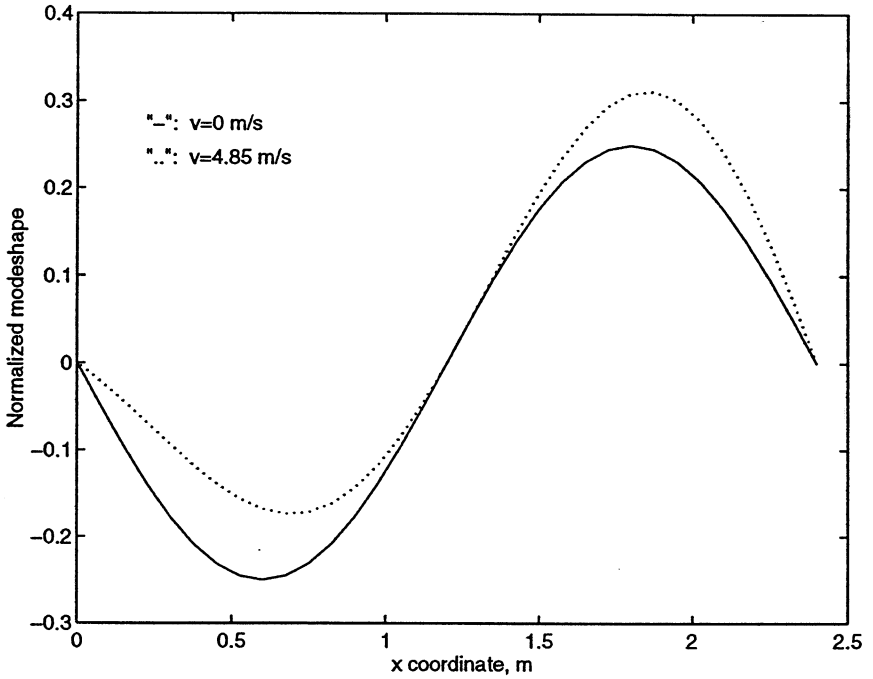

Figure 4-4: The second modeshape of the web with and without traveling speed.

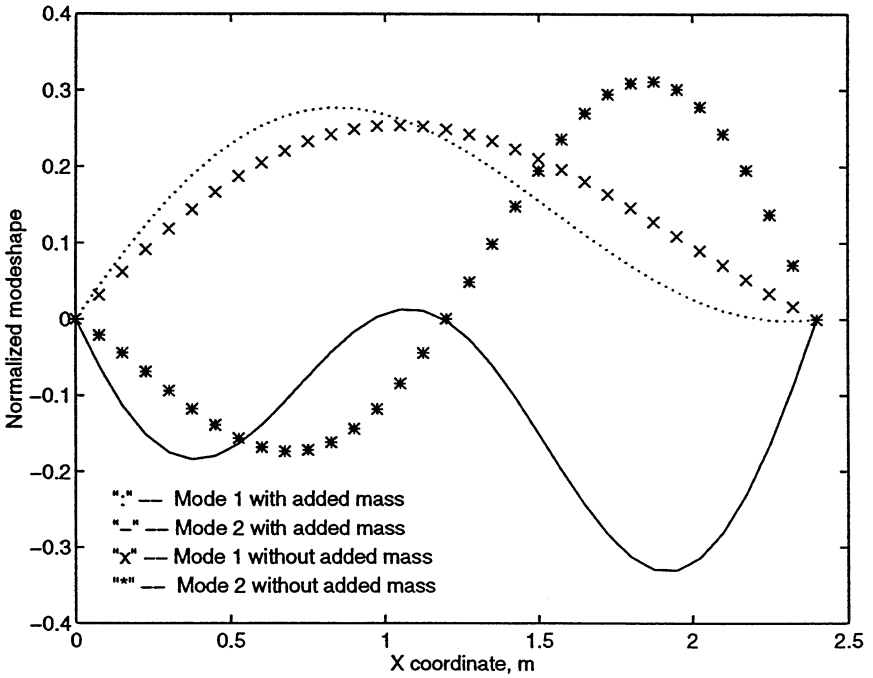

Figure 4-5: The added mass effects on the first and second modeshapes.

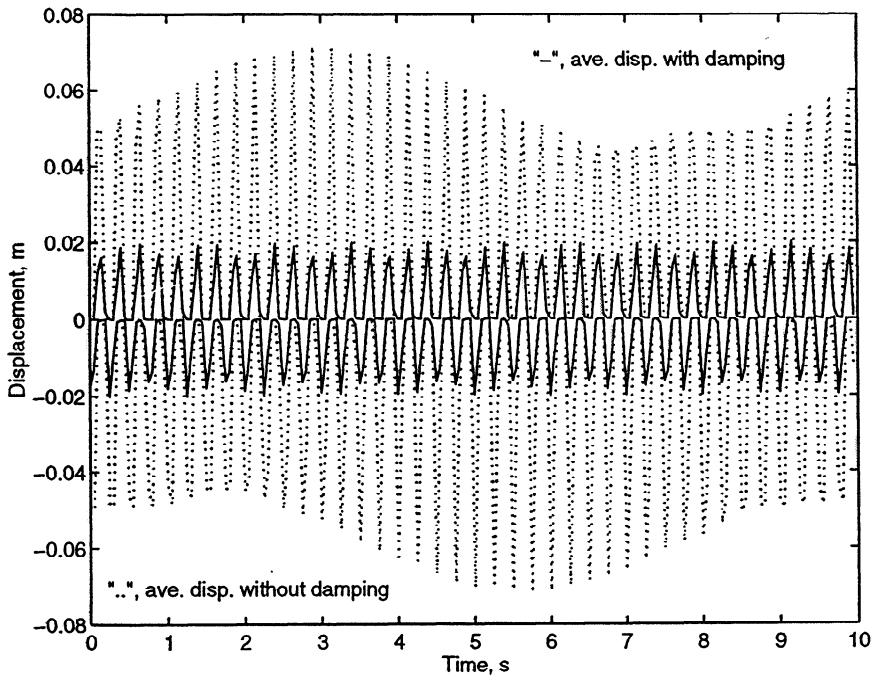

Figure 4-6: The up and down average displacement history with and without damping during the 16.0 Hz forced vibration.

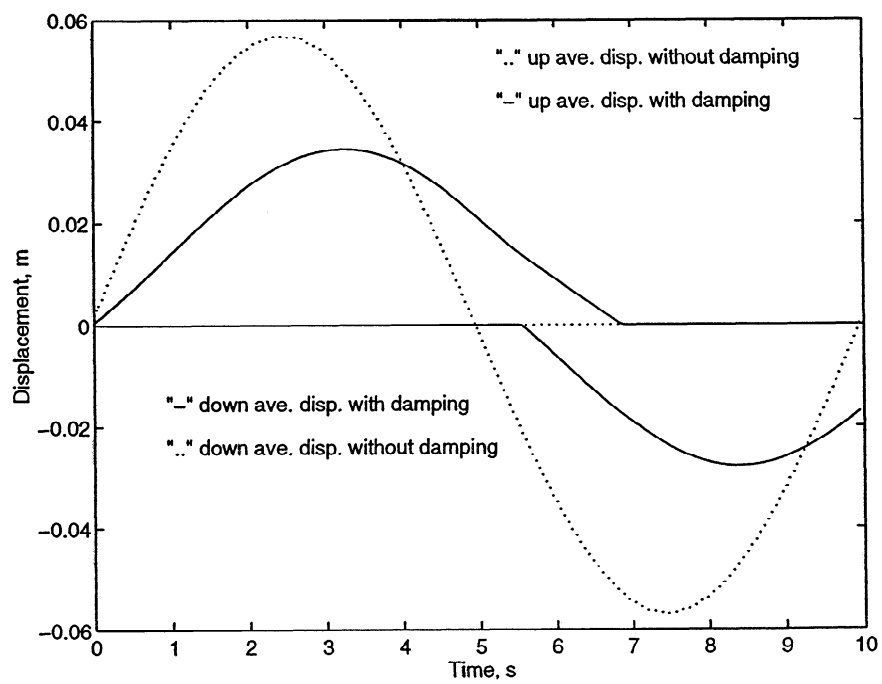

Figure 4-7: The up and down average displacement history with and without damping during the 0.1 Hz forced vibration.

HAPID Water Removal Data

- Water removal was proportional to platen temperature,
- And independent of ambient pressure at nip opening.

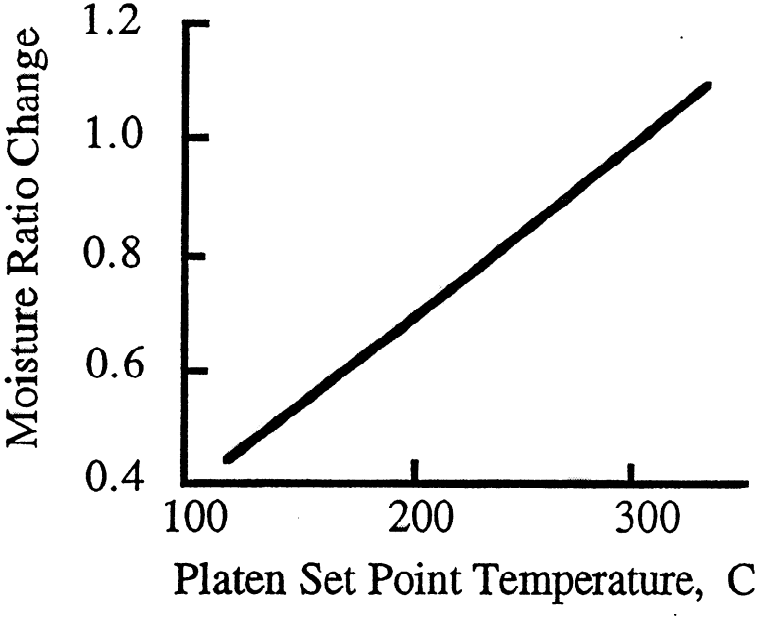

Mesh No. of elements	First frequency with 2-node elements (Hz)		First frequency with 3-node elements (Hz)	
	$v = 4.85\ (m/s)$	$v = 0$	$v = 4.85\ (m/s)$	$v = 0$
2	20.3712	20.4016	18.5191	18.5191
4	18.9323	18.9807	18.4520	18.5069
8	18.5679	18.6213	18.4473	18.5025
16	18.4772	18.5320	18.4471	18.5022
32	18.4546	18.5096	18.4470	18.5022
Analytical results [9]	18.4470	18.5022	18.4470	18.5022

Table 4-1: Comparison of analytic and numerical solutions.

$$\bar{w}^{+} = (\sum_{i=1}^{N} W_i \quad \text{if } W_i > 0)/N \tag{4.1}$$

$$\bar{w}^{-} = (\sum_{i=1}^{N} W_i \quad \text{if } W_i < 0)/N \tag{4.2}$$

where N is the total number of nodal displacement unknowns, we can compare the time histories of the amplitudes with and without the suppression device. The amplitude reductions with both high frequency (shown in Fig. 4-6) and low frequency (shown in Fig. 4-7) excitation forces are significant. Similar dynamic effects of suppression devices are also shown in Figs. 4-8 and 4-9.

Conclusions

For the traveling pretensioned paper web, there are many main sources of excitation forces, namely, (a) the surrounding aerodynamic influence; (b) eccentricity effects of the rollers; (c) both MD and CD basis weight variation effects; and (d) tension variation due to the out-of-plane displacements. Most of the effects are highly nonlinear and the response is really not as simple as when natural frequency is close to the excitation frequency, which is when the most severe vibration of the paper web happens. In fact, many critical frequencies are only a fraction of the natural frequencies, due to subharmonic effects in nonlinear dynamics. In this report, we use the "threadline" model, in which the entire width of the web deflects uniformly, in order to focus on the total transverse displacement.

The nonlinear finite element formulations are developed to analyze the newly proposed flutter suppression device. It is perceptible that a small active damping device, based on aerodynamic means, can be achieved to suppress the flutter. Consequently, we can improve the runnability of webs and reduce the likelihood of sheet wrinkling and breakage. Further research will focus on the following issues:

- to actually design a suppression device and to establish an experimental setting to confirm the computational predictions;

- to include the basis weight variation and tension variation (both CD and MD) in the dynamical analysis of the traveling pretensioned web;
- to extend the research to the 3D model and to focus on the thin structure edge flutter behavior; and
- to include a turbulence model in the aerodynamic effects.

Over the work of this project, the developed softwares as well as the training program will be provided openly to the PAC member companies, with which we hope that the researchers in individual member companies will be able to further the design process incorporating their specific interests.

References

[1] D. Qi and C.K. Aidun. Free edge flutter based on 3-D structural characteristics of paper. *Proceeding of TAPPI Engineering Conference*, 1995. To appear.

[2] S.-J. Liang, G.P. Neitzel, and C.K. Aidun. Finite-element computations for unsteady fluid and elastic membrane interaction problems. *International Journal of Numerical Methods in Fluids*, 1995. Submitted.

[3] R.A. Sack. Transverse oscillations in travelling strings. *British Journal of Applied Physics*, 5:224–226, 1954.

[4] F.R. Archibald and A.G. Emslie. The vibration of a string having a uniform motion along its length. *Journal of Applied Mechanics*, 265:347–348, 1958.

[5] C.D. Mote. A study of bandsaw vibrations. *Journal of the Franklin Institute*, 279:430–444, 1965.

[6] J.A. Wickert and C.D. Mote, Jr. Classical vibration analysis of axially moving continua. *Journal of Applied Mechanics*, 57:738–744, 1990.

[7] Y.B. Chang and P.M. Moretti. Interaction of fluttering webs with surrounding air. *TAPPI Journal*, pages 231–236, March 1991.

[8] A. Pramilla. Sheet flutter and the interaction between sheet and air. *TAPPI Journal*, pages 70–74, July 1986.

[9] A. Pramila. Natural frequencies of a submerged axially moving band. *Journal of Sound and Vibration*, 113(1):198–203, 1987.

[10] A.S. Mujumdar and W.J.M. Douglas. Analytical modeling of sheet flutter. *Svensk Papperstidning*, 6:187–192, 1976.

[11] K.J. Bathe and W.F. Hahn. On transient analysis of fluid-structure systems. *Computers & Structures*, 10:383–391, 1979.

[12] N. Akkas, H.U. Akay, and C. Yilmaz. Applicability of general-purpose finite element programs in solid-fluid interaction problems. *Computers & Structures*, 10:773–783, 1979.

[13] M.A. Hamdi, Y. Ousset, and G. Verchery. A displacement method for the analysis of vibrations of coupled fluid-structure systems. *International Journal for Numerical Methods in Engineering*, 13:139–150, 1978.

[14] T.B. Belytschko and J.M. Kennedy. A fluid-structure finite element method for the analysis of reactor safety problems. *Nuclear Engineering and Design*, 38:71–81, 1976.

[15] T. Belytschko. Fluid-structure interaction. *Computers & Structures*, 12:459–469, 1980.

[16] L.G. Olson and K.J. Bathe. A study of displacement-based fluid finite elements for calculating frequencies of fluid and fluid-structure systems. *Nuclear Engineering and Design*, 76:137–151, 1983.

[17] H. Morand and R. Ohayon. Substructure variational analysis of the vibrations of coupled fluid-structure systems. Finite element results. *International Journal for Numerical Methods in Engineering*, 14:741–755, 1979.

[18] G.C. Everstine. A symmetric potential formulation for fluid-structure interaction. *Journal of Sound and Vibration*, 79(1):157–160, 1981.

[19] L.G. Olson and K.J. Bathe. Analysis of fluid-structure interactions. A direct symmetric coupled formulation based on the fluid velocity potential. *Computers & Structures*, 21(1/2):21–32, 1985.

[20] C.A. Felippa and R. Ohayon. Mixed variational formulation of finite element analysis of acoustoelastic/slosh fluid-structure interaction. *Journal of Fluids and Structures*, 4:35–57, 1990.

[21] K.J. Bathe, C. Nitikitpaiboon, and X. Wang. A mixed displacement-based finite element formulation for acoustic fluid-structure interaction. *Computers & Structures*, 56(2/3):225–237, 1995.

[22] X. Wang and K.J. Bathe. Displacement/pressure based finite element formulations for acousto/slosh fluid-structure interactions. *International Journal for Numerical Methods in Engineering*, 1995. To appear.

[23] X. Wang and K.J. Bathe. On mixed elements for acoustic fluid-structure interactions. *Mathematical Models & Methods in Applied Sciences*, 1995. To appear.

[24] W.C. Müller. Simplified analysis of linear fluid-structure interaction. *International Journal for Numerical Methods in Engineering*, 17:113–121, 1981.

[25] J.A. Wickert. Analysis of self-excited longitudinal vibration of a moving tape. *Journal of Sound and Vibration*, 160(3):455–463, 1993.

[26] J.A. Wickert. Non-linear vibration of a traveling tensioned beam. *International Journal of Non-linear Mechanics*, 27(3):503–517, 1992.

[27] T.Y.T. Wu. Hydromechanics of swimming propulsion Part 3. *Journal of Fluid Mechanics*, 46:545–568, 1971.

[28] K.J. Bathe. *Finite Element Procedures.* Prentice Hall, Englewood Cliffs, N.J., 1995.

[29] O.C. Zienkiewicz and P. Bettess. Fluid-structure dynamics interaction and wave forces. An introduction to numerical treatment. *International Journal for Numerical Methods in Engineering*, 13:1–16, 1978.

[30] W.K. Liu and R.A. Uras. Variational approach to fluid-structure interaction with sloshing. *Nuclear Engineering and Design*, 106:69–85, 1988.

[31] B. Hamrock. *Fundamentals of Fluid Film Lubrication.* McGraw-Hill, Inc, 1994.

[32] S. Müftü and R.C. Benson. Transient study of the two dimensional foil bearing probelm. *Proceedings of the International Tribology Conference*, 1995.

[33] S. Müftü and R.C. Benson. Modelling the transport of paper webs including the paper permeability effects. *Proceedings of ISPS at the ASME-International Congress and Exposition in San Fransisco, CA*, November 1995.

[34] K.J. Bathe and V. Sonnad. On effective implicit time integration in analysis of fluid-structure problems. *International Journal for Numerical Methods in Engineering*, 15(6):943–948, 1980.

[35] J.A. Wickert and C.D. Mote, Jr. Current research on the vibration and stability of axially moving materials. *The Shock and Vibration Digest*, 20:3–13, 1988.

ON THE RESEARCH AREA OF APPROACH PIPE SYSTEMS

PROPOSAL

TO THE

PAPERMAKING
PROJECT ADVISORY COMMITTEE

Xiaodong Wang

March 18 - 19, 1996

Institute of Paper Science and Technology
500 10th Street, N.W.
Atlanta, Georgia

New Project Proposal

ON THE RESEARCH AREAS OF APPROACH PIPE SYSTEMS

by

Xiaodong Wang, Assistant Professor of Engineering

Submitted to the Institute of Paper Science and Technology
on March 18, 1996

Abstract

In this report, the results from the informal survey on the research areas of approach pipe systems are summarized. Current guidelines from TAPPI Technical Information Sheet (TIS), Valmet, Voith, and Beloit are also reviewed and discussed. Based on the survey results and the available information of the past research done in this area, after having completed many telephone interviews, field trips in the three major papermaking machine suppliers, and several mill visits, let alone dozens of papers in this field, it is concluded worthwhile to establish a corresponding funded project on approach pipe systems at IPST. The objectives of this project are to solve some immediate problems relating to approach pipe systems and to obtain deeper fundamental understanding that can be used in the future designs. Specifically, based on the state-of-art computational procedures and the development of concepts in fluidics and hydraulics, computer simulations of different approach flow components and their interactions within the whole system will be developed and analyzed. Some softwares for analyzing and optimizing the approach flow systems according to different mill conditions are to be delivered through this research project.

The project will provide general information for all of our membership companies and focus on the fundamental research of our paper industries facing the coming information era. Although it is not the intention to associate this project with any particular companies or interests, some specific research of particular interest to individual companies can be arranged separately.

With projections for the future, the commencement of this project will help to establish an expertise center at IPST in the approach flow system areas and eventually for the whole wet end papermaking processes.

Acknowledgments

First, I would like to thank Professor David Orloff for suggesting this interesting field to me.

I am very grateful to Dr. David White and his papermaking PAC members, especially Mr. Richard Reese, Mr. Louis M. Vance, and Mr. Karl Christianson, who serve as the approach pipe system subcommittee.

It is my pleasure to have the privilege to work at IPST with so many wonderful faculty, research staff, and students. Part of the inspiration of getting evolved in this area is due to Professor Cyrus Aidun's recent success in applying numerical procedures to the coating and headbox analyses for our paper industries.

My utmost gratitude is due to Mr. Seppo Laaksonen, Dr. Jay A. Shands, Mr. Michael MacGregor, and the engineers working with them; their tremendous support and generosity during the preparation of this proposal mean the most to me.

Introduction

1.1 Overview

The approach pipe (or flow) system is comprised of numerous individual components between the stock preparation section and the headbox [1] [2] [3]. These components include fan pumps, piping, deaeration system, attenuator, pressure screens, cleaners, control valves and white water recycling systems. The effects of each component in the approach pipe system will directly influence the performance of paper machines.

As the development of more high production rate forming devices and short distance forming units (such as hydraulic headboxes and twin-wire forming sections) [4], the pressure pulsation tolerance and consistency fluctuation within the stock (mixture of wood fibers, chemical additives, and water) are getting more strict. In fact, the good performance of stock approach pipe systems is essential to the smooth operation of the entire paper machines with higher and higher machine speeds.

From a design standpoint, the stock approach system is one of the most critical areas of the paper machine and is often called "plumbers' nightmare." The current design guidelines are normally used to avoid the following difficulties:

- non-uniform fiber delivery;

- unstable flow, pulsations and surges;
- formation of stack lumps from stagnant zones, trapped air, rough surfaces; and
- vibration.

Although the arrangement, design, and operation of stock approach equipment will vary greatly from mill to mill and machine to machine, and the available guidelines and research information are often found to be inadequate and even confusing [5] [6] [7] [8] [9], there is no tool available to analyse the approach flow system as a whole under the circumstance of component changes, consistency and stock variations [10] [11] [12]. Therefore, to provide engineers the general design guidelines, more feasible analysis tools for both the specific components within approach flow systems and the whole system design are imperative.

It is the intention of this project to identify the fundamental research areas of approach pipe systems [13] and to provide the state-of-art solution techniques. The research results and procedures shall be widely applicable to both paper machine suppliers and mills.

In order to establish a robust and worthwhile project in this area, the needs and interests of the IPST membership companies were investigated, and based on the available published research results, the following three main research areas are identified:

- **flow-induced vibration**, including pressure pulsation and dynamic analysis of approach pipe systems [14] [15] [16];
- **fluid flow control**, including chemical additive (such as retention aids) mixing [17] [18], uniform consistency, stock and white water mixing; and
- **deaeration systems**, including cavitation, flow separation, and deculator system [10] [19].

The other areas related to approach pipe systems are surface finish [20] and pipe system design. The surface finish problem is mainly an issue of metallurgy and corrosion analysis; therefore it is not considered as one of our main research focuses.

The comments from papermaking PAC members were gathered through an informal telephone survey.

1.2 Project Objective

In engineering sciences, much effort has gone into the application of computer simulations. With the development of more powerful computers and more effective computational procedures, the traditional hydraulics and fluidics are merging with the concepts of computational mechanics [21]. We will, through this research project, develop computer simulation models for the field engineers to use in accordance with the specific mill and machine arrangement. The computer surrogates will contain:

- the mixing simulation within the pipe for fibres, water, and chemical additives;
- the computer simulation of individual components within the approach pipe system;
- the nonlinear dynamics computer simulation of the hydraulic design of approach flow systems; and
- the pressure pulsation simulation.

The specific objectives of this project are:

- to optimize the pressure pulsation attenuator for all ranges of frequencies, especially the lower range;
- to better understand the white water silo design;

- to better understand the mixing between stock and white water before the fan pump;
- to better understand short- and long-term consistency variations;
- to optimize the pipe system design including the location of valves, elbow, and pumps; and
- to develop a nonlinear dynamic model including the disturbance or perturbation dampening mechanism.

1.3 Project Outline

Based on the evaluation of our membership industry needs, we will include three steps in this project.

- Step 1: To identify the problems of individual components within approach pipe systems and to form corresponding computer simulation models;
- Step 2: To incorporate all approach pipe system components into a whole computer model and to develop an algorithm of computer system design simulations; and
- Step 3: To implement the developed software in any of the test approach pipe systems within our membership companies and to improve the current TAPPI TIS guideline (if necessary, individual company's guideline as well, depending on the separate arrangement.)

Evaluation of Industry Needs

Stimulated by some membership industries' research needs [13], a telephone survey was conducted on a potential project in the areas of approach pipe systems.

The following topics are discussed: fan pump, flow stability, flow-induced vibration, piping, valves, recirculation, cleaners, pressure screens, chemical additive mixing, consistency control and design issues. However, discussions are focused on the aforementioned three main issues; i.e. **flow-induced vibration**, **fluid flow control** and **deaeration systems**.

The papermaking PAC members were asked how important these areas are, and what aspects of approach pipe systems are of most interest to them. In addition, they were asked to comment on the other areas related to approach pipe systems.

2.1 Flow-Induced Vibration

Ten out of 11 interviewees agree that this is an important issue. It is reflected in their comments that low frequency pulsation is more difficult to attenuate. In general, the vibration of the approach pipe system will be introduced to the headbox and eventually causes MD and CD base weight variations. The problem should be particularly considered for hydraulic headboxes. The sources of pulsation could be induced

by insufficient pipe supporting systems, flow-induced vibration, defective rotors, and acoustic resonance with the flow.

2.2 Fluid Flow Control

Almost all papermaking PAC members I talked to consider this area to be interesting. It was pointed out that the uniform consistency needs to be well understood. The flow pattern which influences the stock consistency and floccuation conditions, thin stock, thick stock, and chemical additive mixing are of most interest to these industry representatives. They feel that the existing guidelines are inadequate and more hydrodynamic parameters are needed in practice.

2.3 Deaeration Systems

Six interviewees think that this is not an important issue in their perspective, compared with five others on the other side. However, this problem is dependent on the paper grades that individual mill and machine produce. For light weight grade paper machines, it is still an issue of concern. Some PAC members mention the need for a deeper understanding of cavitation and flow separation problems within different pipes. The silo and wire pit are also of some interest. Some mills found that whether or not to have deculator systems did not make much difference, and in order to save room space, these deculators were withdrawn.

2.4 Other Areas

In addition to the three main topics, some papermaking PAC members commented on the system design problem. The concern is about the placement of various components, including the system design for new machines in old mills.

Area of study in approach pipe systems	How important is this area of study?	What aspects are of interest to your industry?	Other comments
Flow-induced vibration	Important	Less tolerance for MD and CD base weight variation as the machine speed increases	
Flow control	Important	Machine chest, blend chest, pressure screen, fan pumps, and valves	Guideline inadequate
Deaeration system	Important	Flow consistency, all kinds of mixing problems, more hydrodynamic parameters	Pipe elbow cavitation needs to be investigated
Other areas	Systems design is an important area	Placement of various components	

Table 2-1: Sample #1 survey results.

Area of study in approach pipe systems	How important is this area of study?	What aspects are of interest to your industry?	Other comments
Flow-induced vibration	Important	Pipe support and headbox vibration causes MD & CD base weight variations	Press section dynamic behavior may affect the headbox
Flow control	Important	Retention aids mixing, silo water level and pressure variation	
Deaeration system	Important	Fan pump, multisection pressure drops	
Other areas			

Table 2-2: Sample #2 survey results.

Area of study in approach pipe systems	How important is this area of study?	What aspects are of interest to your industry?	Other comments
Flow-induced vibration	Important	Influence on the headbox	
Flow control	Important	Good way of consistency control, zero variation	
Deaeration system	Important		
Other areas		System design, not enough space for various components	Air deculator has limited effects

Table 2-3: Sample #3 survey results.

Area of study in approach pipe systems	How important is this area of study?	What aspects are of interest to your industry?	Other comments
Flow-induced vibration	Important		
Flow control	Important	Thin stock, thick stock mixing, fan pump	
Deaeration system	Not so important		Deculator is good for lightweight print
Other areas			

Table 2-4: Sample #4 survey results.

Area of study in approach pipe systems	How important is this area of study?	What aspects are of interest to your industry?	Other comments
Flow-induced vibration	Not so important		
Flow control	Important	Retention aids mixing, uniform consistency, thin stock, thick stock mixing	
Deaeration system	Not so important		Depending on different mills
Other areas			

Table 2-5: Sample #5 survey results.

Area of study in approach pipe systems	How important is this area of study?	What aspects are of interest to your industry?	Other comments
Flow-induced vibration	Important	Low frequency vibration affects the headbox and is difficult to deal with	High frequency vibration is easy to fix
Flow control	Important	Swirling affects additive & stock mixing, consistency, CD base weight variation	Poor guideline
Deaeration system	Not so important		
Other areas			Surface finish is a CH.E. problem

Table 2-6: Sample #6 survey results.

Area of study in approach pipe systems	How important is this area of study?	What aspects are of interest to your industry?	Other comments
Flow-induced vibration	Important		More and more interests
Flow control	Important	Machine chest, consistency control, and faster silo water	
Deaeration system	Not so important	Pipe design	
Other areas			

Table 2-7: Sample #7 survey results.

Area of study in approach pipe systems	How important is this area of study?	What aspects are of interest to your industry?	Other comments
Flow-induced vibration	Important	Pressure pulsation and recirculation line	
Flow control	Important	Thick stock & white water mixing, uniform mixture, and where to put additives	
Deaeration system	Important	Deculator system, Silo and wire pit	
Other areas			

Table 2-8: Sample #8 survey results.

Area of study in approach pipe systems	How important is this area of study?	What aspects are of interest to your industry?	Other comments
Flow-induced vibration	Critical	Fan pump pulsation	
Flow control	Critical	Short circulation system on paper machines	
Deaeration system	Critical		
Other areas		Fan pump design	The design of *entire* system is of interest

Table 2-9: Sample #9 survey results.

Area of study in approach pipe systems	How important is this area of study?	What aspects are of interest to your industry?	Other comments
Flow-induced vibration	Important	Too much pressure drop, MD base weight variation	
Flow control	Important	Mixing velocity, stock & white water mixing, headbox circulation line	
Deaeration system	Important	Upset fan pump, too much pressure drop, cavitation, diffuser, MD variation	
Other areas		Fan pump cracks	Practical side of research

Table 2-10: Sample #10 survey results.

Area of study in approach pipe systems	How important is this area of study?	What aspects are of interest to your industry?	Other comments
Flow-induced vibration	Important		
Flow control	Important	Thick stock and thin stock mixing	
Deaeration system	Not so important	Pipe design	
Other areas			Hope to know more about how we are doing

Table 2-11: Sample #11 survey results.

Current Guidelines

The design guidelines of approach flow systems are results of accumulated field experiences with installations, combined with basic hydraulic principles. These guidelines are generally recommendations for good system designs and should not be misconstrued as absolute design parameters. Therefore, for each individual system, due to the mill condition, specific recommendations are necessary.

Recommendations of TAPPI TIS, Valmet, Voith, and Beloit's guidelines on some approach pipe components' design are extracted in this chapter [5] [6] [7] [8] [9]. In the discussion section, we compare these design recommendations, and rationalize why these guidelines are not adequate, how some of them conflict, and what the future work will be to make the design process more practical and mill-specific.

3.1 Stuff Box

To ensure a stable heavy stock supply to the headbox approach pipe systems, some design guidelines suggest the proper use of a stuff box (shown in Fig. 3-1.)

3.1.1 Valmet's Recommendation

In Valmet's engineering instructions [8], the following two criteria are proposed:

1. **General**

The thick stock is fed into the fan pump suction either with stuff box or pump. The stock (controlled about 3% consistency) is fed through basis weight valve and quick release, or only through quick release valve, to the fan pump suction side.

2. **Stuff box construction**

The stuff box shall be placed at least 4.5 m (14.8 ft) above the white water off machine silo level to ensure sufficient inlet flow speed and pressure of the thick stock.

The connection of the thick stock inlet pipe and feed pipe to the stuff box should be made with a conical pipe to calm the thick stock flow in connection with the stuff box.

In regard to the optimum flow conditions of the fiber suspension, the stock inlet connection is situated in one end of the stuff box bottom, discharging connection in the center compartment and overflow connection in the far end.

The overflow amount of thick stock in the stuff box can be best adjusted with the adjustable-speed pump between the machine chest and stuff box, and thus avoid too much overflow from the stuff box back to the machine chest. Suitable overflow amount is $10 - 20\%$ of the inlet flow. The overflow shall take place laminarily.

The basis weight valve is to be dimensioned for its best possible operational range and placed at least 1.5m (4.9 ft) below the wire pit liquid surface to avoid risk of cavitation. (Dimensioning instructions for stuff box is referred to in ref. [8])

3.1.2 TIS' Recommendation

In the TAPPI 1995-1996 Technical Information Sheets (TIS), the following guidelines are listed:

- Uniformity of basis weight in the machine direction can be no better than the uniformity of fiber supplied by the thick stock pipe. Slurry consistency, volume, and stability must be controlled with precision.

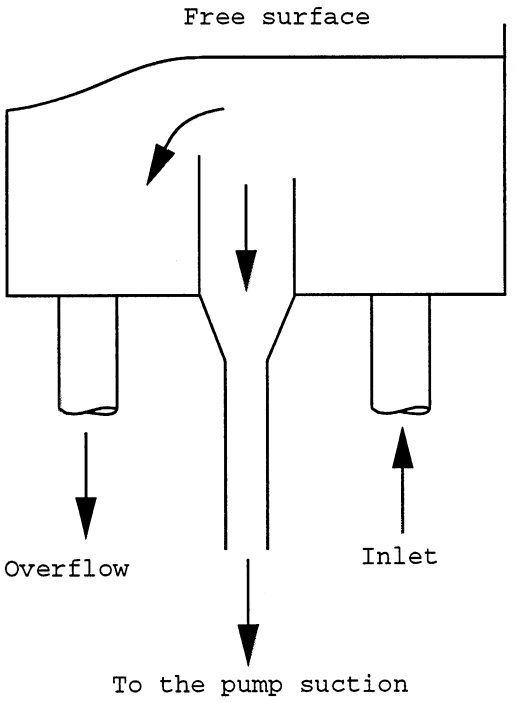

Figure 3-1: Stuff box arrangement.

- Monitor flow with stuff box or magnetic flow meter.
- Locate stuff box as close as possible to the pump suction.
- Figure 3-1 shows the stuff box arrangement.

3.1.3 Voith's Recommendation

If possible, the thick stock to the inlet of the fan pump should be controlled by means of a constant level (stuff) box [5].

- This box must be designed to avoid dead corners or uneven flow characteristics, while allowing a free surface to provide free air an opportunity to be released.
- When the stuff box is positioned very near the machine chest, the constant overflow can be returned directly to the machine chest.

- Use of a constant overflow provides a slight cushion against minor upsets in the thick stock system, and helps avoid foam or dirt build up on top of the stock.
- In order to provide sufficient dP for the basis weight control valve, the stuff box level should be 4m (13 ft) above the silo/wire pit level from which the fan pump draws its water.
- The control valve can be either a motor operated V-port ball valve or a special inclined regulating gate valve (with a narrow gate).
- Regardless of the design of the valve, it must be located below the silo/wire pit level, to avoid cavitation in the line. For best response time, the valve should be located as close to the fan pump as feasible.

3.1.4 Beloit's Recommendation

A stable system begins with a stable flow of heavy stock to that system. Proper use of a stuff box is the best way to insure this stability. By feeding the bottom of one end, discharging to the machine through a vertical dropleg from the center compartment and overflowing the far end, the box accomplishes five things:

- It eliminates much of the free air in the stock.
- It isolates the refining system from the headbox flow loop, minimizing the effects of pulsations from the preceding system. (Valves, Refiners, Pumps, etc.)
- It allows proper back pressuring of refiners, independent of head and flow requirements to the machine.
- It provides a constant head reference for the basis weight valve.
- It allows relatively constant thick stock flow to the refiners by bypassing the excess back to the machine chest.

Correct stuff box operation can be achieved with the following guidelines [9]:

- All interior surfaces in contact with stock or additives must be adequately corrosion resistant. All interior welds and surfaces must pass cotton tests.
- Eight seconds deaeration time are required from points "X" to "Y."
- Liquid level is to be 180 to 240 in (4500 to 6000 mm) above silo liquid level.
- The minimum submerged depth in feet should equal the maximum velocity in fps at "E" or 48 in (1200 mm), whichever is greater.

Notice that the basis weight valve in the machine supply dropleg must be located at a low level to insure submergence and reduce valve cavitation. This prevents erratic pressure pulsations which accompany cascading flow, as well as promotes line cleanliness. Always overflow the stuff box in the direction of flow to eliminate possible foam build up. The stuff box should be located as close as possible to the silo to minimize the length of piping to the fan pump suction.

3.2 Wire Pits and Silos

The other necessary supply to the headbox approach pipe system is the white water from wire pits and silos, which are the major factors in system stability. Besides being a collector for former drainage, they provide a stable suction head for the fan pump and act as a deaeration device.

In order to maintain stock consistency in the machine chest, no return flow or make-up flow should be fed into this chest without having its consistency controlled.

The consistency control, as well as any brush refiners, should be positioned before the machine chest. This will allow the large volume of the chest to act as a buffer against consistency variations, as it mixes and equalizes the stock.

This requires an adequate mixing action within the machine chest to avoid separation of stock and water. Inefficient or faulty consistency control after the machine chest will have a direct effect on MD weight variations as well as CD profiles.

The use of properly designed wire pits and silos will provide deaeration and stability. Two basic types of silos are the under- and off-machine silo. The design criterion is to remove free air, to provide a constant fan pump head without vortexing, to provide constant back pressure, and to have a receptable for introduction and deaeration of make-up waters.

3.2.1 Beloit's Recommendation

Beloit is concerned with the design of wire pits and silos primarily because of their utility in providing deaeration and stability. A considerable amount of air ($2-4\%$ by volume) is entrained in the white water in passing through the forming wires. This is unavoidable. Most of this air can be removed, however, with proper wire pit and silo design techniques [9].

The two basic types of silos are the under-machine type, where the pit is located directly below the former and contained within the sill beams, and the off-machine silo [9], located on the drive side of the former with connecting flow channels to the saveall troughs. The basic requirements are the same for either, and are independent of the former type for proper operation.

The under-machine type is normally used to save space on conventional Fourdrinier machines. Downspouts discharge the water drained by the table elements into the channel at the breast roll end of the pit. The flow is directed to the couch end at slow average velocities (1 to 1.25 feet per second, or 0.3 to 0.4 mps) where the flow reverses and is returned to the silo located at the breast roll end. The relatively long period of open channel flow is desirable to release air and dissipate turbulence (up to 60 seconds if possible).

The off-machine silo is often used when clays and other fillers are present and with

most twin-wire arrangements. Channels are often shortened and some deaeration time sacrificed to prevent settlement of filler. A 30-sec dwell time is still minimum with this design for flow stability. An inherent feature of the off-machine silo is the automatic separation of table drainage and shower water.

The following design principles are offered as guidelines:

- The minimum dwell time for deaeration in the flow channel is 30 sec at the required velocities [9]. (60 sec is a desirable target to achieve maximum deaeration if filler separation is not a factor.)
- Liquid level in channel should be 6 to 24 in below bottom of former saveall to prevent possible flooding of the saveall pans.
- The bottom floor should slope downward as shown, to maintain self-drainage at shut down.
- Typical slopes, shown upwards to prevent air accumulation and subsequent slime build up.
- Adjustable weir to permit level control at least 6 in (150 mm) below to 12 in (300 mm) above design weir setup dimension.
- A minimum continuous silo overflow of approximately 1000 gpm is recommended to maintain a stable and foam free liquid level at the fan pump suction.
- Assuming 100% of total gallonage through wet end downspouts, use 1.25 fps (0.4 mps) to find liquid depth. (Maximum for good deaeration is depth 3 to 5 ft or 0.9 m to 1.8 m). (Nominal design depth should be 42 in.)
- All interior surfaces of the silo and wire pit to be tile-lined or equivalent.
- Use line size giving 6.0 to 8.0 fps between basis weight valve and fan pump suction.

- Alt. 1 of section Y-Y or Alt. 2 of section Y-Y can be used for entrance into the flow channel [9].
- Use Alt. 1 of section X-X for single dilution system.
- Use Alt. 2 of section X-X for double dilution system.
- Outlets may be positioned at any 90^o angle to the silo.
- Use baffle with double dilution to prevent migration. Baffle height should be approximately 3.0 ft above top edge of pump suction.
- The end of pipes going concentric to the pump suction should be cut at a 30^o to 45^o angle to prevent "burping."

A properly designed wire pit/silo arrangement will remove free air, provide a constant fan pump head without vortexing, provide constant back pressure for the basis weight valve, and provide a receptacle for introduction (and deaeration) of make-up waters. A properly designed wire pit/silo arrangement should reduce air content in stock to under 1.0%.

3.2.2 Voith's Recommendation

The level of the white water supply reservoir (silo, wire pit, or seal pit) must be kept constant. Variations in this level will directly effect the quality of the final product [5].

- This is best accomplished by means of an overflow. This allows a cushion for sudden process changes, and long-term drainage variations.
- The maintenance of a constant level is essential. This level provides the inlet pressure against the fan pump and the back pressure against the basis weight control valve and various return flows.

The white water supply reservoir must provide adequate deaeration of the water.

- Retention time should be 0.5 to 1.0 min or greater.
- Downward velocities should not exceed 0.5 fps, to allow air a chance to rise to the surface.
- Maximize surface area to provide maximum opportunity for the release of air.
- Discharges into the reservoir should avoid high velocities and "waterfalls" that may entrain additional air.

Reservoir design must avoid stagnant areas (dead corners). Whenever possible, if space is available, the use of a white water silo over a wire pit or tank is recommended.

- This minimizes the potential cascading of white water.
- Reduction in air entrainment reduces the need for and expense of foam retardants.
- Inlet pressure to the fan pump is increased, reducing head and energy requirements.
- Operation of an auxiliary screen (vibrating) is enhanced as its discharge (if set on the machine room floor elevation) can be directed into a flooded collection tank.
- Start-up requires less "filling" of the system. Hence, stable operation is achieved more readily.

3.2.3 Valmet's Recommendation

The silo is another area in which sufficient retention should be allowed for the liberation of air. The downward velocity in the silo should be around 0.5 ft/sec to allow

entrained air to escape and the retention time should be approximately 60-90 sec. Often, the silo level is raised in order to increase the NPSHa for the fan pump or mixing pump. This is detrimental to the process because the retention time is lowered and the air must travel a greater distance to be liberated, possibly worsening the problem. The tray water must not be allowed to cascade into the silo for the same reasons indicated in the overflow lines.

3.3 Fan Pump

In sizing a fan pump, care must be taken that the pump will operate at a maximum impeller rpm over the entire range of flows and consistencies. There are two types of fan pumps, one is the variable speed centrifugal and the other is the constant speed one.

3.3.1 Voith's Recommendation

For the variable speed pumps, the following guidelines are suggested:

- Vane frequency at low rpm conditions should not be less than 60 Hz.
- Normally used when variation in flow downstream of the fan pump is not detrimental to system performance. Such as no flow sensitive cleaning equipment, double dilution system, or a modified bypass system (if cleaners are not extremely sensitive to flow variations a small bypass can be utilized after the cleaners to control a dP range across the cleaners, while offering variable speed pump flow control to the headbox.)
- Energy efficient.
- Simplified, cleaner, and smaller approach flow system, through the elimination of bypass flows and throttling control valves.

- Reduce opportunity for pulsation generation.
- Reduce opportunity for consistency variations.
- Smooth headbox pressure control.
- During operation, the high points of the pump casing should be bled continuously for air.

3.3.2 Beloit's Recommendation

- Pumps should be selected for a maximum impeller rpm to help raise the frequency beyond the troublesome area.
- The impeller should have a maximum number of vanes.
- The impeller vanes should be split, staggered, and skewed if a double suction pump is selected.
- The impeller must be properly balanced and obviously must not operate near critical speeds. The impeller must be hydraulically as well as mechanically balanced; that is, there should be provision for equal flow through each of the impeller channels.
- Impeller deflection must be minimized.
- The suction head of the pump should well exceed maximum NPSH ("Net Positive Suction Head") requirements.

3.3.3 TIS' Recommendation

- Double suction type; split impeller with staggered vanes is recommended.
- Variable speed drive with good controls is recommended.

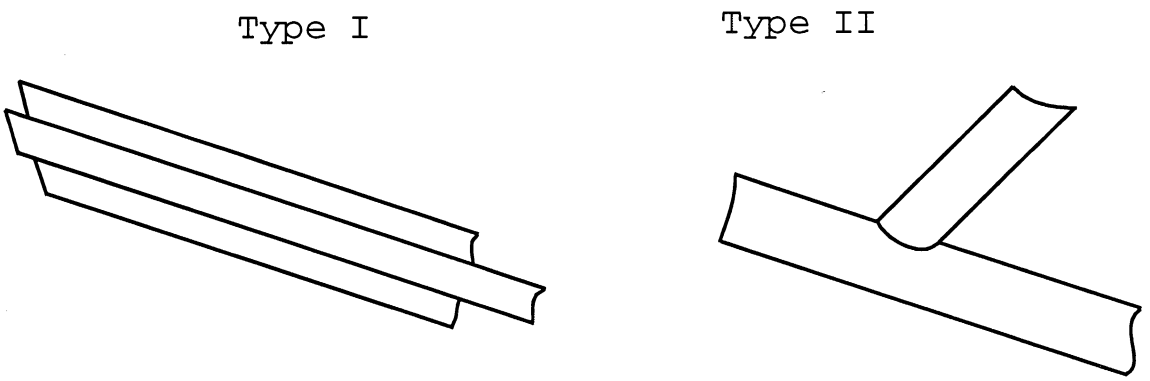

Figure 3-2: Mixing pipe arrangement.

- If oversized, avoid excessive throttling; reduce impeller diameter (check pump manufacturer's recommendations) or reduce speed.
- The inlet should be large to maintain a low velocity.
- Locate inlet to obtain a symmetrical flow to the pump whenever possible.

3.4 Piping Arrangement

Proper flow velocities must be maintained in any piping system. As stock travels through a system, it has a tendency to flocculate. If the proper velocity range is maintained, the stock will be less likely to flocculate and remain well mixed without creating undue turbulence.

Suppose we now have the uniform flows from thick stock, white water, and chemical additives, the mixing before the fan pump will determine the final stock approaching the headbox. There are two ways of mixing the lines shown in Fig. 3-2, one is to use concentric design and the other is to use an alternate top entry arrangement.

For the concentric design, the velocity of thick stock is higher than the white water from the wire pit and silo. For the pipe intersection, less than 45^o is recommended to avoid burping.

One of the most important design considerations for this system is how to provide the best mixing of cleaned stock with white water in the fan pump. Cleaned stock normally increases the velocity of the mixture as it flows toward the fan pump, the final mixing takes place in the pump.

3.4.1 General Recommendations

- Make pipe lines as short as possible.
- Maintain flow velocity in the range of 5 to 15 ft/sec.
- Use noncorrosive pipe with smooth inside finish.
- Grind internal welds, remove weld spatter and polish with fine abrasive to assure acceptable smoothness. Check for residual roughness using the cotton ball test, particularly for pulps which easily form lumps and strings.
- Pipes should fit together smoothly. Fit gaskets carefully to avoid protrusion into the flow. Particularly between screens and headbox, use ground metal-to-metal flanges (Metlap, Vanstone or equivalent).
- Avoid stagnant pockets of stock.
- Install drains at low points. Drain plugs should be flush with the inside wall.

3.4.2 TIS' Recommendation

- Piping to the headbox header should consist of a straight length which is two or more pipe diameters long and is preceded by a long radius elbow, Venturi elbow, or gradual transition.
- Slope pipes upwards (1 in or more per foot) from the fan pump to the header to eliminate air pockets. This will also give better back drainage when the fan pump is shut down.

- When it is impossible to maintain a continuous upward slope to sweep out air pockets, high points (such as the top of a pressure screen) should be vented continuously. Successful venting, of course, requires that the vented area is always above atmospheric pressure.
- High flow velocities (10 ft/sec and faster) will sweep air out of lines that do not slope upward.
- Avoid air entrainment by cascades or vortices.
- Consider removal of troublesome air by a vacuum system.
- Adjustment of the recirculation flow from the end of a side entry tapered header can be overly sensitive if this line and valve are over-sized. Each header is designed for a specific recirculation, which is typically between 2 and 10% of the headbox flow. The line and valve should be sized to pass approximately one and a half times the design recirculation with the control valve fully open.
- A sight flow indicator on the header will assist in adjustment of the recirculation flow.
- Walls should diverge from the mean flow direction at less than 5^o to avoid separation, and walls should converge at less than 45^o.

3.4.3 Voith's Recommendation

As a general rule, all horizontal piping should be up hill (in the direction of the flow).

- Thick stock $(3-4\%)$ piping should be set at a minimum of 1.5 in rise per foot.
- Short runs of low consistency stock flow $(0.25-1\%)$ may be set at 0.5 in rise per foot.

- Pipe velocities (other than controlled mixing points) should be no less than 6 fps to prevent settling of stock and slime generation.

- Provide for deaeration all high points in the piping lines. Deaeration lines should be left slightly open at all times. Air vent lines should be separately piped to a free surface discharge point.

3.5 Flow-Induced Vibration and Variations

The wire pit and screens, the screens and headbox, and parts of the headbox may all form oscillating systems. In the case where the damping is not effective and the resonance occurs, these oscillations will approach the headbox and eventually cause basis weight variations by changing both head and consistency in the stuff box [5] [7] [8] [9].

It is essential that with the piping system layout, all high-fiber content flows are mixed in a uniform and smooth manner. The most efficient way to assure thorough mixing is through the use of a collecting pipe. This method mixes individual return flows and thick stock flow into a single pipe, prior to mixing with dilution water and being introduced into the suction of the fan pump. Assuming mixing considerations are properly followed, this method will eliminate the possibility of basis weight variations due to poor mixing, and it can also premix the return flows some distance away from the fan pump. It is feasible to bring high fiber flows individually into the suction line of the fan pump. This requires additional space to achieve proper mixing conditions. Uncontrolled mixing by free discharge into the white water supply must be avoided at all times.

Headbox recirculation should be returned to the fan pump suction through the white water supply. This must be done in a manner that ensures uniform mixing, while offering a separation between the recirculation piping and the remaining piping in the approach flow system. Since pulsations introduced into the recirculation line

will have a direct effect upon the headbox, by disconnecting the recirculation from the rest of the system, the influence of pulsations in the pump and the collecting pipe upon the headbox can be greatly reduced.

To eliminate flow-induced vibration, the following general guidelines are commonly used [22]:

- Simple hangers alone are not adequate for headers that are located under the floor.
- Cross bracing must resist motion in the other two directions.
- Support or brace all piping, particularly at the headbox inlet.
- Support headers front and back; anchor to prevent CD vibration.

System sized for anticipated future higher volumes can be troublesome during the start-up period. Temporary modifications to the fan pump system should be considered, if a long period of sub-capacity operation is anticipated.

Immediately before the headbox (downstream of the screen) should be considered a critical piping area and all design guidelines should be stringently followed.

For step diffuser headboxes on Fourdriniers which are equipped with a P.E. Tank (Pulsation Elimination System), the tank serves as a hydraulic elbow, uniformly distributing the flow (as delivered to the tank) across the full width of the inlet. This provides a uniform distribution across the width of the machine. However, the tank will not completely compensate for inefficiently distributed retention aid, etc., and prior to the P.E. Tank, there should be a minimum of 3 pipe diameters of straight run.

For pressure headboxes with highly filled sheets, the possibility of flow separation (uneven filler distribution) in the elbows should be given special consideration. The straight run of pipe should be 8 pipe diameters (minimum of 5). If the straight run must be less than 6 diameters, then it is advisable to utilize a Venturi type

(aka acceleration) elbow. Further information is available on this design from Sulzer Papertec Middletown Inc. (SPMI) as required [5].

Separate branch lines by 2 (branch) pipe diameters. Enter at 60^o or, better, 45^o. Flow velocity should be low, less than 10 ft/sec. Match with main flow velocity. The inlet closest to the pump should be the highest consistency. Avoid branch lines entering diametrically opposite each other to prevent the flow of one affecting the discharge of the second. Arrange branch inlets to avoid asymmetrical flows into the fan pump suction.

3.6 Location of Valves

Valves control the pressure, rate of flow, and direction of fluids in accordance with basic principles of flow [5] [6] [7] [8] [9].

No valve should be within eight pipe diameters of the header entrance. Variable speed fan pump with good controls preferred. No in-line valve required. Coarse control by a suitable control valve. Operate valves within optimum operating range to avoid cavitation. Install valves before the screens, none between the screens and headbox.

Use suitable control valve on the fan pump bypass, sized to give a maximum of 20% run-around. A second recirculation line with coarse control can be used to bring the control valve into an optimum operating position.

Precede by 5 (preferably 8 or more) pipe diameters of straight pipe, and follow by 5 (preferably 8) pipe diameters of straight pipe before tees or elbows. In locations with space limitations, consider the use of vaned elbows.

Low elevations (submerged with respect to downstream pressure) for valves on return lines are advisable to minimize the possibility of surging, resulting from the trapped air after the valves. (This also minimizes negative pressures that can develop from back flow at shutdown). All recirculation lines should go into pipeline leading

to the pump suction, not into the wire pit.

All control valves should be located to ensure there is a back pressure at all times. This can be accomplished by locating all valves below the surface of the white water supply. Valves may be located as to have downstream flow at a higher elevation than the valve. When conditions dictate, a valve in a vertical flow downward line may be placed above the surface of the white water supply, if there is a downstream pressure drop greater than the physical elevation difference between the valve location and the white water supply. The guiding factor is that the flow in the approach flow system should be under positive pressure (except in specifically designed areas - i.e., deaeration tanks) at all times. Allowing flows in the approach flow system to generate a natural vacuum will increase free air entrainment, foam generation, and pulsation generation due to cavitation.

3.7 Elbow

3.7.1 Voith's Recommendation

Bends in flow should be made with long radius (Radius = 1.5× Normal Diameter), smooth flow elbows.

- Do not use mitred elbows due to the possibility of generating pulsations.
- Do not use vaned elbows due to the potential of fiber hang ups.

3.7.2 TIS' Recommendation

- Medium radius or vaned elbows are preferred. Medium radius elbows should be followed by at least two pipe diameters of straight pipe.
- Two successive medium radius elbows should not lie in planes inclined at 90^o to each other.

- Mitred vaned elbows are recommended in locations where uniform flow is desirable and a straight pipe run is impractical. In circular pipes, the vanes can be welded into a band at the mitred section. The chord dimension can be selected to provide a convenient number of vanes for any size of elbow, but generally the vane spacing c/3 should lie between 2 in for small pipes and 5 in for large pipes. The leading edges of the vanes should be wider than the longest fiber, or 3/8 in minimum, and the trailing edges rounded. End welds should be continuous and polished. A modification of the above design includes transitions to a rectangular mitred vaned section. This vaned section may be easier to fabricate and, by including a curved wall at the outside of the bend, gives better flow control. The number of vanes of a vaned bend (no miter) design is based on the feasibility of fabrication. All vanes must be carefully designed to avoid stapling of long fibers. Interior welds must be ground smooth and pass the cotton ball test.

- Discharge velocity from the ends of a tee should be greater than, or equal to, the entrance velocity; the distance may be valved to restrict and stabilize the discharge.

3.8 Discussions

Although many of the extracted guidelines from different companies and TIS are similar, they do not lack confusion and contradictions. In conclusion, the additional need in designing approach pipe systems is to have more precise and clearer guidelines, especially more key parameters based on deeper fundamental understanding. It is found that most of the existing guidelines are based on the past engineering experiences. Some of the design guidelines could be dated back for a few decades. Very little information is available on the nonlinear transient behavior of the approach flow system. A proper way to achieve the optimized approach flow system design is

really to have the computational tools to simulate individual components as well as the whole system.

The common guidelines for the stuff box is to arrange the valve and stuff box over the white water level. It is also conceivable that the stuff box can be treated as a pulsation isolator between the refining system and the flow to the headbox. Although certain hydraulic parameters are given in some guidelines, the detailed design is really hard to master based on these simple rules extracted from the mass conservation law. For example, how to optimize the vortex free stuff box free surface and the outlet is never achieved.

As far as the wire pit and white white silo are concerned, the design is focusing on the appropriate time for deaeration and stable water supply to the fan pump. However, the detail information such as the mixing region before the fan pump is really not available. In fact, Valmet has a very different silo outlet geometry recommendation from Beloit's.

Commonly, variable centrifugal pumps are recommended by paper machine suppliers, the needed controls of the pump are the stable inlet, impeller selections. However, the information on how to avoid the deflection of the vanes, how the fan pump reacts to certain variation during the papermaking process, and the detail design information for low consistency stock is not available. In addition, for the most critical part of pipe mixing, i.e. the mixing between the stock and white water before the fan pump, there has been very little in-depth research done in the past.

Also, the guidelines for flow-induced vibration should really be considered much more specifically than the current ones.

In practice, due to the specific mill conditions and the change of certain components within the approach flow systems, the existing guidelines are not always followed. Therefore, it is very much needed to have a computer model to handle the analysis of the whole approach flow system as well as the individual components.

Research Approaches

The dynamics of the wet end includes pressure variation, flow, and consistency dynamics. The nonlinear dynamics computer modeling of the approach flow system will help to analyze and to design the system with the consideration of perturbation effects. The overall research approach would be two-fold:

- in-depth analysis of all components such as pressure attenuator, fan pump, elbow, pipe mixing section, white water silo, stuff box, deaeration system, pressure screen and cleaner within approach flow systems using finite element and other computational procedures; and
- incorporate the computer simulation results into a global nonlinear dynamic mathematical model, and obtain the solution with computational methods.

4.1 Engineering Approach

Starting from the Navier-Stokes equations, we can derive the following transient control equation between point 1 and 2

$$\int_1^2 \{\frac{\partial \mathbf{v}}{\partial t} + \nabla(\frac{\mathbf{v}\cdot\mathbf{v}}{2}) + \frac{\nabla p}{\rho} + \nabla(gz)\}\cdot d\mathbf{r} = \int_1^2 \{\mathbf{v}\times(\nabla\times\mathbf{v})\}\cdot d\mathbf{r}. \qquad (4.1)$$

where $\mathbf{v}$, p, ρ, $d\mathbf{r}$, g and z stand for the flow velocity, pressure, fluid density, streamline differential distance, gravity, and vertical Cartesian coordinate.

The r.h.s will be zero if either of the following holds:

- Positions 1 and 2 are on the same streamline; or
- $\nabla \times \mathbf{v} = \mathbf{0}$.

Notice here, in applying the above relation to our stock, the density change around the streamline might be considered. In the hydraulic control system, the pressure transient behavior within the pipe can be estimated by the above equation. Of course, the pipe flow direction is assumed to be the streamline direction in practice.

In engineering approach, pressure and flow dynamics have been modeled using Bernoulli equations [12]

$$p_1 = p_2 + \frac{L}{A}\frac{dQ}{dt} + \Delta p + s \tag{4.2}$$

where Q, L, A, Δp and s denote the flow rate, path length, cross section area, pressure source for the pipe containing the elevation difference between point 1 and 2, and any heads provided by pumps. Since pumps receive energy from outside the approach pipe system and are used to raise the energy level of the flow, the output of the pump constitutes the total source of energy available within the hydraulic system. Nevertheless, the total of the energy outputs from the system by components such as the drive motor and hydraulic cylinders is not equal to the total energy available from the pump because of friction and heat losses within the system. The proper determination of the correct pump for a given application essentially involves matching the pump to the required fluid power actuator giving consideration to pressure, flow rates, available drive speeds and power, efficiencies, cost, size, maintenance, and the operational characteristics of the pump and system. These include pump noise, vibration, natural frequency, and flow characteristics.

In addition to functioning in a stable, easily controlled manner, the fan pump system should afford a minimum possibility of forming agglomeration, or bundles, that cause sheet defects or breaks. Obviously, some detail analysis within the pump is necessary in addition to the engineering approaches.

Eq. (4.2) was often found to be inadequate, especially in the modeling of pump impeller vane deflection, screen vibration, and high frequency variations. Its modification is to include the continuous equation by introducing the fluid bulk modulus β.

For the consistency dynamics, the control equation can be often given as

$$\frac{dC_o}{dt} = \frac{1}{\tau}(C_i - C_o) \tag{4.3}$$

where C is the consistency, V is the tank volume, and $\tau = \frac{V}{Q}$ is time constant of the tank.

4.2 Displacement/Pressure (u/p) Formulation

A number of finite element formulations have been proposed to model an acoustic fluid for the analysis of fluid-structure interaction problems, namely, the displacement formulation (see Belytschko [23], Bathe and Hahn [24], Hamdi, et al [25], Belytschko and Kennedy [26], Olson and Bathe [27]), the displacement potential and pressure formulation (Morand and Ohayon [28]), and the velocity potential formulation (Everstine [29], Olson and Bathe [30], Felippa and Ohayon [31]).

Primitive variable formulations have received considerable attention because they do not require any special interface conditions or new solution strategies (for example, in frequency calculations and response spectrum analysis). With the ever-increasing availability of high-speed and large-capacity computers, this approach shows great promise in general applications to the solution of a broad range of problems (specifically nonlinear problems) [32] [33] [34].

In the mixed displacement/pressure formulation, we define a variational indicator

$$\Pi = \int_{V_f} \{\frac{p^2}{2\beta} - \mathbf{u}\cdot\boldsymbol{f}^B - \lambda_p(\frac{p}{\beta} + \nabla\cdot\mathbf{u})\}dV + \int_{S_f} \bar{p}\, u_n^s\, dS$$

where the variables are p, $\mathbf{u}$, and the Lagrange multiplier λ_p. We note that the first two terms correspond to the usual strain energy (given in terms of the pressure) and the potential of the externally applied body forces. The third term enforces the constitutive relation. The last term is the potential due to any applied boundary pressure on S_f.

Invoking the stationarity of Π, we identify the Lagrange multiplier λ_p to be the pressure p and obtain the governing equations, with $\boldsymbol{f}^B = -\rho\ddot{\mathbf{u}}$,

$$\nabla p + \rho\ddot{\mathbf{u}} = \mathbf{0} \tag{4.4}$$

$$\nabla\cdot\mathbf{u} + \frac{p}{\beta} = 0 \tag{4.5}$$

with the boundary conditions

$$\begin{aligned} \mathbf{u}\cdot\mathbf{n} &= \bar{u}_n \quad \text{on } S_u \\ p &= \bar{p} \quad \text{on } S_f. \end{aligned} \tag{4.6}$$

Applying the standard Galerkin discretization procedure, we have for a typical finite element

$$\begin{aligned} \mathbf{u} &= \mathbf{H}\widehat{\mathbf{U}} \\ p &= \mathbf{H}_p\widehat{\mathbf{P}} \\ \nabla\cdot\mathbf{u} &= (\nabla\cdot\mathbf{H})\widehat{\mathbf{U}} = \mathbf{B}\widehat{\mathbf{U}} \end{aligned}$$

where $\mathbf{H}$ and $\mathbf{H}_p$ are the interpolation matrices, and $\widehat{\mathbf{U}}$ and $\widehat{\mathbf{P}}$ are the vectors of

solution variables [35].

The matrix equations of the u/p formulation are given as

$$\begin{bmatrix} \mathbf{M} & \mathbf{0} \\ \mathbf{0} & \mathbf{0} \end{bmatrix} \begin{Bmatrix} \ddot{\widehat{\mathbf{U}}} \\ \ddot{\widehat{\mathbf{P}}} \end{Bmatrix} + \begin{bmatrix} \mathbf{0} & \mathbf{L} \\ \mathbf{L}^T & \mathbf{A} \end{bmatrix} \begin{Bmatrix} \widehat{\mathbf{U}} \\ \widehat{\mathbf{P}} \end{Bmatrix} = \begin{Bmatrix} \mathbf{R} \\ \mathbf{0} \end{Bmatrix} \tag{4.7}$$

where

$$\mathbf{M} = \int_{V_f} \rho \mathbf{H}^T \mathbf{H} dV \qquad \mathbf{L} = -\int_{V_f} \mathbf{B}^T \mathbf{H}_p dV$$

$$\mathbf{A} = -\int_{V_f} \frac{1}{\beta} \mathbf{H}_p^T \mathbf{H}_p dV \qquad \mathbf{R} = -\int_{S_f} \mathbf{H}_n^{ST} \bar{p}\, dS.$$

In the u/p formulation we interpolate displacements and pressure as independent variables, and we employ elements that satisfy the inf-sup condition. It is also important that the slip boundary conditions are introduced such that the requirements of mass and momentum conservation around the fluid boundaries and fluid-structure interfaces are satisfied.

Using the u/p formulation for the solution of frequencies, many (exact) zero frequencies are calculated. The exact number of these zero frequencies can be predicted, and in the solution the eigensolver simply shifts over them [35]. Also, the number of zero frequencies can be reduced by use of the u-p-Λ formulation (see also reference [32]).

This displacement/pressure finite element formulation for the analysis of acoustic/slosh fluid-structure interaction problems can be used effectively in this project.

4.3 Pressure Pulsation Attenuator

Extremely low frequency basis weight variations, from 0.001 Hz to 1 Hz, are often related to thick stock flow. It is essential that the thick stock, at 3 to 4% consistency, be fed at a uniform flow rate and stable consistency to the inlet of the fan pump.

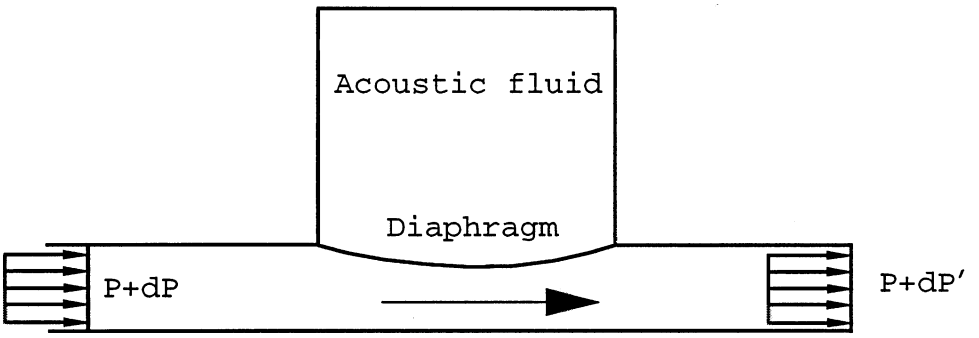

Figure 4-1: Pressure pulsation attenuator mathematical model.

To finally achieve the uniform and consistent stock flow to the headbox, a properly designed pressure pulsation attenuator has to be used to effectively eliminate both the low- and high-range frequencies.

The above-discussed formulation can be directly applied to analyze the pressure pulsation attenuator shown in Fig. 4-1. In fact, computation modeling of this sort can also be applied to obtain optimized designs of different components.

4.4 Pipeline Simulation

Pipelines are nonlinear devices. The flow of fluids in pipes resembles, to a certain degree, the flow of electric current in nonlinear resistances. Kirchoff's laws can be applied directly (see Fig 4-2), however, the Ohm's law is replaced by the nonlinear relation between flow rate Q and the friction loss ΔH

$$\Delta H = S(Q) = LC_2 \frac{4}{(3.6\log(C_1 Q/8d\nu))^2} \frac{Q^2}{d^5} \tag{4.8}$$

and

$$Q = S^{-1}(\Delta H) = \sqrt{\frac{\Delta H d^5}{LC_2}}(-2log(\frac{2.825\nu}{C_1}\sqrt{\frac{C_2 L}{\Delta H d^3}})) \tag{4.9}$$

where C_1 and C_2 are the constants found from experimental results, and ν, L and d are the kinematic viscosity, pipe length, and pipe diameter.

The head loss ΔH can also be written as

$$\Delta H = f(Re, \frac{\epsilon}{d})\frac{L}{d}\frac{U^2}{2g} \tag{4.10}$$

where Re, ϵ, and U are Reynolds number, surface roughness measure, and pipe flow mean velocity, respectively.

From the Karman-Prandtl equation, for smooth pipes, we have

$$\frac{1}{\sqrt{f}} = 2log_{10}(Re\sqrt{f}) - 0.8. \tag{4.11}$$

In actuality, the head loss will include the local head loss in turbulent flow, the head loss due to sudden expansion, the loss in elbow (or pipe bends), the loss at combining and dividing junctions. Of course, the concept of the equivalent pipe length can also be extended.

In the study of transient flow, especially pressure surges in long pipelines, there are close equivalents to the transmission line telegraph and telephone equations. In the approach pipe flow system, fan pumps, pressure screens, cleaners, and elbows can be simulated by different electrical devices.

Notice that to deal with the nonlinear relations in Eqs. (4.8) and (4.9), in practice iterative methods have to be used.

For the complex pipeline systems, we apply the following

Pipelines in Series:

$$\sum_{i=1}^{N} \Delta H_i = \sum_{i=1}^{N} S_i(Q) = \Delta H \tag{4.12}$$

Parallel Pipelines:

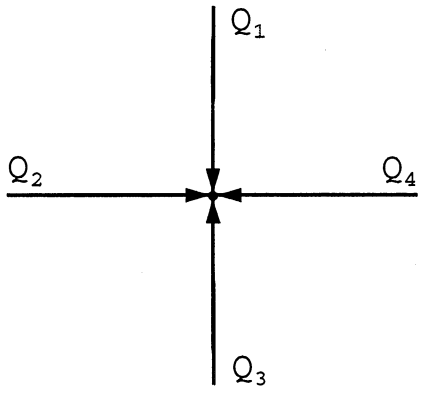

$$Q_1 + Q_2 + Q_3 + Q_4 = 0$$

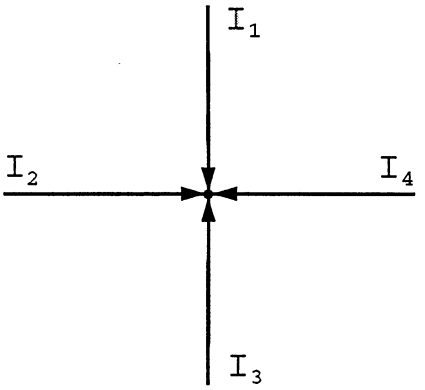

$$I_1 + I_2 + I_3 + I_4 = 0$$

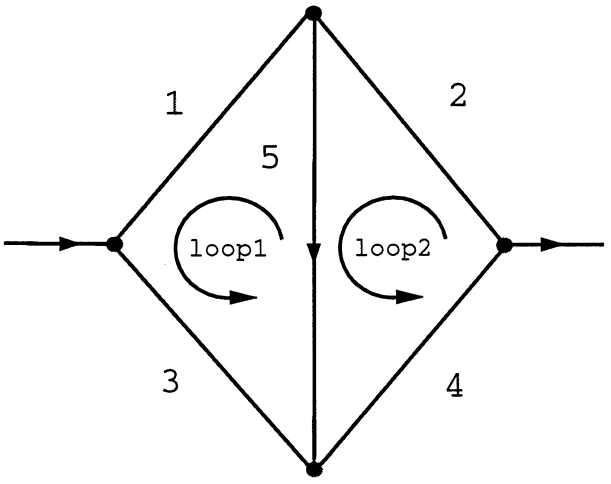

$$\Delta H_1 + \Delta H_5 + \Delta H_3 = 0$$
$$\Delta H_2 + \Delta H_4 - \Delta H_5 = 0$$

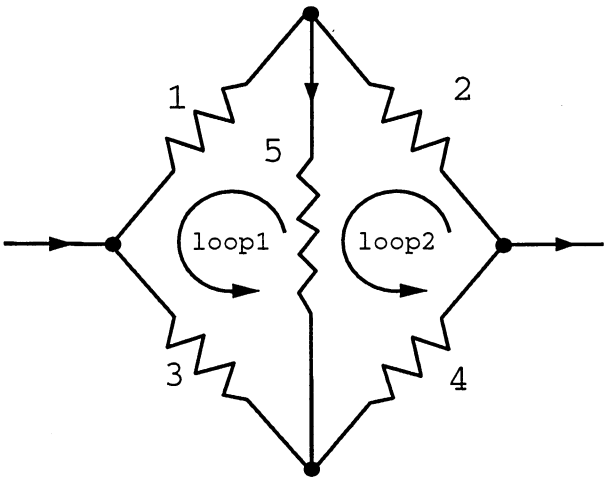

$$\Delta V_1 + \Delta V_5 + \Delta V_3 = 0$$
$$\Delta V_2 + \Delta V_4 - \Delta V_5 = 0$$

Figure 4-2: Analogy to electrical devices.

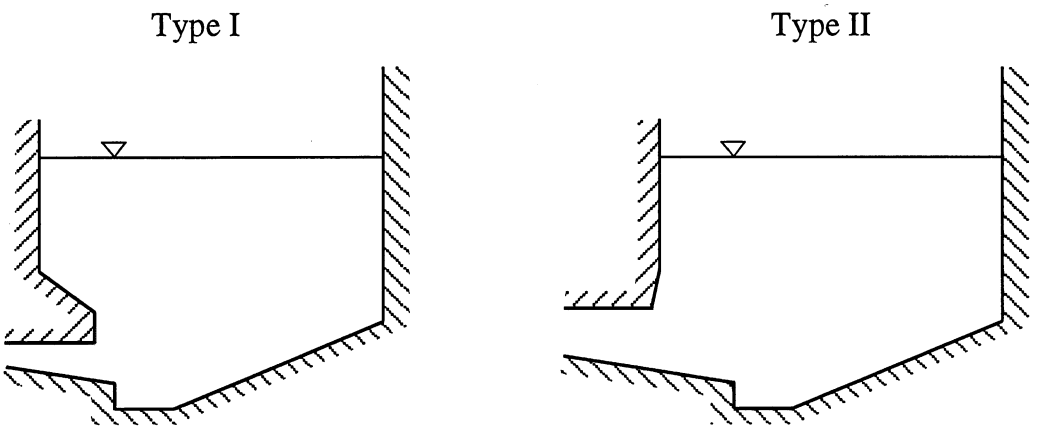

Figure 4-3: Silo design.

$$\sum_{i=1}^{N} Q_i = \sum_{i=1}^{N} S_i^{-1}(\Delta H) = Q \tag{4.13}$$

and Kirchoff's laws to *Partial Looped Pipelines*, *Branching Pipelines*, and *Pipeline Networks*. As discussed before, computational models of different approach flow system components are going to be used to get the simplified equations such as Eqs. (4.8) and (4.9). For example, in the analysis of the free vibration of fluid submerged impeller, the computational procedure with the u/p formulation as described above is efficient and sufficiently accurate. A similar computational model can be applied to the other components as well. Finally, we can incorporate the equations such as Eqs. (4.8) and (4.9) into a global model of the approach flow system, and apply the computational nonlinear dynamics procedure to analyze the effects of individual components' variation on the system. A schematic hierarchy is shown in Fig. 4-4.

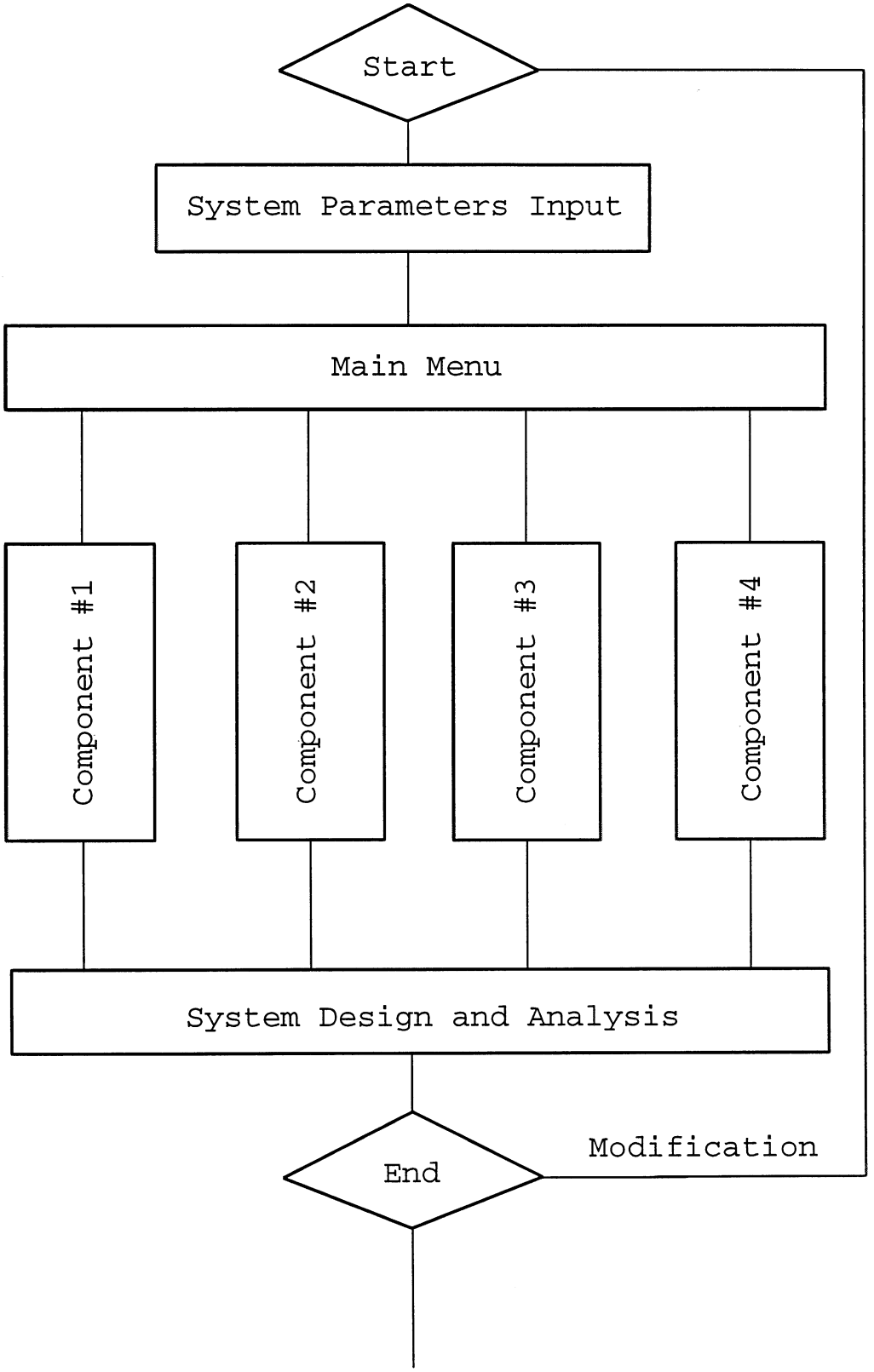

Figure 4-4: An overview of the computer simulation of the approach flow system (eventually the whole wet end processes.)

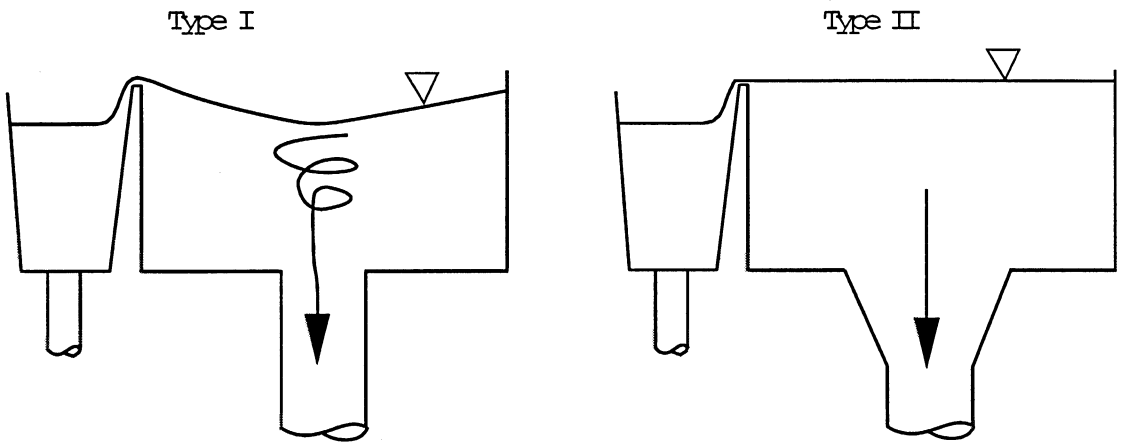

Figure 4-5: Development of vortices.

4.5 Silo Design

Due to the different silo design guidelines [7] [9], in this research project, we will develop a computer model to analyze some white water silo prototypes (shown in Fig. 4-3) and discuss the advantages and disadvantages.

4.6 Vortex Forming

Air entrainment in the stock can result in pressure variations, machine direction basis weight variations, slime and dirt spots, foaming, and pinholes. One of the interesting problems is the vortices forming during the discharge outlets of chests, stuff boxes, and wire pits (shown in Fig. 4-5). It is anticipated that proper CFD models can be used to optimize the design process.

4.7 Application of Fluidics and Hydraulics

Fluidics is the technology of employing the general fluid phenomena of wall-attachment and stream interaction in specially designed devices to perform the functions of sensing, logic, and control [21] [36] [37] [38] [39] [40]. Some of the control procedures will have the potential application to papermaking industries.

Major innovation in the utilization of fluids occurred in the 18th century as the Newcomen steam pump (1711) and Watt's steam engine (1769) were harnessed for the rapidly increasing power requirements of the industrial revolution. In 1904 a German aerodynamicist, Prandtl, proposed the control of flow separation in a wide-angled diffuser illustrated in Fig. 4-6. Nicola Tesla filed a patent in 1916 for a "Valvular condult" which performed as a fluid diode, causing high resistance to fluid flow in one direction and low resistance in the opposite direction shown in Fig. 4-7.

Figure 4-8 shows the effect upon the velocity profile caused by shifting the separation point. It can be seen that the velocity of the flow near the outer wall is increased [41].

Figure 4-9 shows the turbulence amplifier. A laminar jet is produced from the supply port. When the jet is disturbed and becomes turbulent before reaching the outlet channel, the output signal falls from its previous value to a much smaller one. Notice that the jet does not become laminar again immediately on removal of the control signal, probably because of the feedback of turbulent flow from the region of the outlet channel towards the control ports. The delay is found to be four times the time for transport of a particle along the length of the jet.

4.8 Unsteady Flow in Piping System

Unsteady flow in piping systems is a common occurrence. Indeed, steady flow is so rare that one might question the advisability of devoting so much time to a study of its behavior. Although most of all hydraulic design is based on steady flow analysis and,

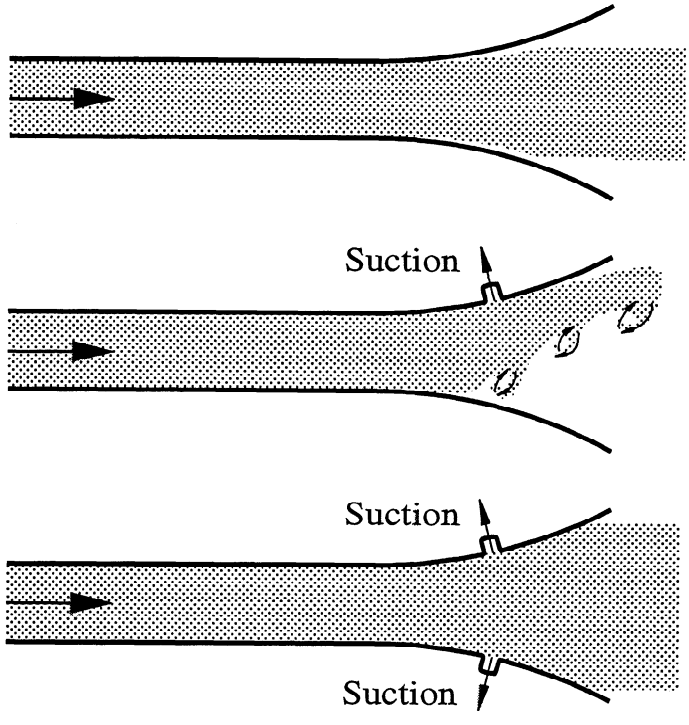

Figure 4-6: Prandtl Diffuser.

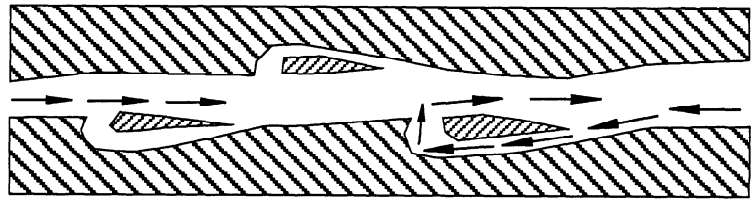

Figure 4-7: Tesla's Diode.

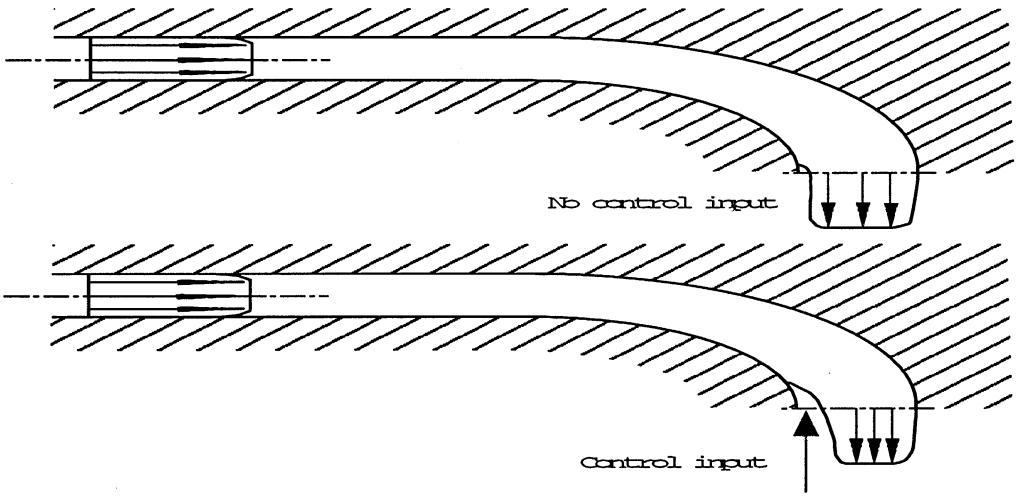

Figure 4-8: The velocity profile is changed by varying the control input.

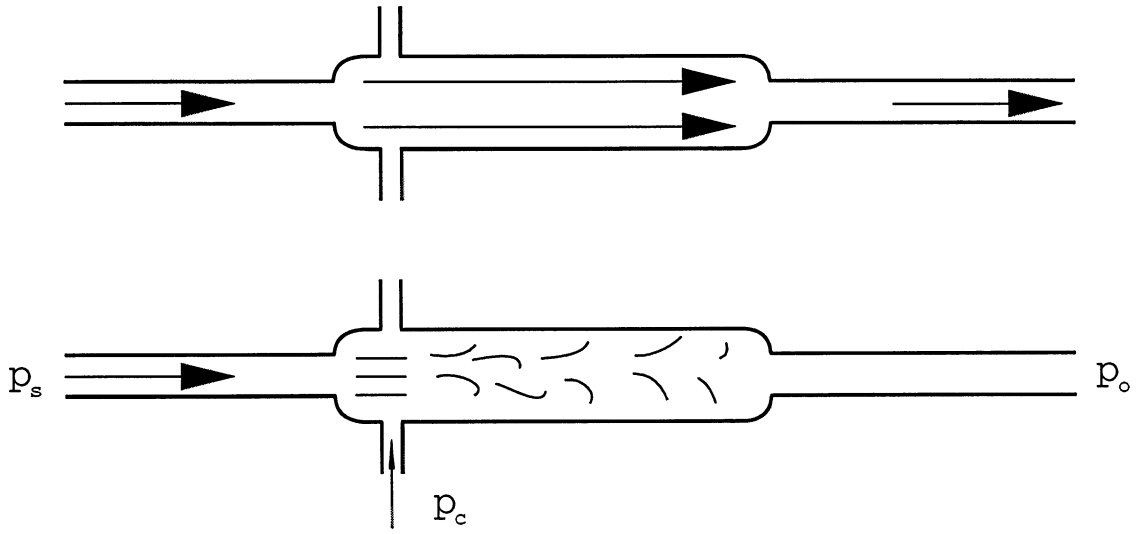

Figure 4-9: Turbulence amplifier.

in many cases, the unsteadiness occurring in a pipeline system is of little consequence because of its transient nature and small magnitude of change, in paper industry, the unsteady flow within the approach flow piping is detrimental to the papermaking process.

The control equation for the transient behavior within the pipe can be written as [42]

$$\frac{\partial p}{\partial s} + \rho g \frac{\partial z}{\partial s} + \frac{4\tau}{d} = \rho \frac{dv}{dt} \tag{4.14}$$

where d is the pipe diameter, τ is the shear stress at the wall, and v is the average velocity. Notice that none of the existing research in this area deals with nonlinear dynamics involving consistency and pressure variations, although in practice the perturbation due to various sources can be detrimental to the manufacturing processes. It will be part of the approach flow system project to simulate the nonlinear variations.

Research Planning

The following M.S. and Ph.D. projects could be generated from the research in this area

(1) Computer Simulation of Approach Pipe System Dynamic Behaviors (M.S.)

(2) Mixing Behavior of White Water and Stocks Before the Fan Pump (M.S.)

(3) Mixing Behavior of Chemical Additives and Uniformity of Consistency (Ph.D.)

(4) Flow Separation and Cavitation (Ph.D.)

(5) Flow-induced Vibration of Approach Pipe Systems and Headboxes (Ph.D.)

(6) Nonlinear Dynamical Behavior of Approach Pipe Systems Subjected to Perturbation (Ph.D.)

The fundamental research topics related to the above five projects are multidisciplinary. It includes the following hot subjects in computational mechanics areas:

(1) Turbulence Theory and Nonlinear Dynamics

(2) Fluid-Structure Interactions

(3) Both Spatial and Temporal Stability of Numerical Procedures

It is justified that a funded project should be established in the approach pipe system area. This project will help to form an education and research center for study in this area as well as the whole wet end papermaking processes.

Once the research is funded, we will start by analyzing the individual components

	1	2	3	4	5	6	7	8	9	10	11	12	1	2	3	4	5	6
Pulsation attenuator	-	-	-	-	-	-												
Pipe flow mixture							-	-	-	-	-							
White water silo												-	-	-				
Elbow															-	-	-	-
Writing report												-						-

Table 5-1: Tasks and time line.

within approach flow systems. The following problems will be focused on first:

- pressure pulsation attenuator;
- White water silo;
- Pipe mixture;
- Fan pump;
- Elbow; and
- Stuff box.

The second stage will be two-fold, firstly, we will continue to analyze specific components within approach pipe flows; secondly, the whole system model will be developed and analyzed.

Although at this stage, it would be hard to exactly follow the time lines, Table 5-1 is used to illustrate the tentative planning of this project for the first one and a half years.

Conclusions

Regardless of dampening features of individual headbox designs, it is important to minimize the system variations prior to delivery of stock to the headbox. This will maximize the capability of the headbox to provide a uniform and consistent delivery of fiber to the machine. The more stable the approach pipe system, the better the end product. In fact, in modern paper machine designs, consistency variations are of specific importance and it is nearly impossible to compensate for a swing in fiber flow within the short dwell time of any headbox. This will only be accentuated as the paper industry turns to more and more hydraulic headboxes and shorter forming sections.

From the information provided by papermaking PAC members and other resources, it seems that many possibilities exist for specific research focuses with the proposed project. In fact, some of them can be ideal candidates for external projects funded by individual companies or groups.

Based on the survey results and available guidelines from TAPPI TIS, Valmet, Beloit, and Voith, it is concluded that more in-depth research is imperative in this area. Since following the guideline does not mean trouble-free, and the details of the approach flow system must be determined for individual cases, including the type of plant, product, speed, and quality requirements for the specific application, the

development of computer simulators for the analysis as well as design purposes will contribute tremendously to the paper industry.

In summary, the need for this project is strong and the support from the industry is overwhelming. The main objective of this project is that through the development of computer surrogates, we will finally be able to achieve, maintain, and master the uniform rates and consistencies for all inflows, outflows, return flows, level controls, in-line mixing, i.e., the complete process within the approach pipe flow system even if the individual components and the whole system are under certain transient variation or perturbation during the papermaking processes.

References

[1] G.A. Smook. *Handbook for pulp & paper technologists.* Angus Wilde Publications, second edition, 1992.

[2] S. Pantaleo. Stock piping principles and their effect on paper machine performance. *Adapted from 'Design Principles for Approach Piping' by D.J. Wolf*, April 1976. Beloit Corp.

[3] O.L. Heissenberger, Jr. Design aspects for approach flow systems. *Papermakers Conference*, pages 273–278, 1986.

[4] J.C.W. Evans. Paper machines in the year 2000: higher speeds, new press designs. *Trends and Developments in Papermaking*, pages 50–51, 1985.

[5] Sulzer Papertec Middletown Inc. Approach flow recommendations. September 1992.

[6] Fluid Mechanics Committee TAPPI. Headbox piping system: General design guide. *Technical Information Sheet(T.I.S.)*, 0410-06, 1995.

[7] Valmet Paper Machinery. Engineering instructions. April 1992.

[8] Valmet-Tampella Ltd. Board Machinery Group. Special requirements for the board machine short circulation. September 1985.

[9] Beloit Corporation. Headbox piping recommendations: Design information. November 1994.

[10] P. Boettcher. Headbox approach flow systems. *Stock Preparation Short Course*, pages 41–45, 1984.

[11] D. Byers. Proper component fit is key design factor for headbox approach system. *Pulp & Paper*, pages 126–129, November 1991.

[12] P. Virtanen, H. Koivo, and F. Cameron. Computer simulator for paper machine wet end. *Tampere University of Technology at Finland*, 1987.

[13] D. Orloff. *IPST Internal Communication*, September 1995.

[14] M. Barasch. Dynamic analysis of the approach flow system. *CPPA 75th annual meeting, technical section*, pages A33–A37, 1989.

[15] M. Barasch. Dynamic analysis of the approach piping system. *TAPPI Engineering Conference*, pages 73–80, 1989.

[16] M. Rajala. Viscosity perturbation damper connected with distribution header of papermaking machine headbox. *United States Patent*, 3865687, February 1975.

[17] J.C. Kerr. Stock prep approach systems. *Stock Preparation Short Course*, pages 93–98, 1990.

[18] M.W. Day and J.C. Kerr. Stock approach technology: Systems design. *Stock Preparation Short Course*, pages 91–95, 1988.

[19] K.D. Kurtz. Deaeration and the approach system. *Stock Preparation Short Course*, pages 179–193, 1994.

[20] M. Johnson. The headbox approach system. *TAPPI Papermakers conference*, pages 515–522, 1991.

[21] C.B. Lester. *Hydraulics for Pipeliners*, volume 1: Fundamentals. Gulf Publishing Company, second edition, 1994.

[22] M. Barasch. Dynamic analysis of the approach flow system. *Pulp & Paper Canada*, pages 49–52, 1991.

[23] T. Belytschko. Fluid-structure interaction. *Computers & Structures*, 12:459–469, 1980.

[24] K.J. Bathe and W.F. Hahn. On transient analysis of fluid-structure systems. *Computers & Structures*, 10:383–391, 1979.

[25] M.A. Hamdi, Y. Ousset, and G. Verchery. A displacement method for the analysis of vibrations of coupled fluid-structure systems. *International Journal for Numerical Methods in Engineering*, 13:139–150, 1978.

[26] T.B. Belytschko and J.M. Kennedy. A fluid-structure finite element method for the analysis of reactor safety problems. *Nuclear Engineering and Design*, 38:71–81, 1976.

[27] L.G. Olson and K.J. Bathe. A study of displacement-based fluid finite elements for calculating frequencies of fluid and fluid-structure systems. *Nuclear Engineering and Design*, 76:137–151, 1983.

[28] H. Morand and R. Ohayon. Substructure variational analysis of the vibrations of coupled fluid-structure systems. Finite element results. *International Journal for Numerical Methods in Engineering*, 14:741–755, 1979.

[29] G.C. Everstine. A symmetric potential formulation for fluid-structure interaction. *Journal of Sound and Vibration*, 79(1):157–160, 1981.

[30] L.G. Olson and K.J. Bathe. Analysis of fluid-structure interactions. A direct symmetric coupled formulation based on the fluid velocity potential. *Computers & Structures*, 21(1/2):21–32, 1985.

[31] C.A. Felippa and R. Ohayon. Mixed variational formulation of finite element analysis of acoustoelastic/slosh fluid-structure interaction. *Journal of Fluids and Structures*, 4:35–57, 1990.

[32] K.J. Bathe, C. Nitikitpaiboon, and X. Wang. A mixed displacement-based finite element formulation for acoustic fluid-structure interaction. *Computers & Structures*, 56(2/3):225–237, 1995.

[33] X. Wang and K.J. Bathe. Displacement/pressure based finite element formulations for acousto/slosh fluid-structure interactions. *International Journal for Numerical Methods in Engineering*, 1995. To appear.

[34] X. Wang and K.J. Bathe. On mixed elements for acoustic fluid-structure interactions. *Mathematical Models & Methods in Applied Sciences*, 1995. To appear.

[35] K.J. Bathe. *Finite Element Procedures.* Prentice Hall, Englewood Cliffs, N.J., 1995.

[36] P. Dransfield. *Hydraulic Control Systems - Design and Analysis of Their Dynamics.* Springer-Verlag, third edition, 1981. Lecture Notes in Control and Information Sciences.

[37] R.P. Benedict. *Fundamentals of Pipe Flow.* John Wiley & Sons, 1980.

[38] A. Lencastre. *Handbook of Hydraulic Engineering.* John Wiley & Sons, 1987.

[39] *Pipework Design and Operation.* IMechE Conference Publications, 1985.

[40] A. Conway, editor. *A Guide to Fluidics.* Macdonald & Co. Ltd., 1971.

[41] R.S. Powell, M.M. Smith, and M.J.H. Sterling. Robust on-line data validation for real-time monitoring of water distribution networks. In Č. Maksimović and M. Radojković, editors, *Computational Modelling and Experimental Methods in Hydraulics*, pages 279–288. Elsevier Applied Science, 1989.

[42] G.Z. Watters. *Analysis and Control of Unsteady Flow in Pipelines.* Butterworths, 1984.